Tailoring Hyaluronic Acid and Gelatin for Bioprinting

Dissertation zur Erlangung des naturwissenschaftlichen
Doktorgrades der Julius-Maximilians-Universität Würzburg

vorgelegt von

Junwen Shan

aus Peking

Aschaffenburg 2022

This document is licensed under the Creative Commons Attribution-ShareAlike 4.0 International License (CC BY-SA 4.0):
http://creativecommons.org/licenses/by-sa/4.0 This CC license does not apply to third party material (attributed to another source) in this publication.

Tailoring Hyaluronic Acid and Gelatin for Bioprinting

Dissertation zur Erlangung des naturwissenschaftlichen
Doktorgrades der Julius-Maximilians-Universität Würzburg

vorgelegt von

Junwen Shan

aus Peking

Aschaffenburg 2022

In Andenken an meine Oma

Eingereicht bei der Fakultät für Chemie und Pharmazie am

Gutachter der schriftlichen Arbeit

1. Gutachter:

2. Gutachter:

Prüfer des öffentlichen Promotionskolloquiums

1. Prüfer:

2. Prüfer:

3. Prüfer:

Datum des öffentlichen Promotionskolloquiums

Doktorurkunde ausgestellt am

This work was conducted from May 2016 till September of 2020 at the Department of Functional Materials in Medicine and Dentistry, University Hospital of Würzburg, Würzburg, Germany under supervision of Prof. Dr. rer. Nat. Jürgen Groll.

Der Weg ist das Ziel.

Konfuzius (551 – 479 v. Chr.)

List of Publications

As first author:

1) Shan, J.*; Böck, T.*; Keller, T.; Forster, L.; Blunk, T.; Groll, J.; Teßmar, J., TEMPO/TCC as a chemo selective alternative for the oxidation of hyaluronic acid. *Molecules* **2021**, *26* (19), 5963.

* equally shared author contributions

As co-author:

2) Blum, C.; Taskin, M. B.; Shan, J.; Schilling T.; Schlegelmilch, K. Teßmar, J.; Groll, J., Appreciating the first line of the human innate immune defense: a strategy to model and alleviate the neutrophil elastase-mediated attack toward bioactivated biomaterials. *Small* **2021**, *17* (13), 2007551
3) Muir, V.G.; Qazi, T. H.; Shan, J.; Groll, J.; Burdick J. A., Influence of microgel fabrication technique on granular hydrogel properties. *ACS Biomater. Sci. Eng.* **2021**, *7* (9), 4269-4281.
4) Ertl, J.; Ortiz-Soto, M. E.; Le, T. A.; Bechold, J.; Shan, J.; Tessmar, J.; Engels, B.; Seibel, J., Tuning the product spectrum of a glycoside hydrolase enzyme by a combination of site-directed mutagenesis and tyrosine-specific chemical modification. *Chem. Eur. J.* **2019**, *25* (26), 6533-6541.
5) Weis, M.; Shan, J.; Kuhlmann, M.; Jungst, T.; Tessmar, J.; Groll, J., Evaluation of hydrogels based on oxidized hyaluronic acid for bioprinting. *Gels* **2018**, *4* (4), 82.
6) Ortiz-Soto, M. E.; Ertl, J.; Mut, J.; Adelmann, J.; Le, T. A.; Shan, J.; Tessmar J.; Schlosser, A.; Engels, B.; Seibel, J., Product-oriented chemical surface modification of a levansucrase (SacB) via an ene-type reaction. *Chem. Sci.* **2018**, *9*, 5312-5321.

Table of Contents

Table of Contents

Abbreviation and Symbol Index XIII

Chapter 1 - Introduction and Motivation of the Thesis 1

Chapter 2 - Theoretical Background and State of Knowledge 7

2.1 Biofabrication and tissue engineering: Principles and applications 9

2.2 Hydrogels as biomaterials for 3D cell culture 11

2.2.1 Requirements for suitable hydrogels / bioinks 11

2.2.2 Biocompatibility 11

2.2.3 Mechanical properties 13

2.2.4 Rheological features 13

2.3 3D Fabrication of hydrogels 17

2.3.1 Processing of hydrogels 17

2.3.2 Casting of hydrogels 18

2.3.3 Extrusion-based 3D printing 19

2.3.4 Microgel fabrication 20

2.4 Biopolymer-based hydrogels for tissue engineering applications 23

2.4.1 Hyaluronic acid 24

2.4.2 Gelatin 26

2.4.3 Crosslinking mechanisms for stable hydrogel formation 27

2.4.3.1 Schiff Base chemistry 29

2.4.3.2 Thiol-ene reaction 31

2.4.4 Challenges during modification reactions 34

Chapter 3 - TEMPO/TCC as Chemo Selective Alternative for the Oxidation of Hyaluronic Acid 39

3.1 Abstract 41

3.2 Introduction 42

3.3 Materials and methods 46

3.3.1 Materials 46

3.3.2 Syntheses of tetrabutylammonium hyaluronate 46

3.3.3 Syntheses of primary oxidized hyaluronic acid 47

3.3.4 Syntheses of hyaluronic acid dialdehyde 47

3.3.5 Determination of the degree of oxidation 47

3.3.6 Gel permeation chromatography (GPC) 48

3.3.7 SPR measurements for binding affinity of HA derivatives 48

3.3.8 Hydrogel preparation 49

3.3.9 Mechanical testing 50

Table of Contents

3.3.10 Swelling and degradation behavior........51

3.3.11 Cell culture........51

3.3.12 MSC encapsulation in blend hydrogels........51

3.3.13 Cell viability assay........52

3.3.14 Histology and Immunohistochemistry........53

3.3.15 Biochemical Analyses........53

3.3.16 Statistics........54

3.4 Results........55

3.4.1 Syntheses and characterization........55

3.4.2 Hydrogel formation........56

3.4.2.1 Compression tests for Young’s modulus........57

3.4.2.2 Swelling and degradation behavior........58

3.4.3 SPR analysis for determination of binding affinity of proxHA........59

3.4.4 Cell viability of hMSCs........60

3.4.5 Chondrogenic differentiation of hMSCs........62

3.5 Discussion........64

3.6 Conclusion........69

Chapter 4 - Pentenoic Acid Modified Gelatin for Application as Bioink with Light Controllable Mechanics ..71

4.1 Abstract........73

4.2 Introduction........74

4.3 Materials and methods........77

4.3.2 Synthesis of pentenoic N-hydroxysuccinimide ester (PA-NHS)........77

4.3.3 Synthesis of pentenoyl modified gelatin (GelPA)........78

4.3.4 Kinetic studies........79

4.3.5 Gel permeation chromatography (GPC)........79

4.3.6 2D gel electrophoresis........79

4.3.7 Hydrogel formation........81

4.3.8 Mechanical testing........81

4.3.9 Wet weight change........82

4.3.10 Rheological analysis........82

4.3.11 3D (bio)printing........83

4.3.12 Statistical Analysis........83

4.4. Results........84

4.4.1 Synthesis of PA-NHS and GelPA........84

4.4.2 Change of the isoelectric point of GelPA........85

4.4.3 Hydrogel formation........86

4.4.4 Rheology of precursor solutions 90
4.4.5 3D printing and 3D bioprinting 92

4.5 Discussion 94
4.5.1 Material properties 94
4.5.2 3D printing 97

4.6 Conclusion 98

Chapter 5 - 3D Printing of Various Cell Concentrations for Investigation of Scaffold Stability Using Pentenoyl Modified Gelatin and Mesenchymal Stem Cells 99

5.1 Abstract 101

5.2 Introduction 102

5.3 Materials and methods 104
5.3.1 Hydrogel formation with various initiator concentrations 104
5.3.2 Determination of crosslinking degree with NMR 104
5.3.3 Cell culture 104
5.3.4 hMSC encapsulation in GelPA hydrogels 105
5.3.5 Cell viability assay 105
5.3.6 Histology and immunohistochemistry 106
5.3.7 Biochemical analysis 107
5.3.8 3D bioprinting with different hMSC concentrations 107
5.3.9 Statistical analysis 107

5.4 Results 108
5.4.1 Influence of initiator concentration on hydrogel formation 108
5.4.1.1 Compression tests for Young's modulus and swelling behavior 108
5.4.1.2 NMR measurements for determination of reacted ene-functions 109
5.4.2 Cell viability of hMSCs 110
5.4.3 Chondrogenic differentiation of hMSCs in GelPA 111
5.4.4 Scaffold stability with various cell numbers 112

5.5 Discussion 115

5.6 Conclusion 117

Chapter 6 - Concluding Discussion and Outlook 119

Chapter 7 - Summary / Zusammenfassung 125

7.1 Summary 127

7.2 Zusammenfassung 129

Table of Contents

Chapter 8 - References 133

Acknowledgements / Danksagung 145

Abbreviation and Symbol Index

Abbreviation	**Meaning**
2D	two dimension
3D	three dimension
ADH	adipic acid dihydrazide
AGE	allyl glycidyl ether
ANOVA	analysis of variance
bFGF	basic fibroblast growth factor
BSA	bovine serum albumin
CAD	computer aided design
Calcein-AM	calcein acetoxymethyl ester
$CDCl_3$	deuterated chloroform
cm^2	square centimeter
CO_2	carbon dioxide
d	day
DAB	3,3'-diaminobenzidin
DAPI	4',6-diamidino-2-phenylindol
DB	double bond
DCM	dichloromethane
ddH_2O	double distilled water
Disp	displacement
DMEM	Dulbecco's Modified Eagle's Medium
DMF	dimethylformamid
DMSO	dimethyl sulfoxide
DNA	deoxyribonucleic acid
DO	degree of oxidation
DPBS	Dulbecco's phosphate buffered saline
DS	degree of substitution
dsDNA	double-strand deoxyribonucleic acid
DTT	1,4-dithiothreitol
e.g.	exempli gratia (for example)
ECM	extra cellular matrices
EDC	ethyldimethyl-aminopropylcarbodiimide
EDTA	2,2',2'',2'''-(ethane-1,2-diyldinitrilo)tetraacetic acid
EF	extrusion fragmentation
eq.	equivalents
et al.	and others
EthD-I	ethidium homodimer-I
EWG	electron withdrawing group
FCS	fetal calf serum
g	gram
GAG	glycosaminoglycan
GelAGE	allyl glycidyl ether functionalized gelatin
GelMA	methacrylate functionalized gelatin
GelPA	pentenoate functionalized gelatin
GPC	gel permeation chromatography
h	hour
ht	height
H_2O	water

H_3PO_4	phosphoric acid
HA	hyaluronic acid
hBMSC	human bone marrow-derived mesenchymal stem cells
HEPES	4-(2-hydroxyethyl)-1-piperazineethanesulfonic acid
HMPs	hydrogel microparticles
hMSC	human mesenchymal stromal cells
Hyl	hydroxylysine
I2959	2 hydroxy-1-[4-(2-hydroxyethoxy)phenyl]-2-methyl-1-propanone
IEF	isoelectric focusing
KD	equilibrium binding
k_{off}	dissociation rate constant
k_{on}	association rate constant
kPa	kilopascal
L	liter
LAP	lithium phenyl-2,4,6-trimethylbenzoylphosphinate
Lys	lysine
M	molar mass
m	mass
MA	Massachusetts
MALS	mulitple angle light scattering
MBTH	3-methyl-2-benzothiazolinone hydrazone hydrochloride hydrate
MD	microfluidic device
MDa	megadalton
MDA	human breast adenocarcinoma
mg	milligram
$MgSO_4$	magnesium sulfate
MHz	megahertz
µL	microliter
µm	micrometer
µM	micromolar
min	minute
mL	milliliter
mM	millimolar
mm	millimeter
mmol	millimol
M_n	number average molar mass
MN	Minnesota
MO	Missouri
MPa	megapascal
MSC	mesenchymal stem cells
M_w	mass average molar mass
MWCO	molecular weight cut-off
N	Newton
$NaBH_3CN$	sodium cyanoborhydride

NaBrO	sodium hypobormite
NaCl	sodium chloride
NaClO	sodium hypochlorite
$NaIO_4$	sodium periodate
NaN_3	sodium azide
$NaNO_3$	sodium nitrate
NaOAc	sodium acetate
NEPHGE	nonequilibrium pH gel electrophoresis
ng	nanogram
NHS	*N*-hydroxysuccinimide
nm	nanometer
NMR	nuclear magnetic resonance
Nonidet P40	nonyl phenoxypolyethoxylethanol
NY	New York
oxHA	hyaluronic acid dialdehyde
PA	pentenoic acid
PBS	phosphate-buffered saline
PDMS	polydimethylsiloxane
PEG	polyethylene glycol
pH	Potentia Hydrogenii
Phe	phenyl
pK_a	acid dissociation constant
pK_b	base dissociation constant
ppm	parts per million
proxHA	hyaluronic acid with oxidized primary alcohol
PS	penicillin and streptomycin
rad/s	radian per second
RGD	arginine, glycine and aspartic acid
RI	refractive index
RM	regenerative medicine
rpm	revolutions per minute
RT	room temperature
Ru	tris(2,2-bipyridyl)dichlororuthenium(II) hexahydrate
s	second
SDS	sodium dodecyl sulfate
SDS-PAGE	sodium dodecyl sulphate-polyacrylamide gel electrophoresis
SEC	size exclusion chromatography
Ser	serine
sPEG	thiolated 4-arm-star-PEG
SPR	surface plasmon resonance
SPS	sodium persulfate
St.	Saint
TBA	tetrabutylammonium
TBA-HA	tetrabutylammonium hyaluronate
TBAOH	tetrabutylammonium hydroxide
TBC	*tert*-butylcarbazate
TBH	*tert*-butylhydrazine hydrochloride

TBNS	2,4,6-trinitobenzene sulfonic acid
TCC	trichlorisocyanuric acid
TE	tissue Engineering
TEMPO	2,2,6,6-tetramethylpiperidin-1-yl
TGF	transforming growth factor
TX	Texas
UK	United Kingdom
USA	United States of America
UV	ultra violet
V	volume
Vis	visible light

Symbol	Meaning
°C	degree Celsius
%	percent
wt%	weight percent
λ	wavelength
ϒ	strain
ω	angular frequency

Chapter 1

INTRODUCTION AND MOTIVATION OF THE THESIS

The field of tissue engineering (TE) aims to avoid the problems of organ transplantation or even reduce the need for organ replacement by enhancing or maintain tissues and organs before a terminal organ failure [1]. The development of TE started in the 1970's with the transfer of keratinocyte sheets onto patients suffering from burn injuries [2]. TE combines the aspects of medicine, cellular and molecular biology, material science and engineering [3]. The association of all these fields enables scientists to develop natural, synthetic, or semisynthetic tissues which can grow into the required functionality by using expanded cells from the patients [4-6]. Therefore, a central aspect of tissue engineering is the use of three-dimensional scaffolds, which should mimic the extra cellular matrix (ECM) in the human body [6]. The ECMs of different tissues all possess a tissue dependent dynamic structure and support the cells to maintain tissue architecture and function by providing a proper structural and mechanical environment. At the same time, the ECM should allow cells to migrate, restructure and degrade this microenvironment to release signaling molecules.

Main components of the natural ECM are various biopolymers, such as collagen, hyaluronic acid (HA) or fibrin [7]. As materials from biological origin, biopolymers can be found in all types of living organisms, such as bacteria, algae, plants, or animals. The advantages of most biopolymers are their immanent biocompatibility and biodegradability. They are also known to be ecofriendly as renewable raw materials. In contrast to defined synthetic polymers they often have a much higher batch-to-batch variability, depending on the source and the culture conditions they were produced [8]. Additionally, most biopolymers usually need secondary chemical modifications to form stable ECM mimicking hydrogels, since they don't provide an accurate mechanical stability themselves [9], which would be essential for a long term culture of cells on these substrates.

To further adjust and prepare materials or 3D scaffolds specific for each patient and application site, the selection of a proper 3D fabrication technique is of utmost importance to also fulfill the structural prerequisites of the intended replacement tissue. To achieve hierarchical constructs containing cells and biomaterials, different biofabrication techniques are used to provide better tissue constructs than before. Groll *et al.* specified this new "*technology of biofabrication that uses cells and materials as building blocks, which is mainly used for TE and regenerative medicine (RM) applications*" [10]. Nowadays, especially the 3D bioprinting of hydrogels as a biofabrication technique is used to generate the desirable larger

3D printed constructs. But still, also this established technique needs continuous adjustment depending on the used biomaterial and is not suitable for all available hydrogel systems.

This thesis aims to establish new biopolymer-based hydrogel systems for TE as well as biofabrication applications. The biopolymers hyaluronic acid (HA) and gelatin were chosen due to their well-known chemical structures and biocompatibility. The thesis mainly focuses on the development of new synthesis paths for modification of HA and gelatin to obtain crosslinkable hydrogel precursors. The resulting hydrogel systems based on the synthesized biopolymer derivatives are investigated regarding their material properties, their biocompatibility, and the possibility to use them in TE applications such as 3D bioprinting.

Chapter 2 provides an overview and deeper insight in the state of knowledge relating to this thesis. First, applications and general principles of biofabrication are introduced. Afterwards, this chapter focuses on the specific 3D fabrication techniques for hydrogels, the requirements for the used materials and processing techniques for hydrogels. In the end, both used biopolymers (HA and gelatin) are introduced in their chemical constitution, crosslinking mechanism for hydrogel formation and the challenges while working with these biopolymers are described.

The aim of **chapter 3** was to establish an alternative synthesis pathway for oxidized HA besides the very common oxidation reaction using sodium periodate ($NaIO_4$). Here, the oxidation with TEMPO/TCC as oxidation reagents and the investigation of the resulting oxidized HA is described. Hydrogel formation was performed using adipic acid dihydrazide (ADH) and the hydrogels were examined with respect to their material properties, biocompatibility and chondrogenic potential using mesenchymal stem cells (MSCs).

Chapter 4 deals with a novel synthesis pathway of ene-functionalized gelatin derivative for a subsequent thiol-ene crosslinking reaction. The substitution with pentenoic acid (PA) via its *N*-hydroxy succinimide (NHS) ester resulting in pentanoate functionalized gelatin (GelPA) is investigated systematically with respect to reaction conditions and reproducibility. Material properties of GelPA were investigated and the hydrogel formation was accomplished using thiolated 4-arm-star-PEG (sPEG) using tris(2,2-bipyridyl)dichlororuthenium(II) hexahydrate (Ru) and sodium persulfate (SPS) as visible light initiator system. The influence of irradiation time on mechanical properties was examined. 3D printing was performed using an extrusion-based 3D printer and adaptation of the printing temperature to enable 3D biofabrication with three different hydrogel concentrations.

In **chapter 5**, further investigations with the hydrogel system developed in **chapter 4** were performed depending on the concentration of the used initiator system. Additionally, chondrogenesis was studied using a GelPA-sPEG hydrogel system and 3D printing with three different concentrations of MSCs was accomplished to examine the influence of cell concentration on the cell viability in the different bioinks.

Chapter 6 describes the results of **chapter 3**, **4** and **5** in an interrelated concluding discussion, giving insight of possible future perspectives.

The summary of this thesis is written in **Chapter 7** in English and German language.

Chapter 2

THEORETICAL BACKGROUND AND STATE OF KNOWLEDGE

2.1 Biofabrication and tissue engineering: Principles and applications

The term "biofabrication" has been used in many scientific fields to describe completely different processes and circumstances [11,12]. For TE and RM applications, Groll *et al.* defined biofabrication as "*the automated generation of biologically functional products with structural organization from living cells, bioactive molecules, biomaterials, cell aggregates such as micro-tissues, or hybrid cell-material constructs, through Bioprinting or Bioassembly and subsequent tissue maturation processes*" [10]. They described also for TE and RM, biofabrication can be divided into two approaches, which is bioprinting and bioassembly (**Figure 1**).

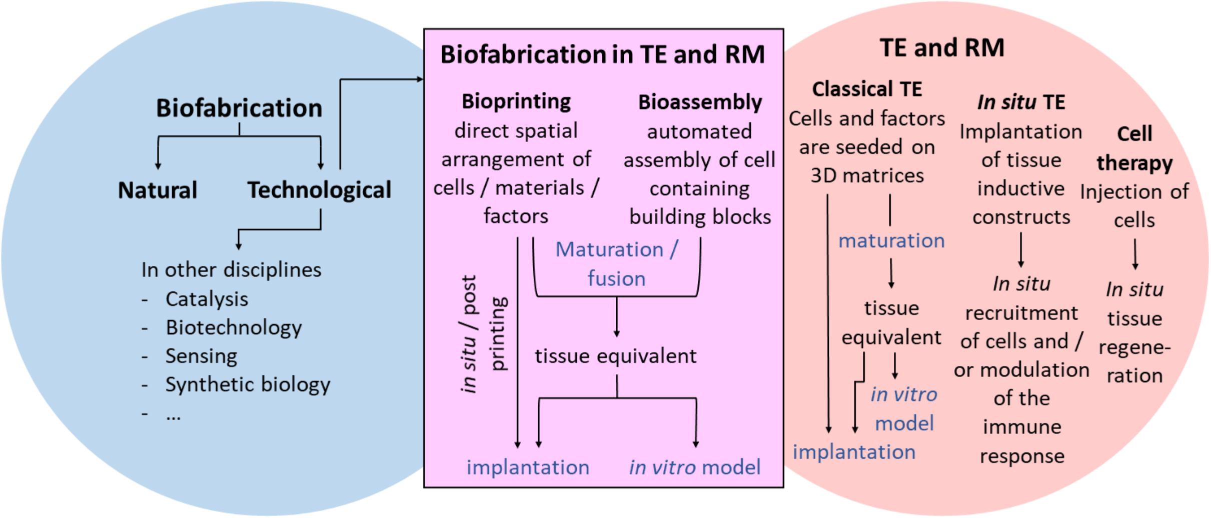
Biofabrication
Natural
Technological
In other disciplines
- Catalysis
- Biotechnology
- Sensing
- Synthetic biology
- ...
Biofabrication in TE and RM
Bioprinting
direct spatial arrangement of cells / materials / factors
Bioassembly
automated assembly of cell containing building blocks
Maturation / fusion
in situ / post printing
tissue equivalent
implantation
in vitro model
TE and RM
Classical TE
Cells and factors are seeded on 3D matrices
maturation
tissue equivalent
in vitro model
implantation
In situ TE
Implantation of tissue inductive constructs
In situ recruitment of cells and / or modulation of the immune response
Cell therapy
Injection of cells
In situ tissue regeneration

Figure 1: Interrelation between biofabrication and TE and RM. Natural processes, e.g. biomineralization or technological processes in various disciplines, e.g. in catalysis, biotechnology and others, are described with the term biofabrication, whereas TE and RM describes the use of living cells with various approaches for regeneration processes. Biofabrication with applications within TE and RM combines both disciplines and can be divided into two specifications as bioprinting and bioassembly. Redrawn and information added from reference [10].

Bioprinting as one biofabrication technique enables the fabrication of 3D tissue constructs with desired structures and shapes using additive manufacturing technologies [13,14]. These constructs contain biomaterials with or without living cells, whereas biomaterials printed without cells with subsequent cell seeding are defined as biomaterial inks and biomaterials containing cells during printing process are defined as bioinks [15]. Bioprinting with respect to its application in TE and RM ultimately aims to generate implantable tissues and organs and thereby reduce the need of organ transplantation based on organ donations [16].

However, the bioprinting of whole organs is still a vision and needs to face many challenges. From the material and biological point of view, the right choice of materials, cell types, growth and differentiation factors are crucial to achieve proper tissue mimicking properties. From the technical aspect, the printing methods must also provide proper resolution and cell viability [14,16,17]. All mentioned issues must be considered during design of a new printable biomaterial ink or especially bioink since cell survival during the printing process is crucial for the application as bioink.

Even 3D bioprinting is still only on laboratory level and was not used for implantations in humans yet, it offers many possibilities for tissue and organ fabrication [18]. Therefore, various tissue models, such as bone [19], heart [20], cartilage [21] and other organ tissues [22-25] have been 3D printed in combination with synthetic polymers or biopolymers. One main issue in all 3D bioprinting approaches is still the vascularization of the printed constructs [26,27], even if vascular tissues have already been fabricated by extrusion [28,29], inkjet [30,31] and laser-based bioprinting [32]. In 2019, Noor *et al*. successfully printed vascularized cardiac patches by using personalized hydrogels with patients own cells and 3D printing into a supporting medium [33]. However, they stated that the printing of blood vessels is still limited.

2.2 Hydrogels as biomaterials for 3D cell culture

2.2.1 Requirements for suitable hydrogels / bioinks

Hydrogels, whether formed with synthetic or natural polymers, are formed in order to mimic extra cellular matrices by providing a biocompatible 3D cell environment for TE [34]. Therefore, many criteria must be considered for a successful design of new hydrogels for application as bioinks [6,35].

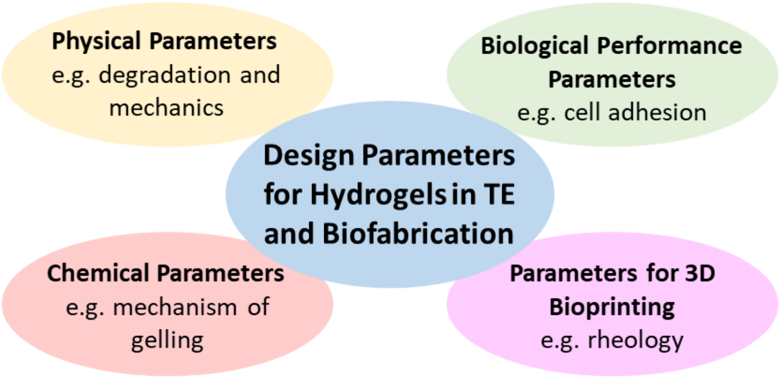
Physical Parameters
e.g. degradation and mechanics
Biological Performance Parameters
e.g. cell adhesion
Design Parameters for Hydrogels in TE and Biofabrication
Chemical Parameters
e.g. mechanism of gelling
Parameters for 3D Bioprinting
e.g. rheology

Figure 2: Design parameters for hydrogels with application in TE and biofabrication. Information added from reference [6,35].

Four design parameters are crucial for a convenient and working hydrogel with application in TE and biofabrication (**Figure 2**). The single parameters are explicated in detail in the following chapters.

2.2.2 Biocompatibility

Cell culture in simple 2D environments differs tremendously from cell culture in 3D, such as the native ECM or alternative 3D constructs [34]. Since many different hydrogels can be used to imitate ECM, their biocompatibility is highly important to enable their application in TE or other biomedical approaches [6,36]. The native ECM as a non-cellular component of tissues provides structural support for cells [37,38] and facilitates many cellular processes such as growth, migration, differentiation and morphogenesis [39,40]. Main components of the ECM are, water [41], carbohydrate polymers like proteoglycans and hyaluronic acid [42,43], and proteins such as collagen, elastin, fibronectin and laminin [44-47]. These components all have their own task in the ECM, e.g. proteoglycans are responsible for buffering, hydration, binding and force-resistant properties of the ECM, whereas collagen and fibronectin are important for tensile strength, regulation of cell adhesion, they support chemotaxis and thereby a directed cell migration and accordingly the tissue development [38,48]. Still, the composition of ECM depends on the functional requirements of the tissues [41]. All in all, ECM is highly complex concerning its structure, its components (**Figure 3**) in proper distributions and resulting functionality.

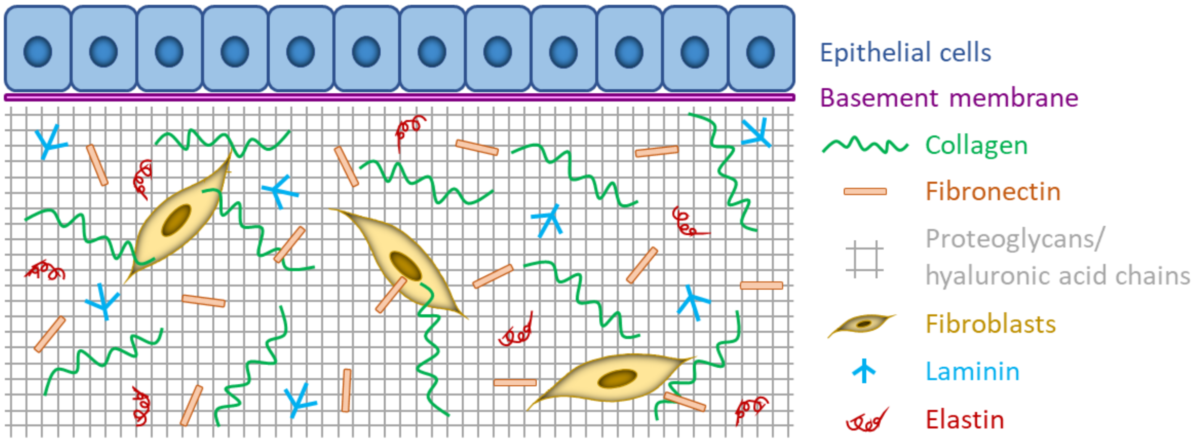

Figure 3: Structure of ECM with main components proteoglycans, hyaluronic acid, collagen, fibronectin, laminin and elastin. Fibroblasts, as presentable example of cells, secret ECM precursors and reorganize the ECM. Redrawn and simplified from reference [38].

The design challenge for an artificial ECM is to fulfill, at least, some of the properties of the natural ECM. The most crucial parameter for synthetic hydrogels with application as factitious ECM is the essential biocompatibility, which should guarantee no rejection reaction, e.g. caused by an inflammatory response or fibrous encapsulation [6]. The used polymers for hydrogel formation can be of synthetic or natural origin [6,49] with the characteristic of an excellent water absorption due to the formation of a stable 3D hydrophilic polymer network [49]. Synthetic polymers offer a wide range of tunable properties, but they have many disadvantages, such as the lack of intrinsic biological activity or adverse effects caused by degradation products [50], which eliminate the biocompatibility of these materials. The absence of active binding sites, for example in polyethylene glycol hydrogels, only provides an inert an unphysiological environment for cells [51,52]. In contrast, biopolymers from natural origin already have, with a few exceptions, biocompatible and biodegradable properties [50]. Common biopolymers used as starting materials for hydrogel formation are proteinogenic biopolymers, like collagen and gelatin [53-55], and/or polysaccharides, such as hyaluronic acid, alginate and chitosan [56-58]. In general, only hydrogels with proper biological parameters, such as non-toxicity, are suitable to mimic natural ECM for applications in TE and RM.

2.2.3 Mechanical properties

Natural ECM also provides mechanical and structural support for cells in tissues [59]. Different tissues have different demands on the structure, composition and mechanical properties of the ECM [60]. For example, Young's modulus of around 0.14 MPa, measured with tensile extension, was reported for human pancreas [61], whereas for human brain 0.1-1 kPa was referred [62]. For cartilage, compressive Young's modulus was determined between 0.24-0.85 MPa [63]. Thus, the natural mechanical strength should be considered during the design of new hydrogel systems for the application in ECM-mimicking of specific tissues. Especially for the chondrogenic differentiation towards cartilage regeneration, it is desirable to develop hydrogels, which show similar mechanical properties than the natural tissue [64].

For the fabrication of more complex shapes of hydrogels, the mechanical properties of the used hydrogels are also important to obtain for example a shape fidelity after the fabrication process [52]. Depending on the fabrication technique and hydrogel material used, hydrogels undergo shear forces and achieve their final mechanical stability after the fabrication process via post crosslinking or a secondary polymerization mechanism [65,66]. Until the material reaches its final mechanical and structural strength, it must be able to keep its shape by cooling for thermo responsive hydrogels [54], pre-crosslinking via enzymes or physical crosslinking [66,67] or using a sufficiently high polymer content for the formation of stable entangled physical hydrogels [52].

2.2.4 Rheological features

The viscosity of a bioink is not only important to avoid cell sedimentation and resulting cell aggregation during printing, but also for proper printability [68]. Additionally, a high shear stress can reduce cell viability of 3D printed cells [69,70]. To investigate the viscosity of a material, its rheological properties need to be determined.

There are two classifications of fluids: Newtonian or non-Newtonian liquids [68]. For Newtonian liquids, shear rate and shear stress are linear related to each other. Polymer solutions can either be shear thickening, for example aqueous corn starch solution [71], or shear thinning (**Figure 4A**), for example a hyaluronic acid solution [72]. Shear thickening behavior leads to increase of viscosity by increasing shear rate due to coalescence of colloids [68] and this can lead to blockage of the needle during 3D printing. However, shear thinning materials show the opposite behavior compared to shear thickening materials. Before reaching a critical shear rate, the viscosity does not change considerably (first Newtonian plateau, **Figure 4B**). When reaching the critical shear rate, the viscosity decreases substantially due disentanglement and elongation of the polymer chains. Finally, the viscosity attains the second Newtonian plateau, where all polymer chains are disentangled and elongated (**Figure 4B**). Since the extrusion through a needle causes high shear rates and shear stress especially at the edge of the needle and can lead to cell death [73,74]. Thus, shear thinning behavior is desirable for materials used for 3D printing to minimize high shear stress during extrusion process through needles.

Whereas the shear thinning behavior of a material is time independent, thixotropy is the reversible decrease of viscosity over time induced by a constant shear rate or shear stress [54,68,75]. If the shear rate or shear stress suddenly stops, the material should, especially when used as bioink, achieve a rapid recovery of the entangled polymer network to ensure shape fidelity after printing (**Figure 4C**) [68,75]. Thus, thixotropic materials with long recovery time are limited for the application as bioink, particularly when multi-layered constructs are aimed [68].

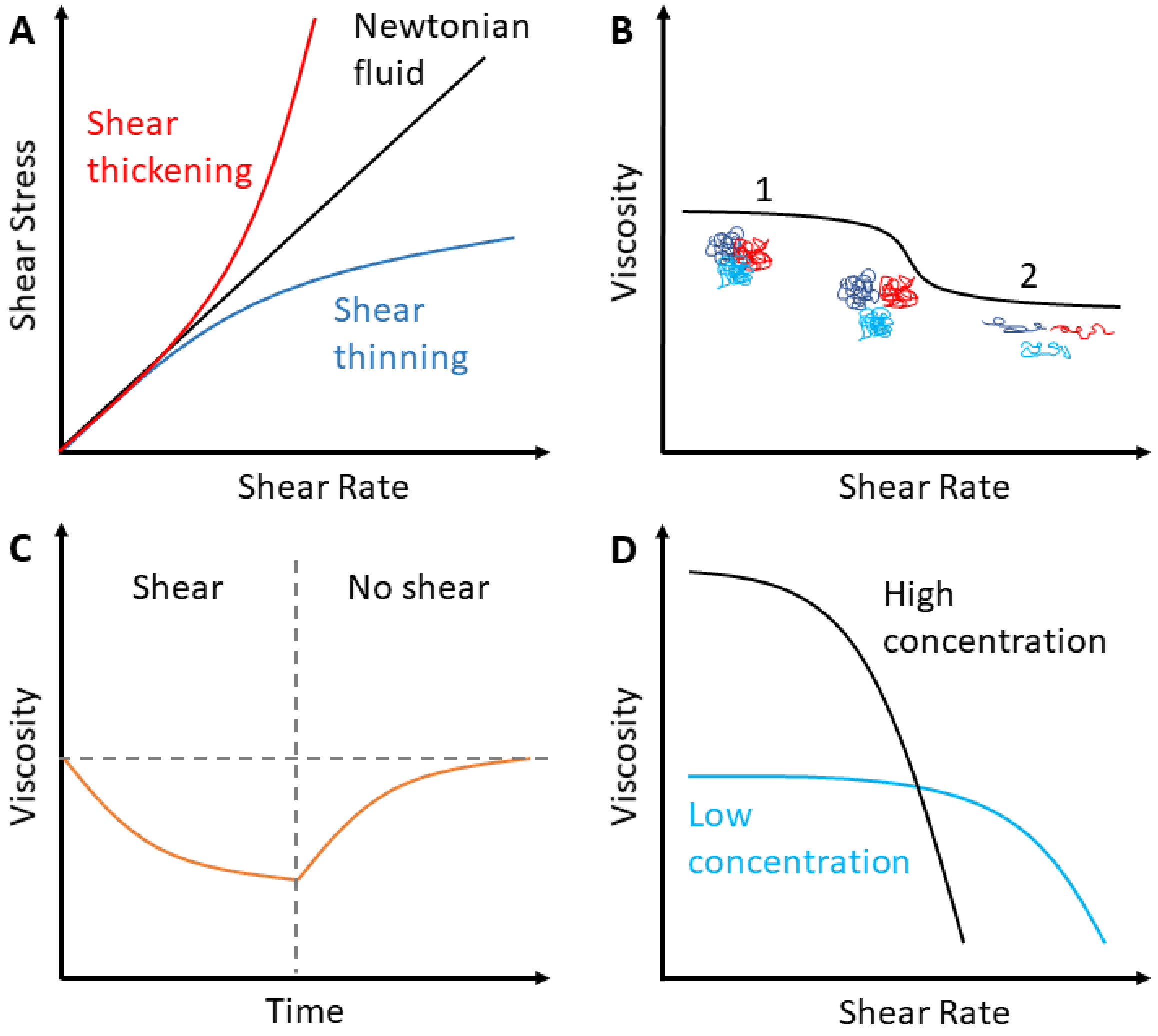

Figure 4: Rheological properties depending on shear rate. (**A**) Flow curves of Newtonian and non-Newtonian liquids with either shear thickening or shear thinning behaviors. (**B**) Shear thinning profile of a non-Newtonian fluid with the first and second Newtonian plateau. (**C**) Change of viscosity of an ideal thixotropic material over time. (**D**) Viscosity of high and low concentrated polymer solutions in dependency of shear rate. (**A**), (**B**) and (**D**) are redrawn from and partially simplified from reference [68].

The viscosity and the shear thinning behavior of a polymer solution is also dependent from the polymer concentration in the solution (**Figure 4D**). By increasing the polymer concentration, the zero-shear rate viscosity also increases, whereas the critical shear rate which initiate the shear thinning is reduced [76]. Still, it is known that high polymer concentration in hydrogels can limit cell growth, migration and differentiation by reducing diffusion of nutrients into the hydrogel network [51,52,77].

Hence, the challenge during design of a new hydrogel system is to ensure all three requirements of biocompatibility, mechanical stability, and printability, which is certainly depending on the subsequent application of the hydrogel. However, various other fabrication techniques have also been developed to process hydrogels, which are not printable due to their unsuited material properties. Accordingly, the next chapter will concentrate on the basic fabrication techniques for 3D processing of hydrogels.

2.3 3D Fabrication of hydrogels

2.3.1 Processing of hydrogels

If the main chemical, physical and biological requirements for an artificial ECM are fulfilled, the hydrogels can be processed to different 3D shapes which is preferential for the subsequent application. Depending on the achieved mechanical and rheological properties of the material, there are various fabrication possibilities for 3D hydrogels (**Figure 5**) or even the usage for other applications such as injectable biomaterials for the delivery of cells or drugs [78,79]. For 3D printable materials, methods such as inkjet, micro extrusion or laser-assisted bioprinting can be used to generate hierarchical 3D structures [16,80]. Other much simpler fabrication methods are film casting, which has been used with an alginate hydrogel system [81]. The state of the art in this work will focus on the casting of hydrogels in predefined molds, extrusion-based 3D printing and microgel fabrication to name fabrication techniques which were used for the materials developed in this thesis and to propose an alternative route how to generate 3D moldable hydrogels, which do not show proper rheological properties.

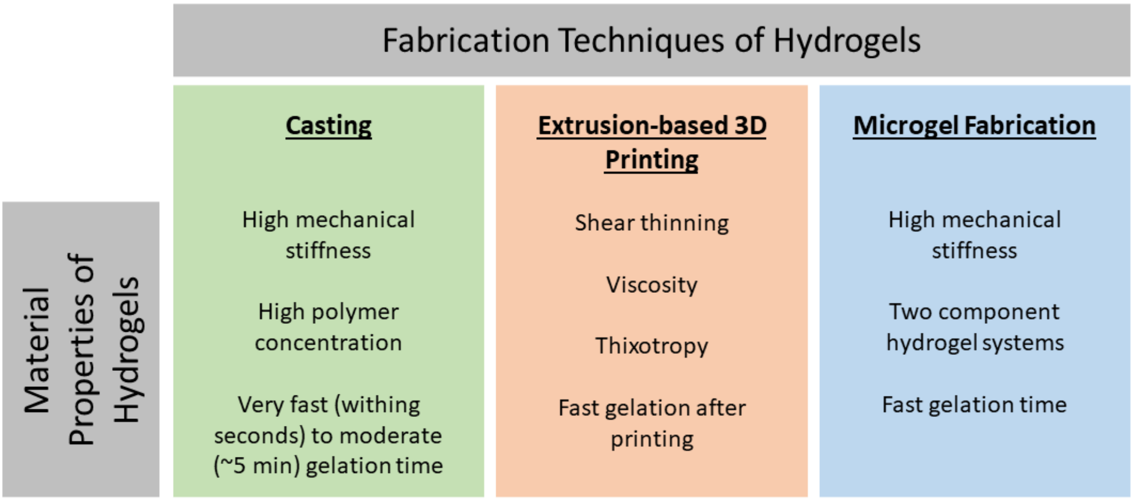
Fabrication Techniques of Hydrogels
Material Properties of Hydrogels
Casting
High mechanical stiffness
High polymer concentration
Very fast (withing seconds) to moderate (~5 min) gelation time
Extrusion-based 3D Printing
Shear thinning
Viscosity
Thixotropy
Fast gelation after printing
Microgel Fabrication
High mechanical stiffness
Two component hydrogel systems
Fast gelation time

Figure 5: Three main fabrication techniques of hydrogels with relevant material properties.

2.3.2 Casting of hydrogels

Hydrogels with high mechanical stiffness, which can also be achieved by very fast gelation time, need high printing pressure to be processed [82-84]. The increase of mechanical strength often relates to increased polymer concentrations and thus an increase of viscosity [85], which causes rise of the shear stress and consequently to more cell damage during extrusion bioprinting. For these hydrogels, which show difficulties in printability or maintenance of cell viability, the fabrication technique of casting is an applicable method.

With casting, special forms can be produced and the method can also be used for commercial production. A very common product generated by a casting method called spin casting are soft contact lenses [86]. Here, the shape of the contact lenses is formed by spinning of the concave mold during polymerization of a silicon hydrogel mixture inside of the mold. Another casting method to produce contact lenses is cast-molding, where the polymer mixture is clamped between two molds during polymerization. Depending on the casting method, Guryča *et al.* found differences between the surface morphology of the lenses by using atomic force microscopy and cryo-scanning electron microscopy [86]. Casting of hydrogel films is often a pre-stage to generate matrices for regeneration of tissues by subsequent drying methods [87,88]. One technique is to cast hydrogel films in petri dishes and let them air dry to receive a thin film. This technique has been used for chitosan-based hydrogels as wound dressing matrix or silk fibroin-graphene oxide hydrogels with potential application in TE [87,89]. Another technique for film casting is to cast the hydrogels into petri dishes followed by treatment with other substance solutions to make the hydrogel insoluble, as performed by Motta *et al* with fibroin hydrogels [88]. Before usage for cell culture, the films were conditioned in PBS for 1 h at room temperature. Film casting of fast gelling HA hydrogels was investigated by Luo *et al*. [90]. Therefore, they functionalized HA with adipic acid dihydrazide to crosslink the product with PEG dialdehyde to load the hydrogel with drugs before film casting. Other possibility for the fabrication of more complex structures is the direct casting of hydrogels. Here, sacrificial templates are needed to specify the desired structure. Zadeh *et al.* therefore used wax templates to receive complex geometries out of cellulose hydrogels, where the wax template was removed by subsequent immersion of the hydrogel-wax construct into a warm water bath to induce the melting of the wax [91]. For the formation of a vascular network, Justin *et al.* used a multi casting approach in cellularized hydrogels [92]. In the first step, the computer aided design (CAD) model vasculature was produced using thermoplastic models in support wax. After removing of the wax, the vascular model was placed into a silicon chamber and then encapsulated with calcium alginate hydrogels. After gelation of alginate, the model was removed by placing the silicon chamber into hot water and washing of the channels with acetone afterwards. To enhance the formation of alginate channels, a calcium chloride solution was injected into the vascular network. After filling of the channels with gelatin, the alginate hydrogel was removed by chelation of the crosslinking calcium ions to achieve the gelatin template which could be then cast in a collagen hydrogel with or without cells. Especially the last two examples of hydrogel casting show that complex structures can be generated by using a very simple stepwise fabrication techniques without using expensive bioprinters or other sophisticated fabrication setups. Regarding the material properties, the casting methods for hydrogels do not impose high demands on the crosslinking time, physical or chemical crosslinking as well as rheological requirements, which makes casting applicable to a wide variety of hydrogel forming polymers.

2.3.3 Extrusion-based 3D printing

When a hydrogel fulfills the rheological requirements, such as proper viscosity and/or shear thinning behavior, extrusion-based 3D printing can be used to fabricate 3D structures with much higher complexity. During extrusion-based 3D bioprinting, hydrogel systems are extruded through a nozzle by using pneumatic pressure or a piston driven system, first to an almost planar 2D structure, which can be turned into sophisticated 3D structures by stacking additional 2D layers on top of each other [14,80,93]. The design of these structures can be realized by CAD techniques and slicing of the 3D structure in several printable layers [94]. The achievable resolution of the printed geometries is mainly limited by the nozzle diameter and other printing parameters, such as the printing pressure and printing speed, and is highly dependent on the used hydrogel properties, such as its viscosity and shear recovery [95-97]. Additionally, the possibility to print multi-material architectures by using multiple nozzles can further enhance complexity of printed constructs [98]. A broad range of hydrogels as bioinks is already used for this approach [8,13,85,93,99]. Still, the best suited hydrogels are those with shear thinning and fast thixotropic behavior or thermo-responsive properties to maintain good printability and shape fidelity after printing, which is achieved by a secondary post-crosslinking in most cases [68,93,99]. Concurrently, when the technique is used for bioprinting, cell viability depends on the necessary printing pressure, since high shear stress during the extrusion causes cell damage [70,94], and the applied post printing crosslinking mechanism can furthermore be detrimental to cell survival.

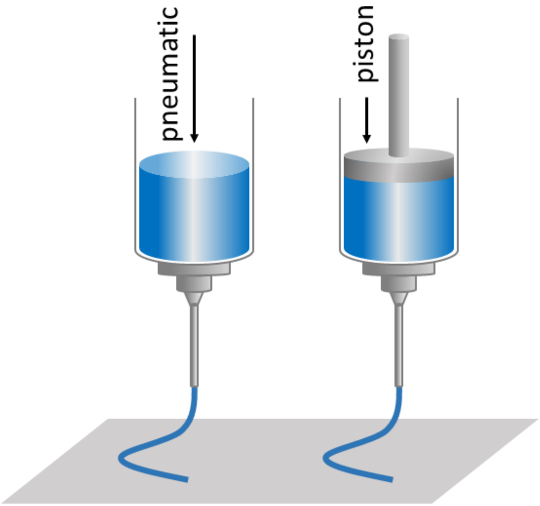

Figure 6: Two common mechanical systems for extrusion-based 3D printing: pneumatic (left) and piston driven (right). Redrawn and simplified from reference [14].

For bioinks, synthetic and natural based polymers, or the combination of both, have been used. Müller *et al.* synthesized diacrylated Pluronic as material for hydrogels which were used for successful extrusion-based 3D printing of bovine chondrocytes [100]. The combination of synthetic and natural polymers as bioinks was demonstrated by Stichler *et al.* [101]. Unmodified high molecular weight hyaluronic acid was added to a precursor solution with allyl and thiol functionalized poly(glycidol) to increase the viscosity but still maintain shear thinning behavior during printing. The encapsulation of human bone marrow-derived mesenchymal stem cells (hBMSC) showed cell viability around 79 %. Most common materials used as bioinks are biopolymers, such as polysaccharides (alginate, hyaluronic acid, chitosan) [65,102,103], proteinogenic polymers (collagen, gelatin and silk fibroin) [104-106] or the combination of at least two biopolymers [107-109]. The importance of biopolymers for the application as bioinks will be discussed later in the material part of state of the art.

2.3.4 Microgel fabrication

Hydrogels with fast gelation and high mechanical strength after gelation are not suitable for extrusion-based 3D printing [110]. These are normally cast as bulk hydrogels as already mentioned in chapter 2.3.2. Additionally, hydrogels with precursor solutions of low viscosity also impede 3D printing [111]. However, fabrication of microgels offers an opportunity to improve the injectability and printability of those hydrogels [112]. Microfluidics, for example, is an emerging method for microgel fabrication. Here, droplets of the aqueous hydrogel precursor solutions are formed within a continuous oil phase in a microfluidic chamber (**Figure 7)** [112]. The polymer containing droplets are crosslinked during their fabrication process and washed afterwards to receive microgels in size range of 5-1000 µm [112-114]. This method is suitable for 2 component hydrogels, which can be mixed within the microfluidic chamber with fast gelation time. Another method for hydrogels with a fast gelation time is extrusion fragmentation, since crosslinked bulk hydrogels are "*subsequently partitioned into microscale components using mechanical force*", resulting in irregular shaped particles from micrometers to millimeters [115]. The hydrogel microparticles (HMPs) with particle sizes between 1-1000 µm can be formed via other methods, such as batch emulsion, emulsion, lithography or electrohydrodynamic spraying methods. With these techniques, formation of droplets (emulsion and spraying techniques), spatial control of HMPs with light from precursor solution (lithography) or the disruption of bulk hydrogels (mechanical or extrusion fragmentation) are possible [112].

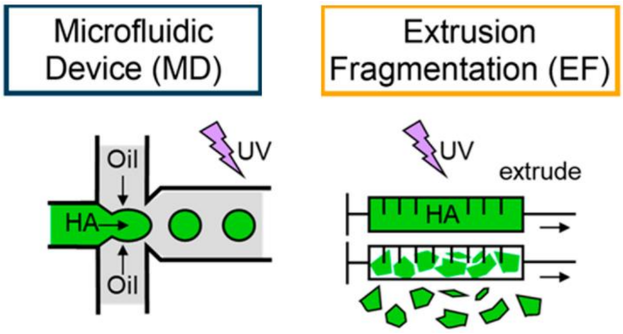

Figure 7: Microfluidic (left) and Extrusion Fragmentation (right) for fabrication of microgels for hydrogel systems with UV crosslinking mechanism. Reproduced and simplified from reference [115] with permission from ACS Publications.

There are few advantages of HMPs. First of all, their size, which fits through thin needles, allows a better shear thinning behavior between the particles due to the granular system and thus enables minimally invasive intervention for cell or drug delivery [112,116]. Second, by combining HMPs made from different hydrogels, cell types or other compositions, bioinks with multiple components can be created [112]. A third advantage is the intentional formation of a microporous structure (void spaces) which can improve and support cell proliferation and migration [117]. In summary, fabrication of HMPs can not only enable printability of hardly printable materials, but also might increase better cell activity. Therefore, HMP fabrication techniques should be kept in mind for the design of novel bioinks.

2.4 Biopolymer-based hydrogels for tissue engineering applications

As already mentioned, biopolymers have, in comparison to synthetic polymers, many advantages from the biological point of view, since most of them are biocompatible with mammalian cells and furthermore biodegradable [8,118]. Biopolymers can be divided in four classes (**Figure 8**): polysaccharides from various sources (e. g. alginate or starch from plants, hyaluronic acid from animals), proteins (collagen/gelatin, elastin), polyesters (polylactid acid), and specialty polymers (shellac, natural rubber) [119]. They can be all extracted from natural origins and are formed under biological conditions by complex metabolic processes in different organisms [8,120]. Thus, the sources for extraction of biopolymers are generally renewable and sustainable [8,118].

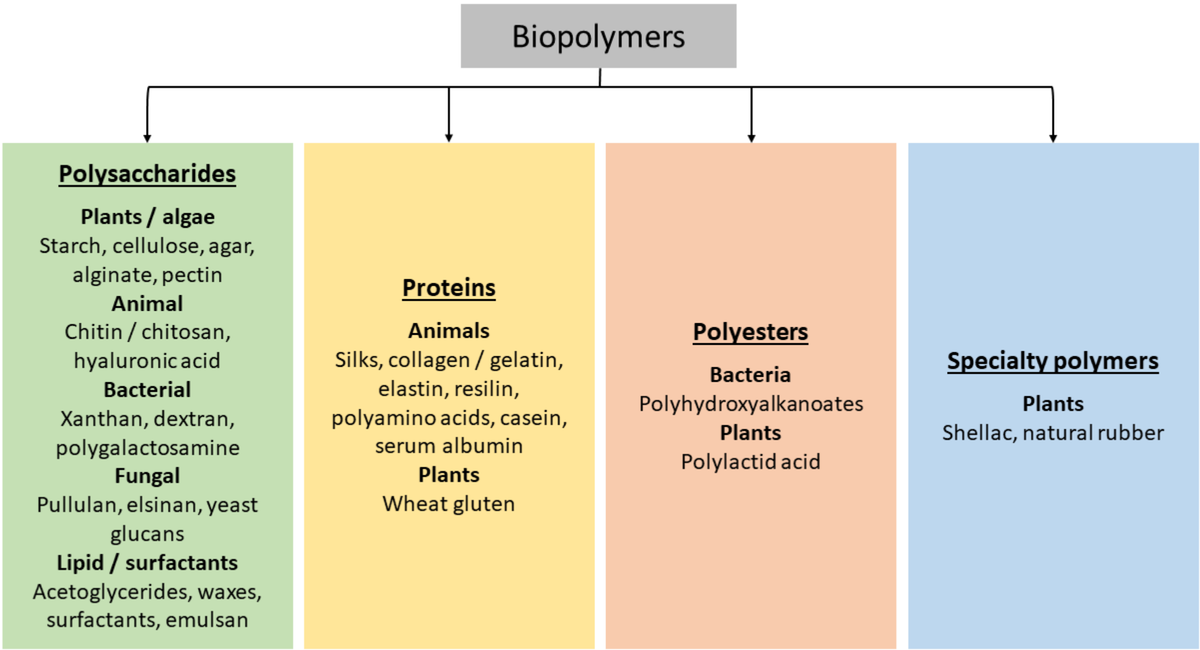
Biopolymers
Polysaccharides
Plants / algae
Starch, cellulose, agar, alginate, pectin
Animal
Chitin / chitosan, hyaluronic acid
Bacterial
Xanthan, dextran, polygalactosamine
Fungal
Pullulan, elsinan, yeast glucans
Lipid / surfactants
Acetoglycerides, waxes, surfactants, emulsan
Proteins
Animals
Silks, collagen / gelatin, elastin, resilin, polyamino acids, casein, serum albumin
Plants
Wheat gluten
Polyesters
Bacteria
Polyhydroxyalkanoates
Plants
Polylactid acid
Specialty polymers
Plants
Shellac, natural rubber

Figure 8: Classes of biopolymers: polysaccharides, proteins, polyesters and specialty polymers. Information added from references [45,119,121-128]

Besides the well-known bioactivity of many biopolymers, most of them only show limited mechanical stability as hydrogels as they are denatured during extraction [129-131]. Therefore, crosslinking of the biopolymers with themselves, other molecules or ions (e.g. alginate) can again increase mechanical strength and improve the hydrogel stability [57,132-134]. Fortunately, biopolymers generally contain various functional groups, which can be easily chemically modified for subsequent physical or chemical crosslinking reactions to compensate the poor mechanical properties and low structural stability in aqueous solutions

[135]. For this work, hyaluronic acid (HA) and gelatin were chosen for functionalization reactions, since both biopolymers are quite promising candidates for an application as artificial ECM for TE or as bioinks [49,136].

2.4.1 Hyaluronic acid

Hyaluronic acid (HA) is a linear anionic polysaccharide, which can be found in all living organisms as part of the connective tissue or in the vitreous humor and synovial fluid [137], and was discovered in 1934 by Karl Meyer and John Palmer [138]. It can be extracted from animal sources, such as rooster combs, or produced by different *Streptococcus* bacterium species [139]. The structure of HA contains repeating disaccharide units of *β*-1,4-D-glucuronic acid-*β*-1,3-D-*N*-acetylglucosamine (**Figure 9**) [140-142] and can reach a molecular weight of more than 10 MDa [143]. Depending on the molecular weight of HA, shorter chains in aqueous solutions are extended, whereas high molecular weight HA chains are coiled [144]. Interactions between the HA chains occur already at low concentrations via hydrogen bonds [144]. At higher concentrations, HA solutions are highly viscous but also shear thinning due to dynamic breakage and formation of hydrogen bonds [144,145]. Still, even at high concentration, HA solutions do not provide proper mechanical stability to mimic ECM sufficiently [146]. Thus, HA generally needs crosslinking reactions to achieve sufficient mechanical strength [146]. Fortunately, HA offers primary and secondary alcohols and acidic group for substitution reactions (**Figure 9**) [141]. Even the *N*-acetyl group of the glucosamine can be used for functionalization after previous deacetylation, but this can result in massive degradation of HA via *β*-elimination of the glucosamine unit [147,148]. The functional groups in HA are not only important for substitution reactions, but also function as binding sites for HA-binding proteins, such as versican or CD44 [149-151]. As a biopolymer, natural degradation of HA is processed enzymatically by hyaluronidase, β-D-glucuronidase and β-D-*N*-acetylhexaminidase [140,152,153]. Chemically, HA can be degraded by pH mediated hydrolysis or free-radical oxidation [154-156].

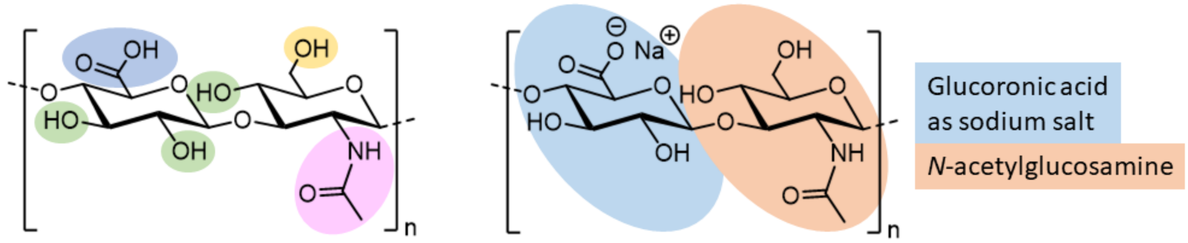

Hyaluronic acid Sodium hyaluronate

Figure 9: Chemical structure of hyaluronic acid (left), containing acidic group (blue), primary (yellow) and secondary (green) alcohol and n-acetyl (purple) groups, and the corresponding HA salt, sodium hyaluronate (right). The repeating dimer unit consist of glucuronic acid and N-acetylglucosamine. Information added from reference [140].

Due to its excellent biocompatibility and biodegradability, HA and its derivatives have been used for cosmetical or medical approaches [157-159]. For cosmetic use, HA is applied in facial creams or subcutaneous injections for wrinkle reduction [157,160]. Pavicic *et al.* showed that wrinkle reduction efficacy of HA creams is dependent on its molecular weight and that low molecular weight HA achieved much better results due to the still possible percutaneous absorption [161,162]. The reduction of wrinkles can be further improved by direct injection of HA based fillers and when complication appears during or after the treatment, it can be easily corrected via injection of hyaluronidase [157,163].

In the human body, HA additionally plays a very important role as lubricant and "shock absorber" to prevent mechanical damage in joints [164]. When arthritis of joints occurs, the overall viscosity of HA solutions in the joints is decreased by reduction of molecular weight as well as concentration of endogenously produced HA [165]. Thus, the injection of exogenous HA to increase the viscosity and HA concentration in the synovial fluid can relieve the symptoms of some patients [158]. Still, recent experiments, summarized by Litwiniuk *et al.*, also indicate that low molecular weight HA from 6 up to 20 kDa is pro-inflammatory, whereas high molecular weight HA shows anti-inflammatory and immunosuppressive behavior [166,167]. Hence, depending on the application, it should be considered whether to use high or low molecular weight HA. As part of the cartilage, HA binds aggrecan as a backbone and forms as HA-aggrecan complex the ECM with type II collagen fibers and regulates the synthesis of proteoglycans during maturation of articular cartilage [158,168,169]. Additionally, HA shows chondroprotective effects *in vitro* and *in vivo* and stimulates chondrocyte proliferation and ECM production in low concentrations [140,170]. Thus, HA is a favored biopolymer for hydrogel formation and has been extensively studied for its application in cartilage repair [171-174]. Due to its poor mechanical properties, HA still needs to be enhanced in its mechanical stability by crosslinking reactions as already mentioned. Since many crosslinking reactions for HA hydrogels are also compatible with other biopolymers, the derivatives of HA and their crosslinking methods are introduced later.

2.4.2 Gelatin

Another common and well-known biopolymer is gelatin, especially with use in food and pharmaceutical industry [175,176]. As denatured form of collagen and proteinogenic polymer, it can be extracted from various animal sources, such as fish or mammalian animals [177]. Depending on the method, whether gelatin is extracted under acidic or alkaline condition, type A (acidic) or type B (alkaline) is obtained [177]. The main differences between these two gelatin types is their viscosity (type A gelatin less viscous) and their isoelectric point (type A 7-9.4 and type B 4.5-5.3) [178]. A characteristic parameter of gelatin is the bloom strength, which describes the rigidity of gelatin gels of a certain concentration, but does not provide any information about the average molecular weight of the hydrolysate [175]. Gelatin of both types with similar bloom numbers show different average molecular weights, whereas gelatin type B shows smaller low molecular weight fraction than type A gelatin. The exact amino acid composition of gelatin is not defined, since it may vary depending on the source the gelatin was extracted from [175]. Nevertheless, it is proven that gelatin does generally not contain any cysteine, which is important for the cross-linking steps performed in this work [179].

For the interaction with cells, gelatin provides arginine, glycine and aspartic acid (RGD) sequences as cell binding site for excellent modulation of cell adhesion [180,181]. In solutions, gelatin chains form triple helices as secondary structure, containing single chains with double loops, single chains with one loop and a non-looped chain or three non-looped chains, depending on the solution concentration and cooling temperature (**Figure 10**) [182]. The disintegration and formation of the triple helix due to hydrogen and van der Waals bonds is responsible for the thermo-reversibility of gelatin [183]. In aqueous solutions, gelatin is soluble at least at 35 °C [176]. The gelation rate of gelatin solutions depends, as the formation of triple helices, on concentration, temperature, and molecular weight [184-186].

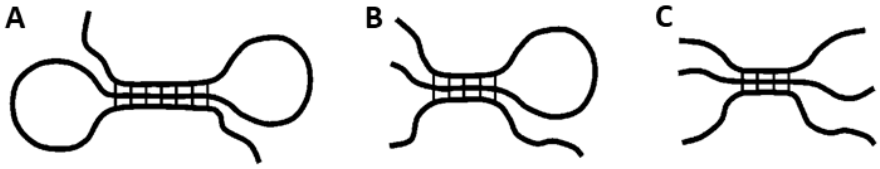

Figure 10: Secondary structure of gelatin, responsible for thermo-reversibility: triple helices containing one double-looped (A), one single-looped and one non-looped (B), and three non-looped gelatin chains (C). Redrawn and simplified from reference [182].

In view of its easy handling, broad range of functional groups due to the contained different amino acids for chemical modifications and an outstanding biocompatibility, gelatin has been widely used as an ingredient for the food industry and as starting materials for many differently modified derivatives in the field of drug delivery and TE [181,187,188]. Gelatin itself without modifications is used as crosslinking partner in hybrid hydrogels, especially using Schiff Base chemistry, with other biopolymers or as stabilizer for 3D printing [189-193]. Still, the physical hydrogel of pure gelatin formed by cooling is not stable for usage under physiological conditions at body temperature [194]. Thus, gelatin needs chemical crosslinking to form stable hydrogels to be used under cell culture conditions thereafter [194]. The most popular gelatin modification is with methacrylate (GelMA), resulting in a photo-crosslinkable hydrogel system [195]. GelMA or hybrid hydrogels have been used for cartilage tissue engineering [196-198], engineering of cardiac constructs [199] or have been studied for development of cardiovascular-like tissues [200,201]. Additionally, GelMA could be already fabricated with various methods, such as microfluidics, photopatterning, micromolding and bioprinting [136].

2.4.3 Crosslinking mechanisms for stable hydrogel formation

As already mentioned, both hyaluronic acid and gelatin need additional physical or chemical crosslinking to form stable hydrogels for use under physiological conditions. For hydrogel formation, two different strategies were developed over the years (**Figure 11**). For physical crosslinking, ionic interaction, hydrogen bonds, polymeric entanglements and π-π stacking are often used as strategies [202], without additional chemical crosslinking agents resulting in better biocompatibility [203]. Simultaneously, reversible physical crosslinking mechanisms have been explored, which improves the shear thinning behavior and additionally can provide self-healing properties [204,205]. Hoverver most of these physical crosslinking mechanisms show poor mechanical properties and often an early dissolution of the hydrogels due to reversible character of the physical interactions [206,207]. Chemically crosslinked hydrogels are instead generated by the formation of irreversible covalent bonds [202]. Therefore, various chemical reactions, including radical polymerization or enzyme induced reactions [208,209], click-chemistry [210], Schiff base formation [211], (thiol-)Michael addition [212,213], can be used for hydrogel formation. The limitation for chemical crosslinked hydrogels is to choose non-toxic and biocompatible crosslinking or initiator reagents. To compensate the poor mechanical and long-term stability of physically crosslinked hydrogels, a secondary crosslinking mechanism via chemical reactions is often used [67,205]. Hydrogels generated as combination of both crosslinking strategies are accordingly also called hybrid hydrogels. This fusion can be used to tune material properties of hydrogels, such as deformation by extreme resilience with following recovery to its original form [214,215] or excellent rheological properties for the 3D printing step and subsequently a mechanical stability after post-printing crosslinking [67,205].

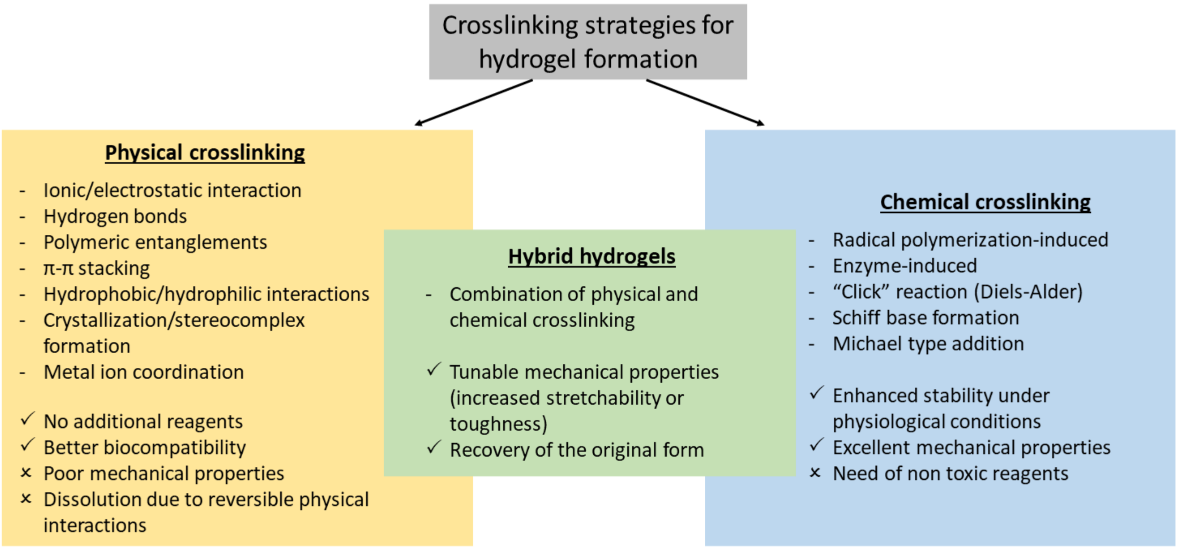

Crosslinking strategies for hydrogel formation

Physical crosslinking

- Ionic/electrostatic interaction
- Hydrogen bonds
- Polymeric entanglements
- π-π stacking
- Hydrophobic/hydrophilic interactions
- Crystallization/stereocomplex formation
- Metal ion coordination

✓ No additional reagents
✓ Better biocompatibility
× Poor mechanical properties
× Dissolution due to reversible physical interactions

Hybrid hydrogels

- Combination of physical and chemical crosslinking

✓ Tunable mechanical properties (increased stretchability or toughness)
✓ Recovery of the original form

Chemical crosslinking

- Radical polymerization-induced
- Enzyme-induced
- “Click” reaction (Diels-Alder)
- Schiff base formation
- Michael type addition

✓ Enhanced stability under physiological conditions
✓ Excellent mechanical properties
× Need of non toxic reagents

Figure 11: Crosslinking strategies for hydrogel formation can be divided into two parts, physical and chemical crosslinking. Hydrogels formed using both crosslinking methods are called hybrid hydrogels and offer special mechanical properties. Information added from references [202,214,215].

Main topic of this thesis is the controlled modification of two different biopolymers to achieve stably crosslinked hydrogel networks. On the one hand, this work focuses on the synthesis of a hyaluronic acid hydrogel system with reversible chemical crosslinking using Schiff base chemistry. On the other hand, a gelatin-based hydrogel which initially uses the thermo reversible crosslinking properties of gelatin for printing and subsequent chemical crosslinking via thiol-ene reaction is investigated. In the following, both these reactions are described with a deeper insight to their chemistry and their advantages and disadvantages are discussed.

2.4.3.1 Schiff Base chemistry

Schiff base is named after Hugo Schiff, who first reported the reaction of amines with aldehydes forming imines (**Scheme 1A**) in 1866 [216]. Under neutral reaction conditions, the first step of the mechanism is the formation of a carbinolamine after internal proton transfer from the nitrogen to the oxygen [217]. Afterwards, the hydroxyl group of carbinolamine is directly protonated and by elimination of water, the reaction results in an iminium ion with a hydroxyl ion as counterion [217]. In the equilibrium state, the iminium ion can be deprotonated by the hydroxyl ion and the imine is formed (**Scheme 1B**). As a pH dependent reaction, the Schiff base formation is most favored at neutral pH [217,218]. The reverse reaction, which is the imine hydrolysis, only occurs with the protonated iminium species [217]. Due to its reversibility, Schiff base chemistry is counted among the dynamic covalent bonds which exhibit self-healing properties of hydrogels for biomedical applications [219]. However, the reversibility of this reaction can also cause a dissolution of the hydrogel when used in amine containing solvents, such as cell media containing amino acids, which consequently will compete with the reversible formation of the imine [84]. Yet, the use of special amine derivatives can further influence the stability of the formed Schiff base, for example by using hydrazide or oxyamines instead of the common primary amines (**Scheme 1C**). The hydrolytic stability of the resulting products hydrazones and oximes compared to imines has been investigated by Kalia *et al.*, showing best hydrolysis stability for oximes, followed by hydrazones [220].

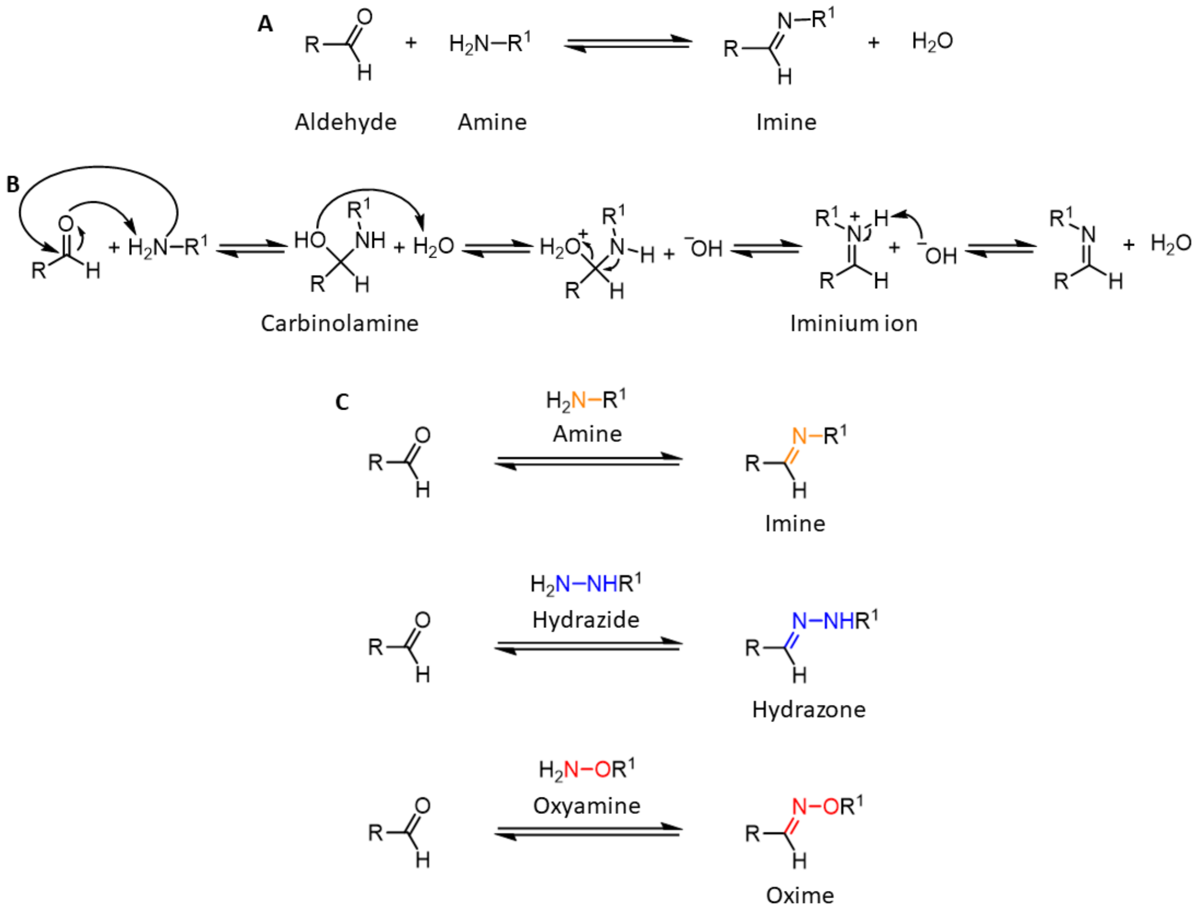

Scheme 1: Schiff base formation with aldehyde and amine (**A**); the reaction mechanism of imine formation under neutral conditions (**B**) via carbinolamine and iminium ion; Schiff base and its derivatives, depending on the amine derivative used for Schiff base formation (**C**).

For a hydrogel formation, the aldehyde functionalization needs to be introduced into the biopolymers, since they do not possess these naturally. The most popular method to generate aldehyde groups is the oxidation of polysaccharides with periodate [221]. The oxidation results in 1,2-glycol scission by formation of a dialdehyde and works very well for carbohydrates due to their poly hydroxylic structure [222]. Many polysaccharides have been oxidized with periodate, e.g. alginate [223], chitosan [224], hyaluronic acid [225] and cellulose [226]. For hydrogel formation, at least difunctional amine derivatives are necessary for crosslinking. Gelatin for example is a potential crosslinker as a multifunctional macromolecule and has been used for crosslinking with aldehyde containing alginate [227]. Adipic acid dihydrazide is a common low molecular weight bifunctional crosslinker, which is often used to generate acylhydrazones with aldehyde functionalized polysaccharides, such as poly(guluronate) [228], alginate [229] and hyaluronic acid [230], to form hydrogels for TE, injection or 3D printing. As a small molecule, it can even be functionalized via 1-ethyl-3-(3-dimethylaminopropyl)carbodiimide activation of the acidic group of hyaluronic acid to transform this biopolymer into a multi-functional crosslinker carrying multiple hydrazide functions [231]. This enables pure hyaluronic acid hydrogels when crosslinked with oxidized hyaluronic acid [67]. Whereas the reversibility can be used for self-healing properties, most Schiff base crosslinked hydrogels need an additional crosslinking mechanism to ensure long time stability, e.g. in cell culture media as discussed above. Therefore, alginate hydrogels were post-crosslinked with calcium ions [227] and hyaluronic acid hydrogels were strengthened by a secondary stable chemical network [67].

2.4.3.2 Thiol-ene reaction

The coupling reaction of mercaptans with olefins was first reported in 1905 by Posner [232]. Yielding the anti-Markovnikov product, which is the linear addition of a thiol to the alkene, two mechanisms, depending on the structure of the olefin, are possible [233]. One mechanism is the free radical reaction, which is mostly photo-induced or metal catalyzed. In the first step, a thiyl radical is generated, followed by its addition to the double bond (propagation 1, **Scheme 2A**). Subsequently, a rapid hydrogen-abstraction of a thiol hydrogen from the carbon-centered radical occurs with the formation of a new thiyl radical (propagation 2, **Scheme 2A**) [234]. However, extremely rapid termination reactions by radical-radical coupling with 10 or even 100 times faster reaction rate can interrupt the main intended thiol-ene reaction [235]. These termination reactions occur when two thiyl radicals form a disulfide bond, one thiyl radical reacts with the carbon-centered radical, or two carbon-centered radical reacts with each other (**Scheme 2B**) [234]. Still, the kinetic of the thiol-ene reaction depends on the chemical environment of the ene structure and has been investigated extensively by Morgan *et al.* [236] and nicely summarized by Hoyle *et al.* [234]. According to Hoyle *et al.*, the conversion rate of the thiol-ene reaction is directly correlated with the electron density of the ene, where electron-rich enes react much faster than electron-poor enes due to better stability of the formed carbon-centered allylic radical with highly conjugated double bonds in the neighborhood. Following this, it is possible to predict the ene-derivatives to their degree of reactivity with thiols:

Norbonene ≥ Vinyl silane > Allyl ether ≥ vinyl ether > fumarate > propene > maleimide > methacrylate > crotonate > styrene > acrylonitrile > butadiene [237].

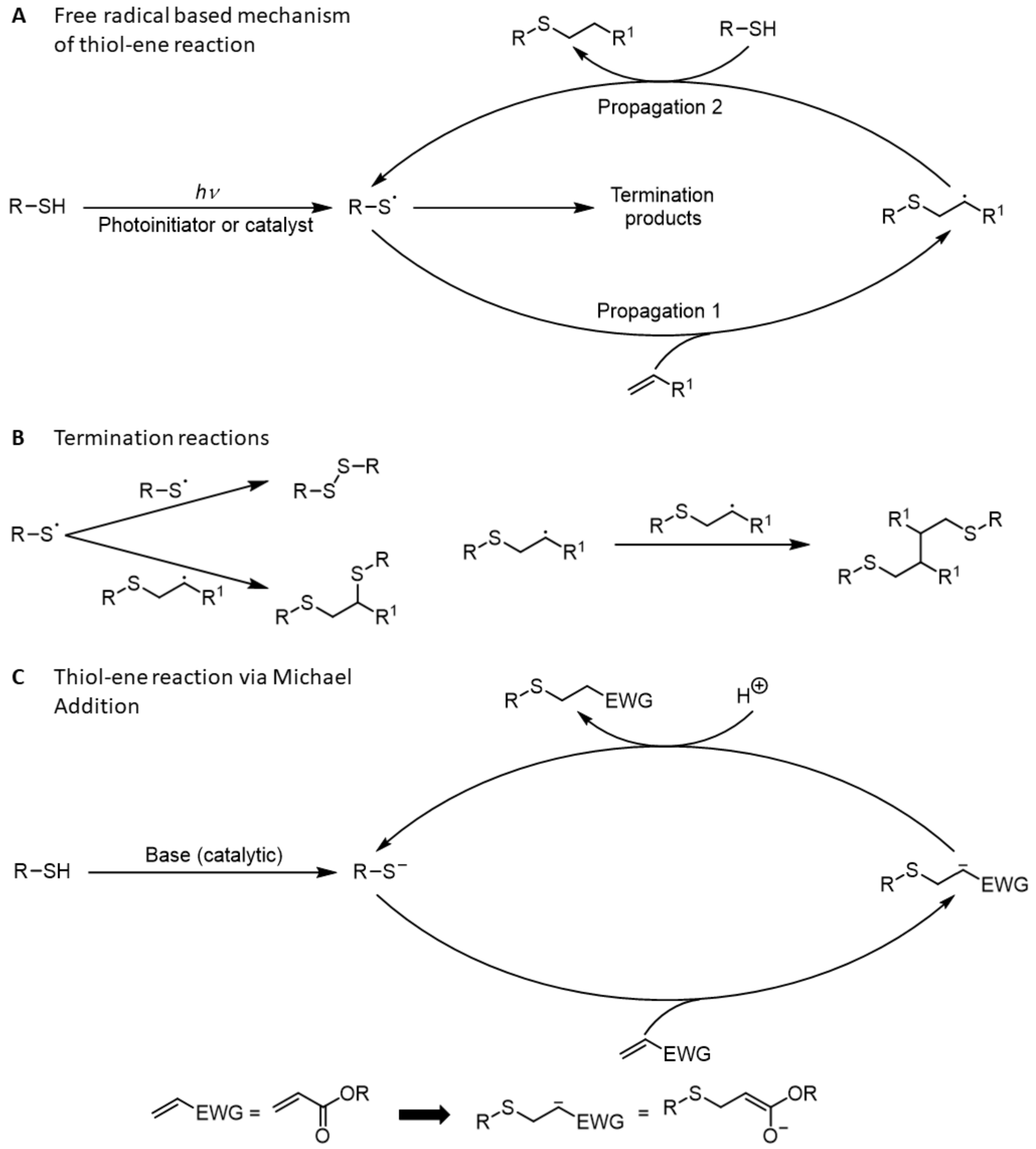
A Free radical based mechanism of thiol-ene reaction
R–SH
hν
Photoinitiator or catalyst
R–S˙
Termination products
Propagation 1
Propagation 2
R–SH
R¹
B Termination reactions
R–S˙
S–R
R–S
R¹
C Thiol-ene reaction via Michael Addition
R–SH
Base (catalytic)
R–S⁻
H⊕
EWG
EWG =
OR
O
O⁻

Scheme 2: Mechanism of thiol-ene reaction, depending on the reaction conditions. For reaction with photoinitiator or metal catalyst, the reaction follows a free radical mechanism (**A**), which can be interrupted by termination reactions (**B**); without photoinitiator, but under catalytic alkaline conditions, the reaction follows Michael addition like nucleophilic mechanism (**C**). When the electron withdrawing group (EWG) is an ester or acidic group, the reaction follows exactly a Michael addition. Redrawn from the references [233,234].

Another possible mechanism is the alkaline catalyzed nucleophilic addition, so called termed thiol Michael addition or conjugate addition reaction [233,238]. The mechanism follows the deprotonation of the thiol, e.g. with triethyl amine or phosphines [239], resulting in the thiolate anion and the corresponding ammonium cation. This anion subsequently reacts as

Michael donor and adds to the via electron withdrawing group (EWG) activated ene-bond to form the electrophilic carbon-centered intermediate anion or an enolate anion, in case of an ester or acidic group as EWG. In the last step, this strong basic carbon-centered or enolate anion abstracts a proton from a new thiol group or the ammonium cation (**Scheme 2C**) [233]. For the reaction kinetic, pK_a of the used thiol, pK_b of the base for deprotonation and the EWG of the vinyl play important roles and impact the reaction rate of the thiol Michael addition [240].

Due to its high yields, stereo specificity, inoffensive byproducts, and mild reaction conditions such as benign solvents (water), which are characteristics for “click” reactions, thiol-ene reactions with both mechanisms are mentioned in many publications as thiol-ene “click” reactions [238,241-243]. Especially photoinitiated thiol-ene reactions possess the advantage, that the reaction can be activated at specific times and locations [238]. The formed thioether products show robust stability in a broad range of chemical environments, such as strong acidic or alkaline media, as well as oxidizing or reducing conditions [244]. The resulting polymer networks are also known to be highly uniform [234]. For photoinitiation, various light sources, depending on the initiator system, can be used. Most common UV-initiator is 2-hydroxy-1-[4-(2-hydroxyethoxy)phenyl]-2-methyl-1-propanone, also known as Irgacure 2959 (I2959), which can be initiated by UV-light between 320-365 nm [245-247]. Still, UV-light can cause genomic instability and damage DNA directly [248]. Therefore, other light initiators which can activated by visible light (Vis) are desirable. Here, lithium phenyl-2,4,6-trimethylbenzoylphosphinate (LAP) [249], riboflavin [250] and the initiator system containing tris(2,2-bipyridyl)dichlororuthenium(II) hexahydrate (Ru) and sodium persulfate (SPS) [251] have been used (**Scheme 3**).

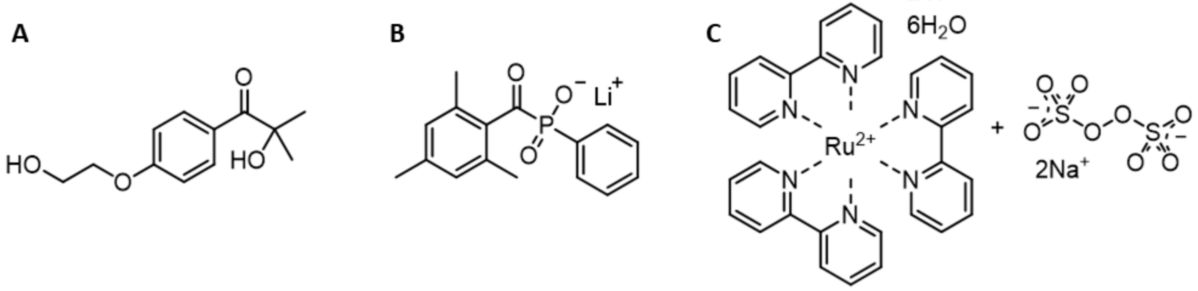

Scheme 3: Common UV initiators or initiator systems. (**A**) 2-hydroxy-1-[4-(2-hydroxyethoxy)phenyl]-2-methyl-1-propanone (I2959); (**B**) lithium phenyl-2,4,6-trimethylbenzoylphosphinate (LAP); (**C**)

Initiator system tris(2,2-bipyridyl)dichloro-ruthenium(II) hexahydrate (Ru) and sodium persulfate (SPS).

Thiol-ene reactions, both free radical induced and thiol Michael addition, have been used in biomedical applications or regenerative medicine for hydrogel formation. Biopolymers which already contain thiol groups have been crosslinked with ene-functionalized polymers, for example silk fibroin [252]. Otherwise, thiol free biopolymers can be functionalized with thiol groups. Here, just to mention a few examples, hyaluronic acid using ethyldimethyl-aminopropylcarbodiimide and *N*-hydroxy-succinimide (EDC/NHS) chemistry for activation of the acidic group and 1,4-dithiothreitol (DTT) [253], collagen or gelatin using 2-iminothiolane to functionalize the lysin residues [254] or amine functionalized acidic groups [255] have been successfully thiol modified and crosslinked with other ene containing polymers. Since biopolymers do not provide ene functions naturally, there are also possibilities to modify biopolymers with ene functions, e.g. norbonene functionalized carboxymethyl cellulose using carbic anhydride or alginate using EDC/NHS chemistry and norbonene-2-methylamine [256,257] and allyl glycidyl ether modified gelatin [54]. Hydrogels containing only one biopolymer, which is both functionalized with thiol and ene functions, have also been investigated, for example using starch [258] or gelatin [259].

2.4.4 Challenges during modification reactions

Although biopolymers offer plenty of functionalization possibilities, there are a few challenges to be considered. To get biopolymers in solution, the most common solvent is water. Otherwise, the biopolymer requires additional treatment, such as ion exchange for hyaluronic acid or chondroitin sulfate, to become better soluble in organic solvents [107,260], or a mixture of water and a miscible organic solvent can be used to improve the solubility of other reagents [261,262]. Many functionalization reactions are performed in organic solvents to provide optimum reaction conditions. For example, pentenoic anhydride or norbornene anhydride are not well soluble or completely insoluble in water and need to be dissolved in organic solvents [263,264]. Furthermore, many chlorides or anhydrides will undergo immediate hydrolysis, partially with high exothermic reactions, in water [265] and are inactivated for a substitution reactions afterwards.

Another challenge for substitution reactions are the reaction conditions and their impact on the modified biopolymer. For hyaluronic acid, a strong hydrolytic degradation occurs under acidic or alkaline conditions on glucuronic acid and *N*-acetylglucosamine moieties via random chain scission. Degradation was also detected at higher temperatures [154]. Even during freeze drying, degradation was observed, especially for the sodium free hyaluronic acid due to presence of free radicals [155]. For gelatin, heating up to 50 °C for 24 h and treatments under strong alkaline conditions cause partial degradation [266,267]. Due to these knowledge, hyaluronic acid and gelatin should only be substituted under mild conditions, such as room temperature, non-radical reactions, or neutral pH to maintain their natural properties. Yet, not all substitution reactions can be performed under mild conditions.

In some cases, reproducibility of a substitution reaction is also an issue. Depending on the source or the provider, there are already enormous batch differences between the raw materials. Additionally, a batch-to-batch variation during synthesis is also known, e.g. GelMA , which is even reported in an article by Zhu *et al.* [268]. During this work, an inconsistency of the periodate oxidation of hyaluronic acid in literature was noticed (**Table 1**). Whether the raw materials were purchased from different providers and the methods of determination of the degree of oxidation were disparate, the degree of oxidation should be in similar ranges when the same ratio of oxidation reagent was used. Since the degree of oxidation is fluctuating between 16 to 70 % when comparing the results from the articles, it can be assumed that the periodate oxidation is not very consistent.

When substitution reactions are performed with reagents, which can react with themselves, e.g. allyl glycidyl ether in a polymerization reaction [269], the determination of the degree of substitution can be quite problematic. Additionally, the batch-to-batch variation of the biopolymers also causes problems when the composition of the raw material is different depending on the sources it was extracted from, which occurs when using proteinogenic biopolymers such as gelatin [178].

All in all, working with biopolymers holds many challenges, which must be faced. Still, the profit they offer to tissue engineering and regenerative medicine is worthwhile to develop new biopolymer-based biomaterials and to investigate their advantages which should be considered for their use as tissue substitutes. For this reason, this work introduces the results of novel synthesis paths for hyaluronic acid and gelatin derivatives and their usage in the field of chondrogenic tissue engineering.

Table 1: Comparison of results of periodate oxidation from four different research articles. HA was purchased from various providers and have different mass average molar mass (Mw), as well as sodium periodate (NaIO4) was from different sources. Even with same equivalents of NaIO4 used, the degree of oxidation (DO) varies massively between 20 and 70 %. Still, determination methods were different. For blue stained line, the reaction was performed for 24 h at RT, whereas the other articles only let the reaction stirring for 2 h. Information added from references [67,84,270,271].

Year	Author	HA provider	$NaIO_4$ provider	M_w (HA, raw)	Equivalents of $NaIO_4$, related to 1 HA dimer	Determination methods of degree of oxidation (DO)	DO [%]
2004	Jia et al.	Genzyme Corp., Cambridge MA	Aldrich (Milwaukee, WI)	1.3 MDa	1	TBC/$NaBH_3CN$, NMR	70
					0.24		16
2010	Su et al.	Q.P. Corporation, Japan	RDH Chemical Co., Spring Valley CA	320 kDa	1	TBNS-Assay, Absorbance (microplate reader)	44
2018	Wang et al.	Lifeforce, Chaska MN	Sigma-Aldrich (St. Louis, MO)	400 kDa	1	TBC, Absorbance (microplate reader)	20
2018	Weis et al.	Dagmar Kohler-BaccaraRose, Alpen Germany	Thermo Fisher Scientific, Waltham, MA, USA	1.3 MDa	0.5 or 2	MBTH-Assay, Absorbance (UV-Vis)	5 or 16
				50 kDa	01.-1		1.4-8

Chapter 3

TEMPO/TCC AS CHEMO SELECTIVE ALTERNATIVE FOR THE OXIDATION OF HYALURONIC ACID

Parts of this chapter are already published (Junwen Shan*, Thomas Böck*, Thorsten Keller, Leonard Forster, Torsten Blunk, Jürgen Groll, Jörg Teßmar, TEMPO/TCC as chemo selective alternative for the oxidation hyaluronic acid).

The content of this article is based on the work of the author of this thesis Junwen Shan, who performed all chemical and material scientifical experiments, data evaluation and composition on the chemical and material scientifical parts of the manuscript.

*: shared author contributions

Chapter 3

The author contribution in the original research article was as followed:

Contributor	Contribution
Junwen Shan	Designed the research; performed the chemical and material scientific part of the research; analyzed all chemical and material scientific data and all statistics; wrote the manuscript
Thomas Böck	Designed and performed all biological research; performed biological, histological, immunohistochemical and biochemistry experiments; provided feedback on manuscript
Thorsten Keller	Performed SPR measurements; provided feedback on manuscript
Leonard Forster	Provided feedback on manuscript
Torsten Blunk	Provided feedback on manuscript
Jürgen Groll	Designed research; provided feedback on manuscript
Jörg Teßmar	Designed research; provided feedback on manuscript

3.1 Abstract

Hyaluronic acid based hydrogels are very commonly applied as cell carriers for different approaches in regenerative medicine. Hyaluronic acid itself is a well-studied biomolecule originating from the physiological extracellular matrix of mammalians and due to its acidic polysaccharide structure offers many different possibilities for suitable chemical modifications, which are necessary to decrease its excellent water solubility and allow the formation of dissolution stable hydrogel networks.

Most of these chemical modifications are performed using the free acid function of the polymer and additionally lead to an undesirable breakdown of the biopolymers backbone. An alternative modification of the vicinal diol of the glucuronic acid is the oxidation with sodium periodate to generate dialdehydes via a ring opening mechanism, which can then be further modified or crosslinked via Schiff Base chemistry. Since this oxidation causes a structural destruction of the polysaccharide backbone, it was our intention to study a novel synthesis protocol frequently applied to selectively oxidize the C6 hydroxyl group of saccharides. Based on this TEMPO/TCC oxidation this study aimed to develop an alternative hydrogel platform based on oxidized hyaluronic acid crosslinked using adipic acid dihydrazide as crosslinker.

3.2 Introduction

Modified biopolymers offer a broad spectrum of hydrogel forming materials, which have become increasingly important in the field of drug delivery, tissue engineering and regenerative medicine in recent years [54,272,273]. As materials from natural origin, they are found in many different extra cellular matrices as hyaluronic acid (HA) or as collagen, respectively the derived and due to processing slightly degraded gelatin [274,275]. Especially the biotechnologically produced HA and its derivatives are already in clinical use for many specific applications due to their excellent biocompatibility and availability in high purity [276]. For a chemical modification hyaluronic acid offers several functional groups available for different modification schemes, additionally the polymer is also known to bind to CD44 receptors [141,277,278] and to enhance the chondrogenic differentiation of mesenchymal stem cells in general [279,280].

Especially in the field of tissue engineering, the dissolution stability and mechanical strength of applied biopolymers-based hydrogels is crucial for the culture and tissue development under physiological conditions, without a stable crosslinking the water soluble polymers will dissolve slowly and disappear from the application site [129]. Natural HA hydrogels themselves possess only very low mechanical properties as physically crosslinked hydrogels and are thereby limited in their applications for tissue engineering approaches [6]. To achieve a proper dissolution and mechanical stability, HA needs to be functionalized and subsequently chemically crosslinked with other non-detrimental molecules to form long term stable hydrogel networks [281]. For these applications the carboxyl group of HA can be modified with e.g. thiol, tyramine, or dihydrazide, whereas the primary 6-hydroxy groups can be alternatively functionalized with methacrylate and bromoacetate for various chemical or enzymatic crosslinking reactions such as thiol-ene, peroxidase or photo-crosslinking reactions. These already applied modifications of HA are summarized in a review article by Burdick *et al.* [141]. Besides the frequently applied chemical networks, there are alternative more stable physical, chemically reversible or irreversible crosslinking mechanisms used for hydrogel formation. For example, physically crosslinked HA hydrogels via a more stable guest-host interaction were introduced by Highley *et al.* by esterification of the primary alcohol with adamantane acetic acid as guest and amidation of the carboxylate with β-cyclodextrin as host. For the later application in cell culture, they still needed a secondary and irreversible chemical crosslinking by applying radical polymerization of methacrylate, which they attached to non-modified primary alcohols for enhanced mechanical stability [204]. Wang *et al.* in a similar fashion introduced HA hydrogels containing adipic acid dihydrazide modified HA as well as periodate oxidized HA. This dynamic covalent system, based on the reversible Schiff Base chemistry, additionally needed chemical fixation by a thiol-ene crosslinked secondary network with norbornene modified HA and a tetrathiol crosslinker to allow long term tissue culture [67].

Many of the physical or dynamically crosslinked hydrogels can also be successfully applied for 3D bioprinting approaches due to their excellent shear thinning properties, but as stated above those systems require a secondary crosslinking to achieve sufficient mechanical strength and long-term stability for subsequent cell culture. Therefore, other common crosslinking mechanisms, which can also lead to hydrogels without any pre-crosslinking systems, were used to generate irreversible covalent bonds via UV crosslinking, e.g. via thiol-ene reaction [253,282] or radical polymerization [283]. However, the here used UV light can harm cells by direct DNA damage and should therefore be avoided or at least applied with the necessary care [284,285]. In general, it is thus desirable to apply mechanisms without any UV crosslinking to provide good cell viability during covalent hydrogel formation. One alternative crosslinking reaction already described for HA hydrogels is based on Schiff Base chemistry, which has already been reported for pre-crosslinking [67,84,270], including different reactive and stable amine derivatives, like imines, hydrazones or oximes [286].

For the necessary aldehyde functionalization, one commonly applied method is the oxidation of HA using sodium periodate to generate a dialdehyde in a ring opening reaction of the glucuronic acid unit, which results in a massive alteration of the HA backbone structure. Linkers containing amine, dihydrazide or aminooxy groups can subsequently be used as crosslinkers [84,270,286,287]. Weis *et al.* showed, that hydrogels formed using these materials are not stable for longer than six days in PBS and even less stable in the amino acid containing cell culture medium. At the same time, the degree of oxidation (DO) varies even with same molar stoichiometry and is normally quite moderate, most likely due to numerous side reactions of the periodate [67,84,270]. Accordingly, hydrogels based on Schiff Base chemistry using low molecular weight crosslinkers always need a secondary networking, e. g. UV crosslinking, to achieve sufficient mechanical and long-term stability.

A promising alternative way to modify HA with aldehyde functionalities is the selective oxidation of the primary alcohol of the *N*-Acetylglucosamine unit with (2,2,6,6-tetramethylpiperidin-1-yl)oxyl (TEMPO)/trichloroisocyanuric acid (TCC) as described for the selective oxidation of glycosides. To enable this reaction of HA in DMF, the solubility of HA needs to be enhanced by exchanging the sodium ion of hyaluronan for a tetrabutylammonium ion (**Scheme 4**). Angelin *et al.* proved the selectivity of the oxidation to primary alcohols with unprotected monoglycosides with high yields already after at least 7 h [288]. For this approach, anhydrous DMF was used as solvent to avoid overoxidation of the primary alcohol to the carboxylic acid and sodium bicarbonate was shown to be most efficient to generate the required alkaline conditions. Buffa *et al.* performed this oxidation in a mixture of water (H_2O) and dimethylformamide (DMF) to generate degrees of oxidation between 5 and 15 %. Additionally, they also tested various secondary oxidation reagent such as sodium hypochlorite (NaClO) or sodium hypobromite (NaBrO). However, a maximum DO of only 18 % was obtained in their studies [289].

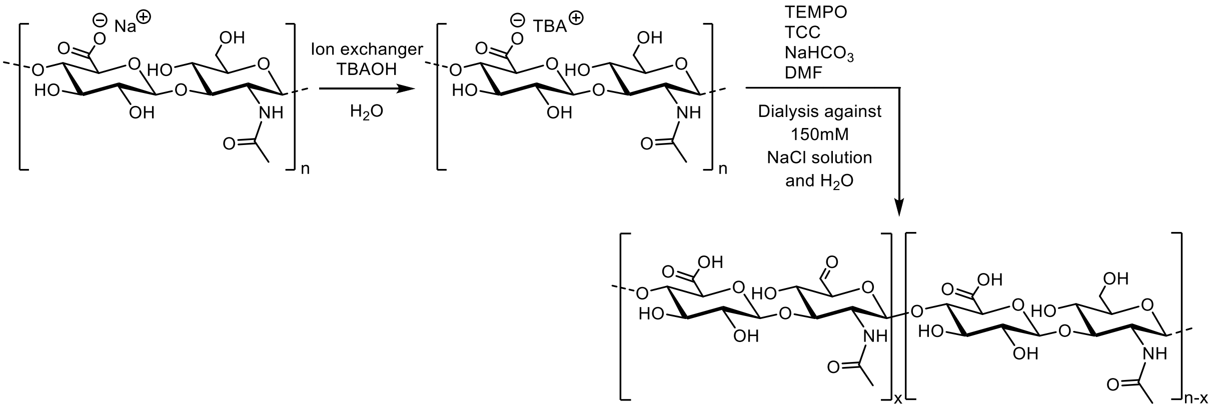

Scheme 4: Synthesis of hyaluronic acid with oxidized primary alcohol (proxHA).

In this study, the aim was to oxidize the primary alcohol of HA selectively by using TEMPO/TCC oxidation in anhydrous DMF. A preservation of the HA backbone without ring-opening and possibly higher DO was expected. It can also be assumed, that due to the intact polymer backbone and higher DO, more stable hydrogels can be prepared even in cell culture medium without any secondary crosslinking systems to achieve higher mechanical and potentially long-term stability. Furthermore, the chondrogenic differentiation potential of human mesenchymal stromal cells (hMSCs) within these hydrogels was analyzed additionally in the research article mentioned above. Since it is known that modifications of the HA backbone can affect the binding affinity to CD44 receptors [290], the binding properties of the primary oxidized HA were studied and compared to periodate oxidized and native HA using surface plasmon resonance (SPR) affinity measurements.

3.3 Materials and methods

3.3.1 Materials

HA (1.0-2.0 MDa, 80-100 kDa), 1-ethyl-3-(3-dimethylaminopropyl)carbodiimide (EDC), *N*-hydroxysuccinimide (NHS) were purchased from Carbosynth Limited, Berkshire, UK. Adipic acid dihydrazide (ADH), anhydrous dimethylformamide (DMF), dimethylhydrazine, DOWEX® 50WX8-400 ion exchanger, Dulbecco's Phosphate Buffered Saline (DPBS), ethidium homodimer-I (EthD-I), sodium azide, sodium chloride, sodium cyanoborohydride, sodium periodate, *tert*-butylhydrazine hydrochloride (TBH), tetrabutylammonium (TBA) hydroxide solution (~40 % in water), trichloroisocyanuric acid (TCC) were purchased from Sigma Aldrich, St. Louis, MO, USA. 2,2,6,6-Tetramethylpiperidine-1-oxyl (TEMPO) was acquired from Alfa Aesar, Karlsruhe, Germany. Human CD44 Fc Chimera Recombinant Protein was obtained from R&D Systems, Minneapolis, MN, USA. Acetic acid, ethylene glycol, potassium chloride, sodium nitrate were purchased from Merck KGaA, Darmstadt, Germany. Proteinkinase K was purchased from Merck Millipore (Burlington, MA, USA). Calcein acetoxymethyl ester (Calcein-AM), Dulbecco's Modified Eagle's Medium (DMEM), 0.25 % trypsin-EDTA, HEPES 1M, penicllin-streptomycin, Quant-iT™PicoGreen® dsDNA Reagent and Kit, sodium hydrogencarbonate was acquired from Thermo Fisher Scientific, Waltham, MA, USA. ROTI®Histofix 4.5 %, ZelluTrans/Roth dialysis tubing (regenerated cellulose, MWCO 3,500 Da) were purchased from Carl Roth GmbH and Co. KG, Karlsruhe, Germany.

3.3.2 Syntheses of tetrabutylammonium hyaluronate

The transformation of sodium hyaluronate into tetrabutylammonium hyaluronate (TBA-HA) was performed according to Oudshoorn *et al.* with slight modifications [291]. The exchange of the sodium counterions was performed with 50 g DOWEX® 50WX8-400. The resin was washed three times with 1 L Millipore H_2O and afterwards suspended in 98 mL TBA hydroxide solution, stirred for two hours at RT and then separated from the solution by filtration. For the preparation of TBA-HA, 5 g HA was dissolved in 600 mL Millipore water overnight at room temperature (RT) and then suspended with 50 g resin. The suspension was shaken for 3 h and the resin was removed by centrifugation. TBA-HA was obtained by lyophilization (Epsilon 2-4 LSCplus, Martin Christ Gefriertrocknungsanlage GmbH, Osterode, Germany).

3.3.3 Syntheses of primary oxidized hyaluronic acid

All subsequently used equivalents were calculated corresponding to one repeating unit of the TBA-HA (M = 621.79 g/mol). TBA-HA was dissolved overnight at room temperature (RT) in anhydrous DMF (0.5 % *w*/*v*) under inert gas. TEMPO (0.0513 eq., catalytical amount) and excess of solid $NaHCO_3$ (30 eq.) was added. The suspension was then cooled down to 4 °C and different amounts of TCC (0.76, 0.5, 0.25 and 0.1 eq.) were added. The reaction was subsequently stirred for 4 h and then slowly warmed up to RT. Afterwards, an excess of ethylene glycol (30 mL for 750 mg TBA-HA and 0.25 eq. of TCC) was added to quench the reaction and remaining oxidative potential. The obtained reaction mixture was then dialyzed against 150 mM NaCl for 2 d and then against Millipore H_2O for another 2 d (MWCO 3,500 Da). The final modified polymer was obtained after lyophilization as a white solid foam. For cell studies and mechanical testing, several batches obtained with 0.25 eq. of TCC were consolidated to receive one larger blend batch to achieve sufficient reproducibility of subsequent experiments and to investigate the influence of batch-to-batch variations.

3.3.4 Syntheses of hyaluronic acid dialdehyde

The synthesis was performed according to Jia *et al.* with slight modifications [270]. HA was dissolved in Millipore H_2O overnight. A 0.4 M sodium periodate solution was added dropwise under exclusion of light with following equivalents: 0.76, 0.5, 0.25 and 0.1. The reaction was stirred for two hours at RT and quenched by adding 30 mL ethylene glycol. The oxidized hyaluronic acid was obtained after dialysis (MWCO 3,500 Da) against ddH_2O and lyophilization as a white solid foam.

3.3.5 Determination of the degree of oxidation

Aldehyde containing HA was dissolved in acetate buffer (pH 5.2) overnight at RT. Stock solutions of *tert*-butylhydrazine hydrochloride and sodium cyanoborohydride (0.5 M) were added. The mixtures were shaken at RT for 24 h at 850 rpm. The solutions were then dialyzed against Millipore H_2O (MWCO 3,500) and lyophilized. ^1H-NMR spectra of the products were measured with 300 MHz NMR (Bruker NMR Fourier 300). The acetyl group of HA (2.05 ppm) was calibrated as 3 protons. The *tert*-butyl signal (1.40 ppm) of each sample was accordingly divided by 9 protons to estimate the achieved degree of oxidation (DO).

$$DO\ [\%] = \frac{integral\ of\ {}^{t}Bu}{9} \cdot 100 \qquad \text{(equation 1)}$$

3.3.6 Gel permeation chromatography (GPC)

Weight and number average molecular weights (M_w and M_n) of proxHA, oxHA were determined by using a GPC system from Malvern (Herrenberg, Germany). The system consisted of a Viscotek GPCmax (in-line degasser, 2-piston-pump and autosampler), a column oven (35 °C) refractive index (RI) detector (Viscotek VE3580), multiple angle light scattering detector (Viscotek SEC-MALS 20, laser wavelength 660 nm) and two Viscotek A-columns (A6000M, length = 300 mm, width = 8 mm, porous poly(methyl methacrylate), particle size 13 µm). An aqueous solution of Millipore H_2O with 8.5 g/L $NaNO_3$ and 0.2 g/L NaN_3 was used as eluent and solvent for the polymers. The samples were dissolved with a concentration of 0.5 mg/ml overnight at RT and filtered with a 0.45 µm regenerated cellulose membrane. The measurements were performed with 100 µl injection volume with an elution rate of 0.7 ml/min. The molecular weights of the HA derivatives were calculated using a MALS calibration performed with a narrow-distributed PEG standard of M_w = 45,000.

3.3.7 SPR measurements for binding affinity of HA derivatives

Interactions between the differently modified HA and the corresponding HA receptor CD44 (R&D Systems, Inc., Minneapolis, MN, USA) were measured by SPR using a Reichert® 4SPR system (Reichert Technologies, Unterschleissheim, Germany). For immobilization of the CD44 receptor on the sensor surface, the carboxylate groups of a carboxymethyldextran hydrogel coated sensor chip (XanTec bioanalytics GmbH, Düsseldorf, Germany) were activated first by perfusing a 1:1 mixture of NHS and EDC (1-ethyl-3-(3-dimethylaminopropyl) carbodiimide) according to the manufacturer's recommendation. Then, CD44 (10 µg/mL in 10 mM NaOAc, pH 4.5) was injected onto the activated sensor for 8 min at a flow rate of 10 µl/min to cause CD44 coating to a final density of 2000 resonance units. Unreacted activated carboxylate groups were quenched by injecting 1 mol/L ethanolamine (pH 8.5) for 300 seconds. Afterwards, measurements were performed at 25°C using HBS150T [10 mM HEPES (pH 7.4), 150 mM NaCl, 3.4 mM EDTA, 0.005% (v/v) Tween 20] as running buffer. Native HA or oxidized HA derivatives were used as analyte at four different concentrations, ranging from 32.7 to 2.7 µM. The flowrate for the acquisition of interaction data was set to 25 µL/min in all experiments. Association was measured for 120 s then dissociation was initiated by perfusing running buffer, and the dissociation phase was monitored for 300 seconds. Regeneration of the chip surface was performed by injecting of two 60-second pulses of 100 mM glycine (pH 2.5) at a flow rate of 100 µL/min. Interaction data were analyzed using the software TraceDrawer version 1.8.1 (Ridgeview Instruments AB, Uppsala, Sweden), applying a simple Langmuir-type 1:1 interaction model and using global fitting for the rate constants. Association rate constant k_{on} values and dissociation rates constant k_{off} values were obtained by fitting data of individual experiments. Equilibrium binding K_D values were deduced using the equation

$$K_D = \frac{k_{off}}{k_{on}} \qquad \text{(equation 2).}$$

All SPR experiments were performed in at least three independent experiments.

3.3.8 Hydrogel preparation

Hydrogels were generally prepared in PBS with final polymer contents of 2, 3, 4 and 5 wt% for proxHA. The polymers were dissolved for 3 h at 37 °C and the 1 or 2 wt% ADH in PBS was also prepared fresh for every experiment. For all hydrogels, equimolar ratios of aldehyde to hydrazide were used. The ADH solution was added to the polymer solution, thoroughly mixed with the pipette and then the solution was immediately transferred to appropriate cylindrical molds. The gels were allowed to cross-link in petri dishes with added wet tissues to avoid drying out, the 3, 4 and 5 wt% hydrogels for 1 h and the 2 wt% hydrogels for 2 h to achieve sufficient cross-linking before adding them into the incubation media. All volumes and masses used for hydrogel preparation are shown in **Table 2**.

Table 2: Volumes and masses used for hydrogels for mechanical tests and investigation of wet behavior.

wt%	DO [%]	m(proxHA) [mg]	V(PBS)	V(ADH 2 wt%)
3	49.5	14.2	385.3	74.7
	55		377	83
	57.2		373.7	86.3
	73.7		348.8	111.2
	53.5 (Blend)		379.6	80.4
2	53.5 (Blend)	9.3	353	107 (ADH 1 wt%)
4	53.5 (Blend)	19.2	350.5	109.5
5	53.5 (Blend)	24.2	321.4	138.6

3.3.9 Mechanical testing

For mechanical testing as well as the swelling/degradation behavior hydrogels were prepared in PBS as described in *3.3.8* using cylindrical molds (4 mm diameter, 4 mm height). The linear compression tests were performed with a mechanical test instrument (ElectroForce 5500, TA Instruments, Eden Prairie, MN, USA) with a load cell of 250 g and a rate of 0.005 mm/s. The height and diameter of each sample were measured with a sliding caliper before each mechanical testing. The strain γ was calculated by dividing displacement (disp) of the measurement by the height h_0 as shown equation 3:

$$\gamma = \frac{displ}{h_0} \qquad \text{(equation 3).}$$

True stress was calculated as follows:

$$True\ stress = load\ (N)\,\frac{h_0 - disp}{V_{sample}} \qquad \text{(equation 4).}$$

By plotting strain *versus* true stress and using the linear fit from the strain ranges showing in the Young's modulus was obtained from the slope of the linear fit. Based on the incubation period of the hydrogels the compression depth and the strain range for the calculation of the Young's modulus were adjusted due to the contraction of the hydrogels (0 and 1h: l = 1 mm, strain 10 to 20%, all other time points: l = 0.5 mm, strain 2.5 to 12.5%).

3.3.10 Swelling and degradation behavior

To observe the swelling or degradation behavior of the hydrogels after incubation in PBS, the hydrogels were taken out of the solution after 1 h, 24 h, 7 d, 14 d and 21 d, blotted dry using analytical tissues, weighed and compared to initial hydrogels at time 0 h. The ratios of the weight of incubated hydrogels (w_s) and weight of non-incubated hydrogels (w) were calculated using the following equation:

$$WB = \frac{w_s}{w} \qquad \text{(equation 5).}$$

3.3.11 Cell culture

Human bone marrow-derived mesenchymal stromal cells (hMSC) were used for biological evaluation of the obtained hydrogels. hMSC were isolated from the cancellous bone of patients undergoing hip replacement (as approved by the Local Ethics Committee of the University of Wuerzburg (186/18) with the written informed consent of each donor patient.) The hMSC were extracted by extensively washing of the bone fragments and bone marrow with PBS. Following this, the cell containing suspension was centrifuged and the obtained cell pellet was resuspended in proliferation medium (DMEM/F12, supplemented with 10 % FCS, 1 % PS, 50 µg/mL L-ascorbic acid, 2-phosphate sesquimagnesium salt hydrate and 5 ng/mL bFGF (BioLegend, London, UK)) and seeded into T175 cm^2 flasks (Greiner Bio-One, Frickenhausen, Germany). After several days the non-adherent cells were removed by washing carefully with PBS and adherent cells were cultured to a sub-confluent level at 37 °C and 5 % CO_2 in proliferation medium. Finally, MSCs were detached with 0.25 % trypsin-EDTA and seeded at a density of 3-5×10^4 cells mL^{-1} into T175 cm^2 flasks.

3.3.12 MSC encapsulation in blend hydrogels

Blend hydrogels were prepared as described in section 3.3.8 for encapsulation of MSCs. Briefly, proxHA was sterilized using germicidal UV light at 254 nm for 20 min (UVL hand lamp with filter, A. Hartenstein, Wuerzburg, Germany). Afterwards, the proxHA was dissolved in PBS to achieve a final hydrogel content of 3, 4 and 5% (**Table 3**). The ADH solution was sterile-filtered through a 0.2 µm syringe-filter.

Initially, MSCs at passage 4 were resuspended in the corresponding blend proxHA solutions. Then, the cell-laden proxHA solution was mixed with the ADH solution separately for each individual hydrogel and immediately transferred into a silicon mold with 6 mm diameter and 2 mm height (60 µL). The hydrogel precursor solutions were allowed to gel for 30 min at 37 °C and 5 % CO_2 in humidified environment. Following that, the hydrogels were transferred into cell culture medium using a spatula and were cultivated *in vitro* for 21 days either in proliferation medium or in chondrogenic medium (Dulbecco's Modified Eagle's Medium high glucose 4.5 g/L (DMEM) supplemented with 1 % ITS+ Premix (Corning, NY, USA), 40 µg/mL L-proline, 50 µg/mL L-ascorbic acid 2-phosphate sesquimagnesium salt hydrate, 0.1 µM dexamethasone, 1 mM sodium pyruvate, 1% PS, and 10 ng/mL transforming growth factor-β1 (TGF-β1, BioLegend, London, UK).

Table 3: Volumina and masses used for hydrogels for cell culture experiments.

wt%	DO [%]	m(proxHA) [mg]	V(PBS)	V(ADH 2 wt%)
3	73.7	23.2	568.7	181.3
	53.5 (Blend)	23.2	617.8	132.2
4	53.5 (Blend)	31.3	572.0	178.0
5	53.5 (Blend)	39.5	525.1	225

3.3.13 Cell viability assay

The viability of encapsulated MSCs cultivated in proliferation medium was analyzed on d1, d7 and d21 using calcein acetoxymethyl ester (Calcein-AM) to detect viable cells and ethidium homodimer-I (EthD-I) for the detection of dead cells. Therefore, the cell containing hydrogels were washed two times with PBS and were subsequently incubated for 45 min at RT in the staining solution (1 µM EthD-I, 2 µM Calcein-AM). Following that, constructs were washed with PBS and top view images were taken using a fluorescence microscope (Axio Observer.Z1, equipped with epifluorescence optics and a MRm camera, Carl Zeiss, Jena, Germany). The ratio of viable and dead cells was determined for three samples per condition, counting at least at eight different locations within each sample using "Find Maxima" (settings for "live" and "dead" channel: prominence=75, strict, exclude edge maxima, output=Count) with Fiji [292].

3.3.14 Histology and Immunohistochemistry

The hydrogel constructs undergoing chondrogenic differentiation were harvested on d21 and fixed in ROTI®Histofix 4 % for 60 min, washed afterwards in PBS and incubated in Tissue Tek® O.C.T. (Sakura Finetek, Torrance, USA) overnight at 4 °C. The next day, the constructs were transferred into fresh O.C.T., shock frozen in liquid nitrogen and stored at −20 °C until cryosectioning. Longitudinal sections of 8 µm thickness were prepared and collected on Super Frost® plus glass slides (R. Langenbrinck, Emmendingen, Germany).

For histology, the samples were stained with Weigert's hematoxylin, fast green and safranin O to analyze the distribution of glycosaminoglycans (GAG) [293], and with Weigert's hematoxylin and picrosirius red to stain for collagen distribution [294].

For immunohistochemistry, the sections were washed in ddH_2O, and antigen retrieval was performed using Proteinase K for 5 min at RT. The blocking was performed with 1% bovine serum albumin (BSA) in PBS for 30 min and primary antibodies were diluted in 1% BSA in PBS and incubated overnight in a humidified chamber at RT. Antibodies against collagen type II (II-4C11, 1:100, Sigma Aldrich, St. Louis, MO, USA) and aggrecan (969D4D11, 1:300, Thermo Fisher Scientific, Waltham, MA, USA) were used. Sections were washed three times in PBS, and secondary antibodies were diluted in 1% BSA in PBS and applied in the dark for 1 h. A goat anti-mouse (Alexa Fluor 488, 1:100, (115-545-068; Jackson ImmunoResearch; Dianova, Hamburg, Germany)) secondary antibody was used. Finally, the slides were washed three times in PBS and mounted with DAPI mounting medium ImmunoSelect®. Images were taken with a fluorescence microscope (Axio Observer.Z1, equipped with epifluorescence optics, a MRm camera and an Apotome; Carl Zeiss, Jena, Germany).

3.3.15 Biochemical Analyses

For analysis of DNA, GAG and collagen content the constructs were digested in 0.5 mL of a papain solution (3 U/mL) for 16 h at 60 °C. Prior to digestion the constructs were homogenized at 25 Hz for 5 min using a TissueLyser LT (Qiagen, Hilden, Germany).

The DNA content of the hydrogels was determined employing Quant-iT™PicoGreen® dsDNA Reagent and Kit (Thermo Fisher Scientific, Waltham, MA, USA) according to the manufacturer's manual. The DNA quantification was carried out fluorometrically at

λ_{ex} = 485 nm and λ_{em} = 538 nm, using a microplate reader (Spark 20M, Tecan, Maennedorf, Switzerland) and a Lambda DNA standard. The amount of produced GAG was measured using the DMMB assay. The GAG amount was determined with a spectrophotometer at 525 nm, using bovine chondroitin sulfate as standard [295]. The content of hydroxyproline was measured, after acid hydrolysis and reaction with DAB and chloramine T. The quantification was carried out with a spectrophotometer at 570 nm, using L-hydroxyproline as standard [296,297].

3.3.16 Statistics

Sigma Plot 12.5 (Systat Software GmbH, Erkrath, Germany) was used for statistical analysis and Origin 2018b (OriginLab Corp., Northampton, MA, USA) for graphical plots. Data are reported as the mean and standard deviation from at least three replicates if not stated otherwise. For GAG and collagen production, multiple groups were compared using one-way ANOVA with Tukey's post hoc test. Two-way ANOVA with Tukey's post hoc test was used with time (day 1 and 7) and blend hydrogel contents (3 %, 4 % and 5 %) for cell viability. Significant differences are marked as follows: *($p<0.05$), **($p<0.01$) and ***($p<0.001$).

3.4 Results

3.4.1 Syntheses and characterization

The syntheses were processed several times (n ≥ 2) for each equivalent of TCC used. To quantify the overall amount of generated aldehyde functions, the aldehyde groups were stably substituted via reductive amination. For this approach, amine derivatives which contain defined number of protons as a *tert*-butyl group were used and NMR spectra of the substituted products were measured. The acetyl group of the HA dimer unit was calibrated as three protons and the integral of *tert*-butyl group was divided by the number of the *tert*-butyl protons. Consequently, the calculated degree of oxidation refers to the overall amount of oxidized HA dimer units. TCC equivalents of 0.76 and 0.5 led to almost same DO of 72.7 % in average (**Figure 12A**). The reactions applying 0.25 eq. oxidation reagent led to strong variations of the obtained DOs between 49.5 and 73.7 % (**Table 4**). Compared to the $NaIO_4$ oxidation (DO between 4.1 - 11.7 %), generally a much higher DO was achieved with TEMPO catalyzed oxidation with lower amounts of secondary oxidation reagents and even the lowest amount of 0.1 eq. TCC achieved a DO of around 22.2 % (**Figure 12A**). In general, TEMPO/TCC oxidation achieves a 3 to 12-fold higher DO than $NaIO_4$ oxidation depending on equivalents TCC used.

Degradation of HA chains during oxidation was investigated by parallel GPC measurements. In comparison with the $NaIO_4$ oxidation, where a weight average molecular weight (M_w) of 101 – 435 kDa was obtained for the different equivalents of periodate, a pronounced degradation occurs during TEMPO/TCC oxidation with achieved molecular weights of M_w 11 – 302 kDa (**Figure 12B**). In both cases, increasing molecular weights M_w with decreasing amounts of oxidation reagent were observed, which can be attributed to a smaller polymer destruction by the lower amounts of oxidation reagents. Since the DOs for the TEMPO/TCC oxidation were at least 3 to 12 times higher, it was decided to investigate the influence of obtained individual oxidation degrees on hydrogel stiffness and incubation stability.

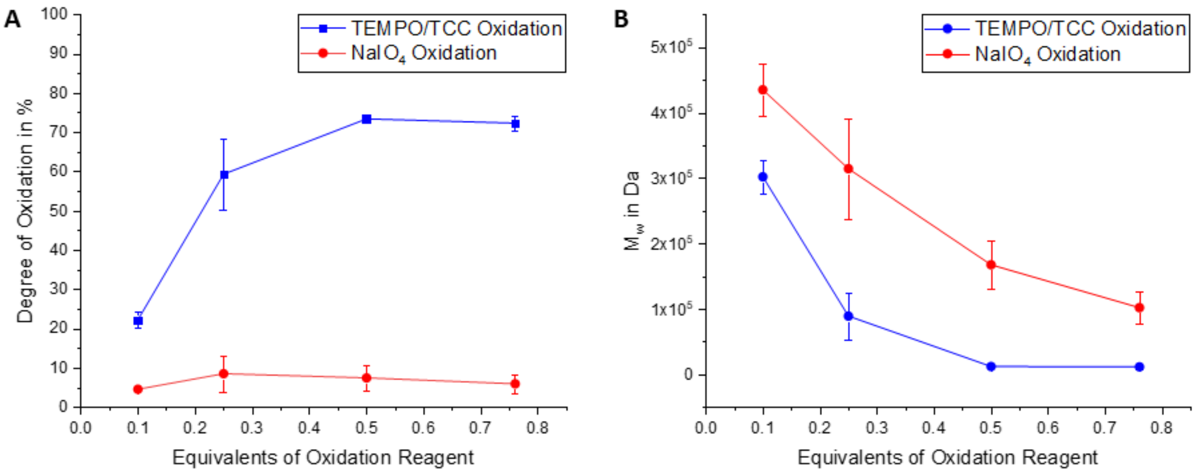

Figure 12: Comparison of TEMPO/TCC and $NaIO_4$ oxidation in (**A**) degree of oxidation in % for different equivalents of oxidation agents and (**B**) weight average molecular weight in kDa for the differently oxidized polymers.

Table 4: DO in % and weight and number average molecular weights (M_w and M_n in kDa) of native HA, oxHA and various batches of proxHA synthesized with 0.25 eq. of TCC; grey marked batches were combined to one blend.

	DO [%]	M_w [kDa]	M_n [kDa]	Sample Name
Native HA	0	61	24	HA
proxHA	73.7	95	27	DO 73.7 %
	63.2	36	11	DO 63.2 %
	57.2	96	44	DO 57.2 %
	55	75	33	DO 55.0 %
	49.5	144	45	DO 49.5 %
Blend	53.3	87	34	Blend
oxHA	11.7	260	121	oxHA

3.4.2 Hydrogel formation

To investigate the influence of oxidation degree on hydrogel formation, different batches with the DOs of 73.7. 57.2, 55.0 and 49.5 % were used. Additionally, batches with similar DOs of 57.2, 55.0 and 49.5 % were combined to a mixed blend and the hydrogels, which were made from the blend and the single batches, were compared at a final content of 3 wt% for their hydrogel formation. Analyses were also performed to investigate the effect of increasing content on the mechanical properties of the hydrogels generated with the blend by using final contents of 2, 3, 4 and 5 wt%.

3.4.2.1 Compression tests for Young's modulus

Right after preparation, the batch with the lowest DO also showed the weakest mechanical properties as indicated by the measured stiffness (2.4 ± 0.04 kPa), whereas the batches with DO 55.0 % (33.2 ± 0.7 kPa) and 57.2 % (40.9 ± 3.9 kPa) showed significantly higher Young's moduli (**Figure 13A**). After 14 days of incubation, the DO 49.5 % hydrogels were already completely swollen and dissolved. The batch with highest investigated DO 73.7 % first showed similar Young's moduli as the hydrogels with DO 49.5 % (2.5 ± 0.7 kPa on day 1), but the stiffness of these hydrogels increased very rapidly compared to the other batches due to significant contraction and finally achieved the highest mechanical strength after 7 d with 222.9 ± 58.3 kPa. The hydrogels of the other batches with DO 55.0 % with 193.3 ± 26.3 kPa and 57.2 % with 191.03 ± 27.46 kPa also achieved their maximum Young's modulus after 7 d. This effect of increasing Young's modulus during long term storage in PBS could be observed for all single batches as well as the mixed blend. After 7 d, almost all hydrogel formulations lost the mechanical strength and became weaker again.

Hydrogels made from the blend in different contents proved that the Young's modulus could be further increased with higher polymer content (**Figure 13B**). Overall, the 2 wt% hydrogels showed 6 times lower Young's modulus than the 5 wt% hydrogels on day seven and even 31 times lower on day one. The 3 wt% hydrogels of the blend appeared at least almost 2 times less stiff compared to the hydrogels of the single batches DO 55.0 % and DO 57.2 % on day one, which can be attributed to the content of lower oxidized HA. At the maximum of mechanical strength on day seven, the 3 wt% blend hydrogels showed with 76.1 ± 8.6 kPa a 2.5 times smaller Young's modulus than the hydrogels made from the batches with DO 55.0 % and 57.2 %. All hydrogels achieved their maximum stiffness at day seven and lost mechanical strength afterwards.

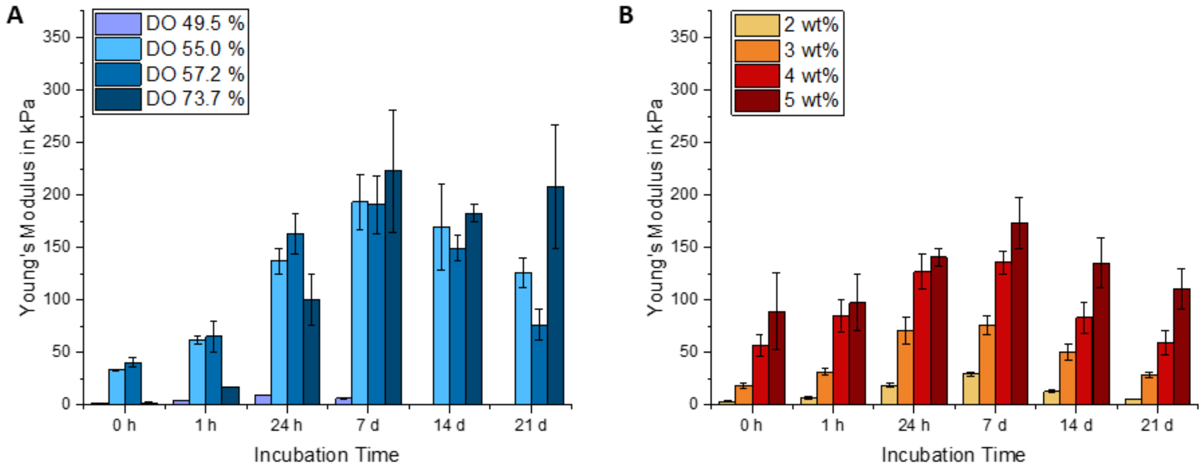

Figure 13: Young's moduli of (**A**) various batches with DO 49.5 %, 55.0 %, 57.2 %, 73.7 % and a polymer content of 3 wt% and of (**B**) the mixed polymer blend (DO 53.3 %).

3.4.2.2 Swelling and degradation behavior

Besides the mechanical properties weight changes of the hydrogels during storage in 1x PBS were also investigated. Here, a shrinkage of all hydrogels based on polymers with a higher DO then 50 % (**Figure 14A**) and 3 wt% polymer content was observed. After 21 d, the hydrogels shrank to about 55.1 ± 0.2 % of their initial weight for DO 55.0 %, 64.0 ± 1.1 % for DO 57.3 % and even to less than the half of the initial weight (39.3 ± 1.4 %) for DO 73.7 %. For the lower oxidation (49.5 %), the hydrogels initially swelled to 143.4 ± 2.6 % of the starting weight, shrank after 1 d to 119.2 ± 0.9 % and swelled afterwards until complete dissolution. The blend hydrogels didn't shrink after 1 h but swelled all over 100 % (**Figure 14B**), the resulting shrinkage then was quite moderate compared to the single batches and stopped between 68.3 ± 2.3 % (5 wt%) and 94.6 ± 1.3 % (4 wt%).

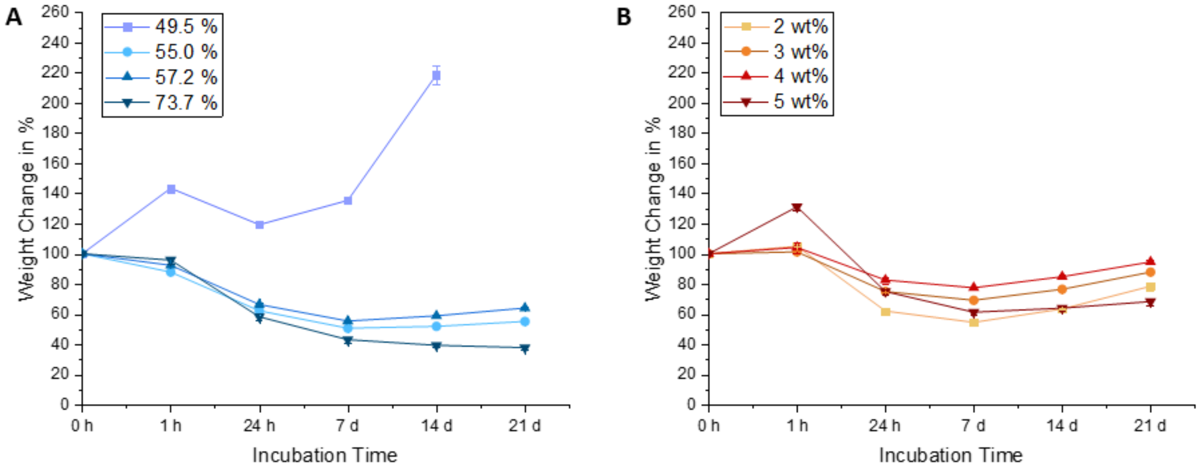

Figure 14: Behavior of hydrogels after storage in 1 ml 1 x PBS: (**A**) various batches with DO 49.5 %, 55.0 %, 57.2 %, 73.7 % with a content of 3 wt%, (**B**) blend (DO 53.3 %) with various contents.

3.4.3 SPR analysis for determination of binding affinity of proxHA

Since chemical modifications of HA can strongly influence its binding properties to the CD44 receptor on cell surfaces [290], their binding to surface immobilized CD44 receptors were studied via SPR measurements. The CD44 binding affinity of following HA derivatives were detected and compared: unmodified HA (HA, M_n = 24 kDa), the $NaIO_4$ oxidized HA (oxHA, M_n = 121 kDa, DO 11.7 %) as well as the primary oxidized HA (proxHA, M_n = 11 kDa, DO 63.2 %) oxidized with the same equivalents of the respective oxidation agents. Despite the fact that proxHA has an almost 6-fold higher DO than oxHA, and a 10 fold lower molecular weight both K_D values were still in a similar range, which can be attributed to the intact backbone structure of the proxHA favoring the interaction with the CD44 receptors and the retention of the polymer on the SPR chip (**Table 5**). However, both the oxidation of the primary alcohol to an aldehyde function and the formation of the dialdehyde seemed to have a major effect on the binding ability compared to the native HA of a comparable molecular weight (**Figure 15**).

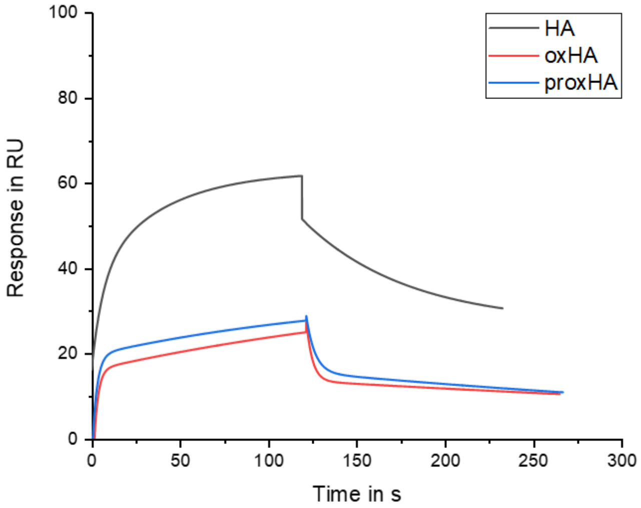

Figure 15: SPR analysis of unmodified HA (black) NaIO4 oxidized (oxHA, red), and TEMPO/TCC oxidized (proxHA, blue) at the highest investigated concentration of 32.7 µM.

Table 5: Values of dissociation constant of unmodified HA, NaIO4 oxidized (oxHA) and TEMPO/TCC oxidized HA (proxHA) with different degrees of oxidation (DO).

Sample	M_w [kDa]	M_n [kDa]	DO [%]	K_D [nM]
HA	61	24	0	533 ± 87
oxHA	260	121	11.7	3546 ± 1052
proxHA	36	11	63.2	3330 ± 911

3.4.4 Cell viability of hMSCs

To evaluate the *in vitro* cytocompatibility of the obtained hydrogels, hMSCs were embedded in hydrogels formed out of the polymer blend to investigate the effect of polymer contents (3, 4 or 5 wt%) on cell survival and differentiation in proliferation medium as well as in chondrogenic differentiation medium for 21 days. Depending on the chosen culture medium there was a quite remarkable difference in hydrogel stability. In proliferation medium the hydrogels with 3 and 4 wt% polymer both dissolved between day 7 and day 21, whereas the 5 wt% blend hydrogels did not disintegrate but became slightly larger during *in vitro* culture. Additional cell-containing hydrogels (3 wt%) based on polymers with a DO of 73.7 % retained their size in cell culture and remained stable even after day 21 (**Figure 16A**). In contrast to that, all hydrogels that were cultured in chondrogenic differentiation medium did not dissolve at all but decreased in size, with 5 wt% hydrogels showing the strongest shrinkage of all studied formulations (**Figure 16B**).

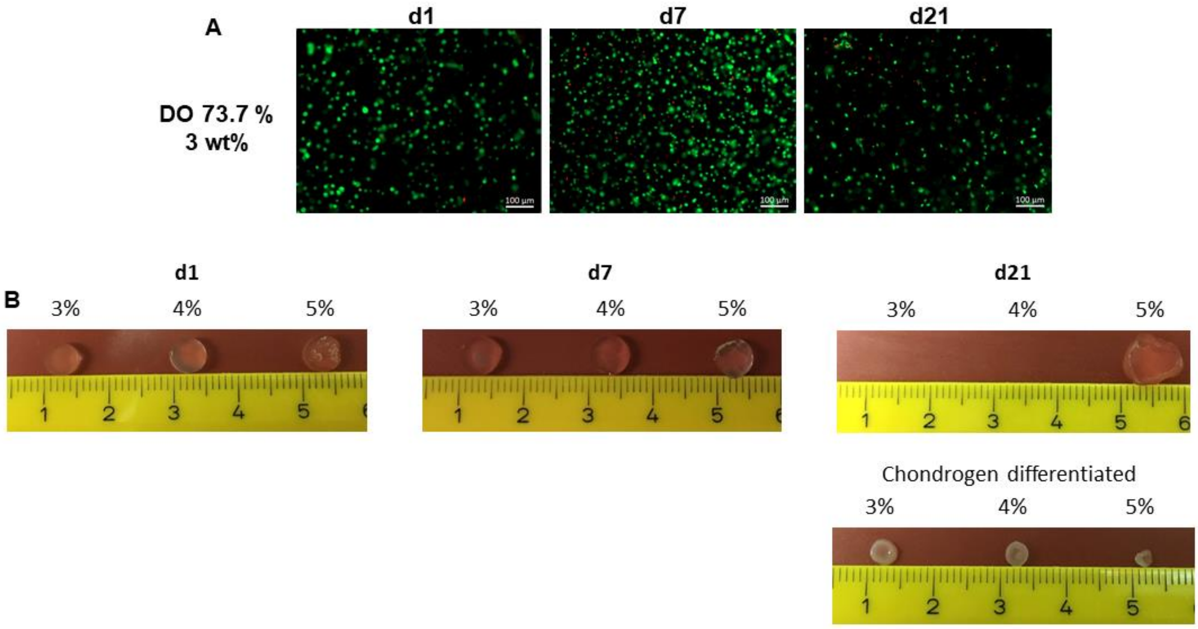

Figure 16: (**A**) Cell viability of in vitro cultured hMSCs in 3 wt% hydrogels (DO 73.7 %) after day 1, 7 and 21, shown by live/dead staining. Viable cells were labeled green with calcein-AM and dead cells with EthD-I. (**B**) Proportion of the hydrogels (3, 4, and 5 wt%) with proliferated cells over 3 weeks in comparison of hydrogels with chondrogenic differentiated cells (3, 4 and 5 wt%).

Live/dead assays were performed for all polymer contents of blend hydrogels and showed excellent biocompatibility (> 85 %) of all investigated hydrogels at day one (**Figure 17A, B**). On day 7, only a slight decrease in cell viability was observed for 3 wt% and 4 wt% hydrogels (77.2 ± 13.5 and 74.8 ± 9.5 %, respectively), whereas significantly less viable cells (61.9 ± 8.3 %) were detected for 5 wt% gels (**Figure 17B**).

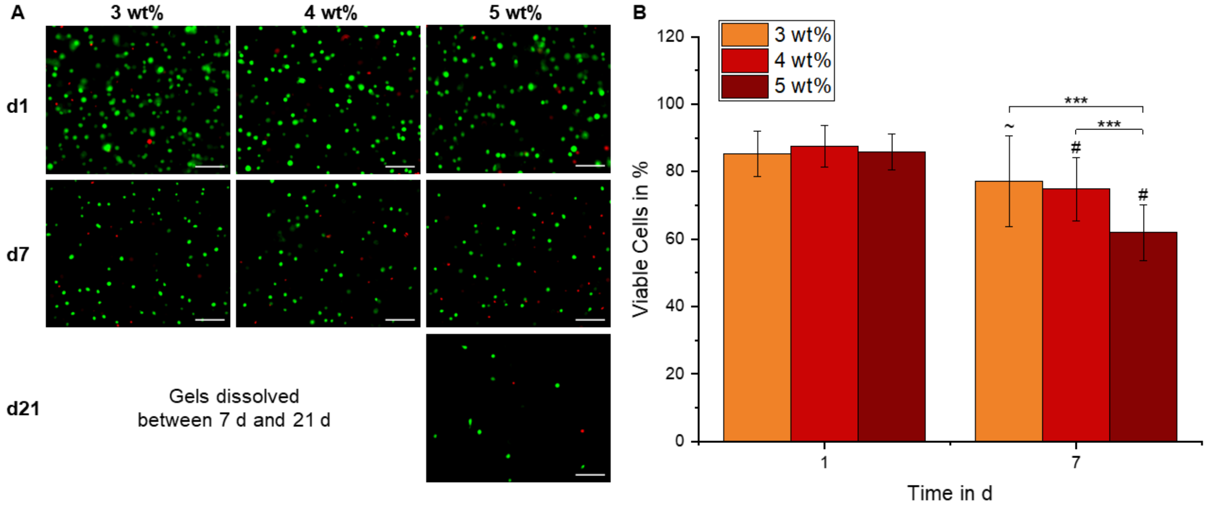

Figure 17: Cell viability in blend hydrogels. (**A**) Cell viability of in vitro cultured hMSCs in 3, 4 and 5 wt% blend hydrogels (DO 53.3 %) after day 1, 7 and 21 in proliferation medium, shown by live/dead staining. Viable cells were labeled green with calcein-AM and dead cells with EthD-I. Scale bars represent 100 µm. (**B**) Quantification of viable cells, after day 1 and 7 of in vitro culture in proliferation medium. Data are presented as means ± standard deviation (n = 3 per condition and time point,

counting at least eight locations each sample). Significant differences between groups at day 7 are marked with *** ($p < 0.001$), labels above bars of groups at day 7 show significant differences compared to day 1, "~" ($p < 0.01$) and "#" ($p < 0.001$).

3.4.5 Chondrogenic differentiation of hMSCs

After culture of hMSCs in chondrogenic differentiation medium, the deposition of cartilaginous extracellular matrix (ECM) within the hydrogels was assessed. Quantitative biochemical analysis of GAG production showed that hMSCs encapsulated in the lowest concentrated hydrogels (3 wt%) produced distinctly higher amounts of GAG/DNA compared to 5 wt% hydrogels (15.9 ± 4.1 µg/µg) (**Figure 18A**). This could also be demonstrated by histological staining with safranin O for GAG and immunohistochemical staining for aggrecan, where the 5 wt% hydrogels exhibited the weakest signals for these cartilage specific ECM molecules (**Figure 18C**). The staining for collagens with picrosirius red and collagen II on the other hand did not show differences in collagen production between the different hydrogel formulations (**Figure 18C**). These findings were furthermore reflected by the determination of the total collagen/DNA ratio, with only slightly, but not significantly lower values for 5 wt% compared to 3 wt% (**Figure 18B**). Altogether the assays confirmed that considerable ECM production during chondrogenic differentiation was achieved in all tested hydrogels and that the lowest concentrated 3 wt% hydrogels showed higher GAG production compared to the highest concentrated hydrogels.

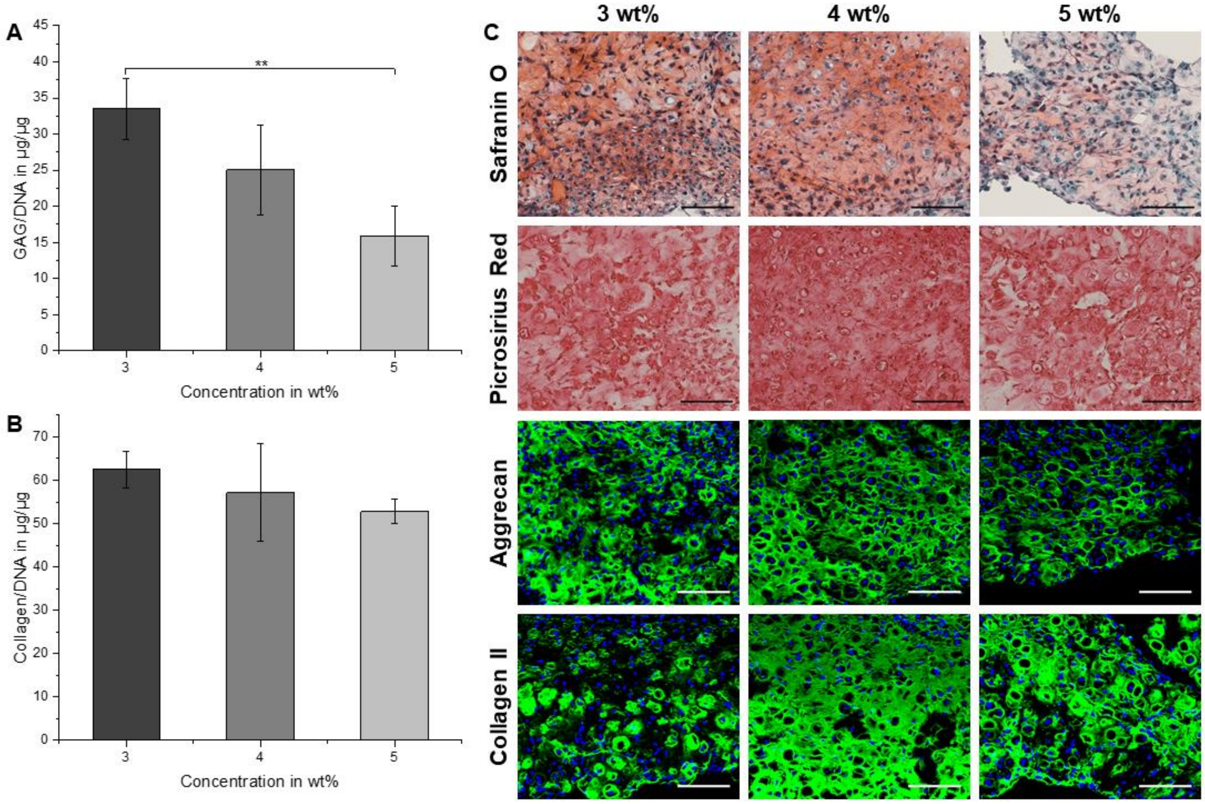

Figure 18: (**A**) GAG and (**B**) total collagen production of in vitro cultured hMSCs in 3, 4 and 5 wt% blend hydrogels (DO 53.3 %) after 21 days of chondrogenic differentiation, normalized to DNA. Data are presented as means ± standard deviation ($n \geq 3$). Significant differences between groups are marked with ** ($p < 0.01$), (**C**) Histological and immunohistochemical staining for deposited ECM components in 3, 4 and 5 wt% blend hydrogels (DO 53.3 %) after 21 days of chondrogenic differentiation. Longitudinal sections were stained for deposition of GAG and collagen with safranin O and picrosirius red, respectively. Immunohistochemical staining for aggrecan (green) and collagen type II (green), nuclei were counterstained with DAPI (blue). Scale bars represent 100 µm

3.5 Discussion

This study established a new synthesis path of a primary oxidized HA for the formation of dynamic chemically crosslinked hydrogels with a high mechanical strength and long-term stability for cell culture. Additionally, the determination method for the aldehyde content of oxidized HA and other comparable biopolymers was optimized. In literature, *tert*-butyl carbazate, a BOC-protected hydrazine, is often used for the quantitative analysis [270], but it is also known that the BOC protection group can already be cleaved under the mild acidic conditions during the modification [298]. Since the reductive amination is performed in acetate buffer with pH 5.2, the use of *tert*-butyl carbazate can deceive the obtained DO. With *tert*-butyl hydrazine, the cleavage of the *tert*-butyl group used for quantification is avoided and stable results are obtained.

During the characterization of proxHA using TBH, it was observed that both higher TCC equivalents of 0.76 and 0.5 led to a similar DO over 70 %. The oxidation of the primary alcohol of HA is performed by TEMPO which is acting as catalyst and needs activation and regeneration by a secondary oxidation reagent. For this, TCC is used both to activate and regenerate TEMPO in a two steps oxidation [288]. Since all three chlorine atoms are active, TCC can function three times as oxidation reagent and finally convert to cyanuric acid with an aromatic ring, which is also the driving force for the reaction [299] (**Scheme 5**). Additionally, the reaction must be performed under strictly anhydrous conditions to avoid subsequent oxidation to carboxylic acid functions [288]. For this reason, 0.5 and 0.76 equivalents TCC should be able to convert nearly all primary alcohol groups of *N*-acetyl-D-glucosamine during the reaction. Still, no complete conversion of all HA dimer units was achieved, wherefore it can be assumed that the oxidation limit is capped at a certain degree of oxidation due to steric effects, since the obtained degrees of oxidations for the higher amounts of TCC were quite similar (**Figure 12A**). Taking the three active chlorine species into account, it was expected to achieve a DO of over 70 % already with 0.25 eq. of TCC, which occurred only once with DO 73.7 % due to excellent reaction conditions. Since HA is a very sensitive and eventually also hygroscopic biomacromolecule, reproducibility of the reactions with HA is often hard to accomplish. Under best conditions, a DO of around 60 % was achieved in average and this is nonetheless 2.4 times higher than the equivalents of added TCC. A similar effect was observed for the reactions with only 0.1 equivalents of TCC, indicating the multiple step oxidation of the secondary oxidation reagent. Compared to the oxidation with $NaIO_4$, at least 3 – 12 times higher DOs were obtained depending on the used equivalents of TCC. Unfortunately, the GPC measurements nevertheless showed a massive degradation of the HA chains also after TEMPO/TCC oxidation. However, it is well-known that degradation of HA chains can occur under oxidative stress (e.g. caused by free radicals) or under non physiological pH-conditions both during chemical reactions as well as in biological systems [156,300-302].

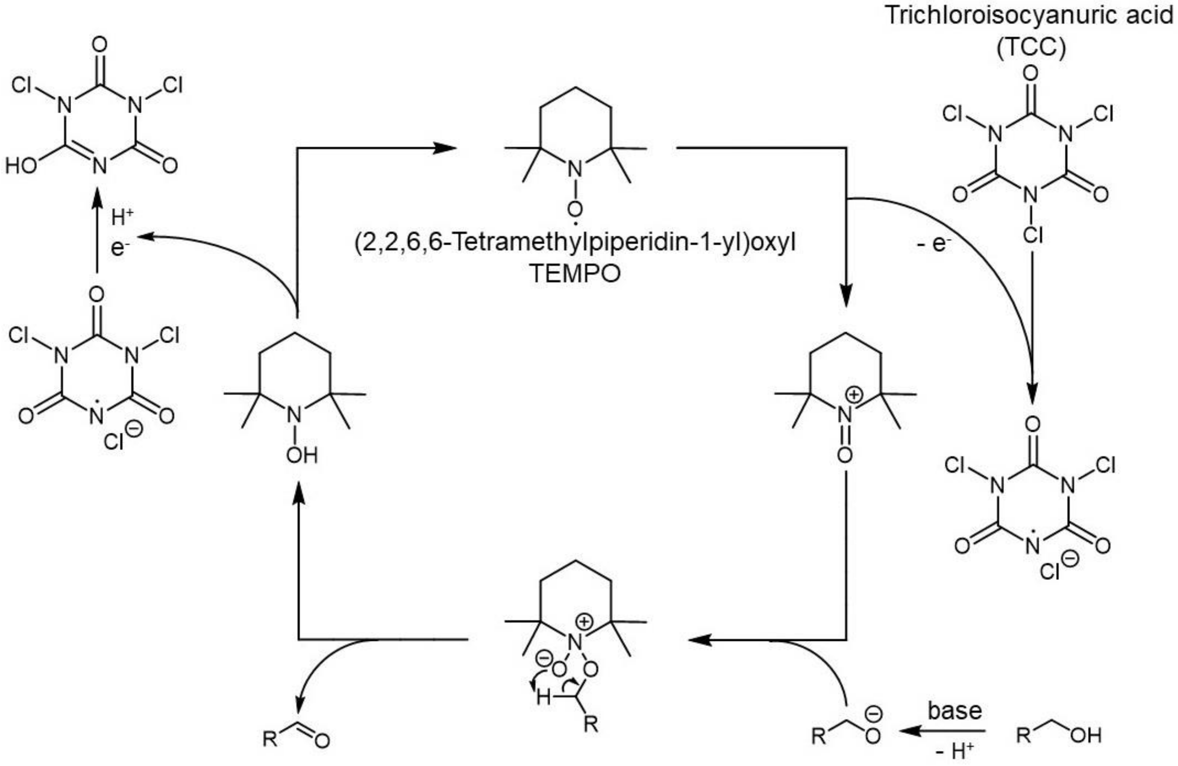
Trichloroisocyanuric acid
(TCC)
(2,2,6,6-Tetramethylpiperidin-1-yl)oxyl
TEMPO
H⁺
e⁻
- e⁻
base
- H⁺
R
OH
O
Cl
N
HO

Scheme 5: Mechanism of oxidation of primary alcohol with TEMPO/TCC.

When using the polymers for the formulation of hydrogel, a very fast gelation with adipic acid dihydrazide appeared within 10 seconds or even faster, especially with higher polymer contents and oxidation degrees. Due to the immediate gelation, the obtained hydrogels were quite stiff and brittle, this is why it can be assumed that these hydrogel systems cannot be used for extrusion-based 3D bioprinting. Since higher DO leads to more crosslinking and consequently higher network density, it is expected that the higher DO also results in higher Young's moduli. Upon incubation in PBS, an increase of the Young's moduli was noticed for almost all hydrogels except the hydrogels with DO 49.5 %, which even dissolved completely between day 14 and 21. One possible explanation for this increase of Young's moduli is the dynamic reversible bond of the Schiff Base chemistry, which can be re-arranged due to the reversibility until the most stable thermodynamic state and consequently highest mechanical stability is reached. Additionally, the occurring shrinkage of the hydrogels after storage in PBS can also be related to this re-arrangement of the network. The higher hydrogel network density caused by syneresis again explains the occurring increase of the mechanical strength at the later timepoints. A similar effect of higher network density can also be achieved by increasing the content of the hydrogel forming polymer solutions, which is demonstrated with the blend hydrogels formed by different polymer contents (**Figure 13B**). Compared to the individual polymer batches the blend hydrogels showed a reduced mechanical strength and rather moderate swelling behavior, which can be attributed to the overall mixed behavior of the differently oxidized polymer batches. Accordingly, the behavior of the hydrogels can be tuned by the oxidation degree of the used polymers. In general, the formed hydrogels with an average oxidation degree above 50 % proved to be stable for extended time even without cells (over 3 weeks), which was never achieved with hydrogels based on $NaIO_4$ oxidized HA and the low molecular weight crosslinker ADH [84]. When compared with other HA hydrogels crosslinked only via reversible Schiff Base, e.g. the hydrazine modified HA crosslinked with $NaIO_4$ oxidized HA [67], our proxHA hydrogels are also mechanically much stiffer. It can be presumed that this is mainly induced by the high degree of oxidation and eventually also the preservation of the HA backbone structure.

Since only the primary alcohol of HA is modified without changing the backbone structure excessively, it was interesting to investigate the receptor binding affinity of this HA derivative in comparison to the commonly performed HA oxidation using periodate. Bhattacharya *et al.* summarized the interactions between the functional groups of HA and the CD44 receptor, showing that hydrogen bonds between the charged glucuronic acid and the amino acids predominate the hydrogen bonds and hydrophobic interaction of the *N*-acetylglucose-amine [151,290]. Oxidation with $NaIO_4$ obviously leads to an opening of saccharide rings, which causes an extreme interference with the retention of HA backbone structure. It can be assumed that this interference by ring opening and oxidation has a much higher influence on the CD44 receptor binding properties of HA than the oxidation of the primary alcohol group to an aldehyde function. However, both binding affinities of the differently oxidized HA derivatives were significantly lower than the native HA, which demonstrates the specificity of CD44 for the preserved structure of HA. Even though $NaIO_4$ oxidized HA only had an almost 6-fold lower DO and a 10-fold higher molecular weight than proxHA, the K_D values of both oxidized HA were in a similar range. This demonstrates that even with preservation of the backbone the high DO negatively affects the binding affinity of the HA derivative (**Table 5**). However, given the fact that the CD44 receptor needs at least four intact HA repeating units for binding [278], which is achievable by oxHA with an DO of 11.7 % (every 10th repeating unit is oxidized), it is impossible to find as much unchanged repeating units in the proxHA, where six out of ten repeating units are already oxidized. Accordingly, it can be supposed that the $NaIO_4$ oxidation massively destroys the backbone structure and thereby interferes with the receptor interaction leading to the weak binding affinity even with lower oxidation degree. The exchange of the primary alcohol to an aldehyde function accordingly seems to have a minor effect on binding ability (**Figure 15**) in this study.

Further striking differences were observed during the *in vitro* cell culture in the formed hydrogels. Here, it was observed that the hydrogels formed out of 3 and 4 wt% polymer dissolved completely during *in vitro* culture in proliferation medium, which was most likely caused by the reversible dynamic Schiff Base system where the formed hydrazones undergo hydrolysis [220]. Additionally, the dissolution of the hydrogels was possibly enhanced by the presence of amino acids in cell culture medium, which can obviously replace ADH as a bifunctional crosslinker. In strong contrast, all hydrogels which underwent differentiation retained their stability in cell culture, which can be attributed to the newly formed ECM by the hMSCs, which was most likely integrated in the reversible hydrogel network. Nevertheless, a higher DO could still be employed to improve stability due to more crosslinking possibilities for ADH and thereby allow longer culture also for non-differentiated cells (**Figure 16A**). In general, all hMSCs (non-differentiated and differentiated) within the hydrogels initially showed an excellent cell viability with over 85 % after encapsulation. The viability of cells decreased after 7 days, especially for the higher polymer containing 5 wt% hydrogels (**Figure 17B**), which was also observed in other HA-based hydrogels and could probably be caused by limitations of nutrient and waste diffusion due to the denser polymer network [303-305].

Furthermore, the deposition of GAG and collagen throughout the hydrogel matrix proved the formation of cartilage specific ECM [306]. The significant reduction of the GAG to DNA ratio in 5 wt% hydrogels when compared to lower concentrated hydrogels, i.e. 3 wt% (**Figure 18A**), is in line with reports for other HA hydrogels which showed that higher polymer content can reduce GAG production of encapsulated cells [307-309]. Besides that, the total collagen content did not indicate significant differences between the different contents (**Figure 18B**). The considerable shrinkage of hydrogels cultured under chondrogenic conditions after 21 days (**Figure 16A**), especially for high concentrated gels with less ECM production, could also be explained with the dynamic bonds of the Schiff Base chemistry, which allow a steady replacement of the ADH crosslinker by the ECM produced by the cells and thereby a further contraction or condensation of the hydrogel. Here, the reversible Schiff Base chemistry also enables a continuous remodeling of the hydrogels without any necessary cleavable crosslinkers. Additional histological and IHC staining accordingly showed an aggregation of cells and homogeneous distribution of cartilaginous matrix components such as GAG, aggrecan and collagen II, especially throughout the lower concentrated hydrogels providing more space for the formed ECM components (**Figure 18C**). The deposition of cellular ECM in these reversibly crosslinked hydrogels appears more even, when compared to other HA hydrogel systems [253,307,308]. Taken together, the here presented hydrogel system based on highly oxidized hyaluronic acid seems to be well suited for the culture of ECM forming cells, especially hMSCs undergoing chondrogenesis in this pilot experiment.

3.6 Conclusion

In this work, a novel synthesis path was developed for a new hyaluronic acid (HA) based material which can be used for the *in situ* formation of biocompatible hydrogels. The study demonstrated that the degree of oxidation by the TEMPO/TCC oxidation can be further increased by using anhydrous DMF as solvent to avoid overoxidation of the primary alcohol group to carboxylic acid functions. With the higher DO, it was able to generate long-term and mechanical stable hydrogels without the need for secondary crosslinking, even in cell culture medium. By using the reversible Schiff Base crosslinking, UV exposure in cell culture was avoided and good cell viability was achieved. The formed hydrogels were successfully applied for the chondrogenic differentiation of hMSC, where the newly formed ECM was essential to retain the hydrogel structure during the long-term culture. Due to the very fast gelation and high mechanical stiffness, this still reversible hydrogel is not immediately suitable for extrusion 3D printing, where a gelation on a longer time scale would be desired. Nevertheless, casting of this fast crosslinking hydrogel in more complex prefabricated shapes could be applied to encapsulate cells also in different geometries. Additionally, this system may be used for the formation of microgels using microfluidic two component mixers with the encapsulation of cells.

Chapter 4

PENTENOIC ACID MODIFIED GELATIN FOR APPLICATION AS BIOINK WITH LIGHT CONTROLLABLE MECHANICS

Parts of this chapter are intended to be published in the future (Junwen Shan, Hannes Horder, Nadine Grummel, Michael Bartolf-Kopp, Ilona Paulus, Khoon Lim, Tim Woodfield, Ben Fabry, Torsten Blunk, Jörg Teßmar, Jürgen Groll, Pentenoic Acid Modified Gelatin for Application as Bioink with Light Controllable Mechanics).

The content of this article is based on the work of the author of this thesis Junwen Shan, who performed all chemical and material scientifical experiments, printing experiments, data evaluation and composition on the chemical and material scientifical parts of the manuscript.

Chapter 4

The author contribution in the original research article was as followed:

Contributor	Contribution
Junwen Shan	Designed the research; performed the chemical and material scientific part of the research; analyzed all chemical and material scientific data and all statistics; wrote the manuscript
Hannes Horder	Designed and performed part of the biological research; performed biological and morphological experiments; provided feedback on manuscript; wrote biological materials and methods part of the manuscript
Nadine Grummel	Designed and performed part of the biological research; performed cell migration tracking experiments; wrote materials and methods (cell migration) of the manuscript
Michael Bartolf-Kopp	Supported G-code design
Ilona Paulus	Provided feedback on manuscript
Khoon Lim	Provided feedback on manuscript
Tim Woodfield	Provided feedback on manuscript
Ben Fabry	Designed research; provided feedback on manuscript
Torsten Blunk	Designed research; provided feedback on manuscript
Jörg Teßmar	Designed research; provided feedback on manuscript
Jürgen Groll	Designed research; provided feedback on manuscript

4.1 Abstract

3D printing of hydrogels as bioinks has gained attention in recent decades. Inherent in this, gelatin hydrogels which have been used for drug delivery systems or injectable hydrogels, have found application as bioinks as well. Well-known gelatin-based hydrogel systems are methacryloyl gelatin (GelMA) and allyl glycidyl ether substituted gelatin (GelAGE). Both systems are crosslinked in a photoinitiated polymerization or thiol-ene reaction via UV light and have been investigated in their application as bioinks. In this study, pentanoate functionalized gelatin (GelPA) hydrogels are established as a potential bioink with light tunable mechanical properties, using thiol-ene reaction with thiolated 4-arm polyethylene glycol (sPEG) and the visible light initiator system tris(2,2-bipyridyl)dichloro-ruthenium(II) hexahydrate (Ru) and sodium persulfate (SPS). For synthesis of GelPA, a selective reaction to substitute the amines of gelatin with ene-functions using *N*-hydroxysuccinimide (NHS) ester of pentenoic acid under mild conditions was provided to preserve thermo responsive properties of the material.

4.2 Introduction

In recent years, biofabrication of biopolymer-based hydrogels has experienced a very fast development, especially as bioinks in the field of 3D printing [192,310,311]. During printing process, the biomaterial must provide proper viscosity, shape fidelity after printing and cell friendly environment to serve as a cell delivery medium [14,312]. Viscosity and mechanical stability of a biomaterial-based hydrogel is strongly depending on the chain length of the used biopolymer [313,314]. Mechanical and viscous properties decrease with decreasing molecular weight. To enhance mechanical stability, higher polymer concentrations must be used especially when the biopolymers have lower molecular weights [315]. However, it is known that high polymer concentrations are not beneficial for cell viability [316,317]. Thus, it is desirable to use low concentrated hydrogels to obtain good cell viability. For 3D printing, the challenge here is to simultaneously preserve proper material properties such as convenient viscosity and form stability after printing.

Therefore, gelatin is a promising material for the application as bioink. As a water-soluble proteinaceous biopolymer, it contains Arg-Gly-Asp (RGD) sequence which modulates cell adhesion [181,251] and is less antigenic than collagen since its denatured [181,187]. Due to its thermo responsive behavior, the triple helical state of gelatin chains converts into disordered coils in aqueous solution above the helix melting point around 32 °C [318]. But for cell culture, which is normally performed at 37 °C, this property is not accessible and must be avoided by chemical crosslinking. Still, the thermal response can be used to achieve the desired viscosity for 3D printing and the mechanical stability can be accomplished by subsequent crosslinking after the printing process. Therefore, a commonly used and 3D printed gelatin hydrogel is methacroyl gelatin (GelMA) [136,319]. The crosslinking is performed via photoinitiated chain growth polymerization under UV light exposure with Irgacure 2959 (I2959) as initiator and no additional crosslinker. Bertassoni *et al.* investigated the printable concentrations of GelMA and reported printability in a range between 7 and 15 % [320]. Another printable gelatin based hydrogel system is allyl glycidyl ether functionalized gelatin (GelAGE) using thiol-ene chemistry as crosslinking mechanism, where a thiol functionalization is coupled with a double bond (“ene”) via light-mediated radical reaction [238]. Therefore, Bertlein *et al*. modified gelatin with allyl glycidyl ether (GelAGE) under harsh conditions of pH between 8 – 13 and a temperature of 65 °C, despite the fact that gelatin is heavily degraded by pH and temperature increase [267]. This synthesis conditions resulted in massive degradation of gelatin chains, but still led to feasible 3D printing at low temperatures between 4-10 °C and very high polymer concentrations up to 30 wt%. Since it is known that UV irradiation can damage cell DNA [284], they used a visible-light photo initiating system based on tris(2,2-bipyridyl)dichloro-ruthenium(II) hexahydrate (Ru) and sodium persulfate (SPS) and compared it with I2959. An alternative gelatin based hydrogel system which is not investigated precisely yet was developed by Russo *et al.* using thiol-ene chemistry. Therefore, they modified gelatin with pentenoic anhydride and *γ*-thiobutyrolactone [259]. Anhydride species can react with alcohol and amines when they are turned into nucleophils by deprotonation [321]. Thus, it is unclear whether penteonic anhydride reacts with alcohol groups, such as serine (Ser) or hydroxylysine (Hyl), and amine group of lysine (Lys) in gelatin simultaneously. To achieve selectivity, *N*-hydroxysuccinimide esters (NHS-ester) of acids are known to be attacked by amines particularly, even in presence of alcohols [322,323]. The synthesis of NHS-ester of acids is normally performed via 1-ethyl-3-(3-dimethylaminopropyl)carbodiimide (EDC) chemistry [324] by activating the acid functionalization (**Scheme 6**, top). Additionally, it is desirable to use milder conditions than for GelAGE synthesis (**Scheme 6**, bottom) to prevent chain degradation of gelatin to preserve this biopolymer in its structure as far as possible. Still, the substitution reaction needs amine groups to react as nucleophils [325,326] and therefore slightly alkaline conditions necessary to deprotonate amines.

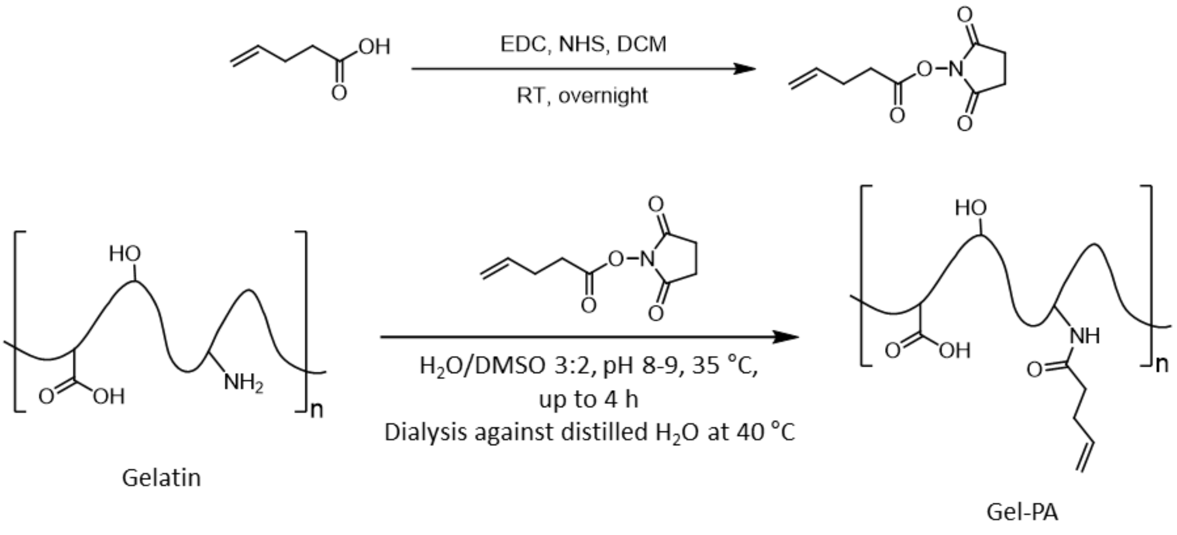

Scheme 6: Synthesis of NHS-pentenoic acid ester (top) and GelPA (bottom).

Chapter 4

This study contains a novel synthesis path of pentenoate functionalized gelatin and the influences of reaction time and amount of substitution reagent on the degree of substitution. Additionally, hydrogels formed with GelPA and thiolated 4-arm-star-PEG with a molecular weight of 5 kDa as crosslinker via thiol-ene reaction are investigated on their properties in mechanical strength and swelling behavior. The biological part with human breast cancer cell line MDA-MB-231 is not shown in this thesis.

4.3 Materials and methods

4.3.1 Materials and reagents

Gelatin, pentenoic acid (PA), dimethylsulfoxide (DMSO), gelatin (gel strength 300, Type A), magnesium sulfate ($MgSO_4$), sodium nitrate ($NaNO_3$), sodium persulfate, tris(2,2′-bipyridyl)-dichlororuthenium(II) hexahydrate were purchased from Sigma Aldrich, St. Louis, USA. 1-ethyl-3-(3-dimethylaminopropyl)carbodiimide (EDC), *N*-hydroxysuccinimide (NHS) were obtained from Carbosynth Limited, Berkshire, UK. Sodium azide (NaN_3) was purchased from Merck KGaA, Darmstadt, Germany. Dichloromethane was obtained from Fisher Scientific, Schwerte, Germany. 4-Arm-star-PEG Thiol (5 kDa, sPEG) was obtained from JenKem Technology USA, Plano, TX, USA.

The used materials for gel electrophoresis were purchased from Bio-Rad, Munich, Germany, if not declared otherwise. Urea was purchased from Merck, Darmstadt, Germany. Sodium dodecyl sulfate (SDS), Ampholine pH 2-11 were obtained from SERVA Electrophoresis GmbH, Heidelberg, Germany. Nonidet® P40 was purchased from AppliChem GmbH, Darmstadt, Germany.

4.3.2 Synthesis of pentenoic N-hydroxysuccinimide ester (PA-NHS)

EDC (23.0 g, 120.0 mmol, 1.2 eq.) was dissolved in 150 ml DCM. NHS (18.4 g, 160.0 mmol, 1.6 eq.) was added and the mixture was diluted with another 150 mL of DCM. Then, pentenoic acid (10.2 mL, 100.0 mmol) was added, the round bottom flask was flushed with inert gas and the reaction was stirred over night at room temperature (RT). The solvent was removed under vacuum and the residue was dissolved in 150 mL diethyl ether and the organic phase was washed with 80 mL H_2O for six times. The organic phase was dried with $MgSO_4$ and the solvent was removed under vacuum. The product was obtained as a beige solid (yield). Nuclear magnetic resonance spectroscopy was used to confirm successful synthesis. ^{1}H-NMR (300 MHz, $CDCl_3$): δ [ppm] = 5.91-5.78 (m, 1H, -CH_2-C*H*=CH_2); 5.16-5.06 (m, 2H, -CH_2-CH=CH_2); 2.83 (s, 4H, *H*-NHS); 2.73 (t, ^3J = 7.35 2H, NHS-CH_2-CH_2-); 2.52-4.45 (dd, 2H, ^2J = 13.94 Hz, ^3J = 7.32 Hz, NHS-CH_2-CH_2-)).

4.3.3 Synthesis of pentenoyl modified gelatin (GelPA)

Gelatin (1 g) was dissolved in water (10 %, *w*/*v*) at 40 °C for 2 h. Afterwards, pH is adjusted to 8-9 with 0.1 mol/L NaOH. Then, PA-NHS (0.1 g (0.51 mmol) 0.25 g (1.27 mmol), 0.5 g (2.54 mmol), 1 g (5.07 mmol) or 2 g (10.14 mmol) per gram gelatin) was dissolved in DMSO to achieve a final H_2O:DMSO ratio of 3:2 and added to the gelatin solution. The reaction was stirred for 2 h at 40 °C, dialyzed (MWCO 1 kDa) against distilled H_2O at 40 °C for 3 days. After freeze drying, Gel-PA was obtained as a white solid foam. NMR (NMR Fourier 300, Bruker Corporation, Billerica, MA, USA) was measured at 40 °C to hold the NMR sample liquid. ^{1}H-NMR (300 MHz, D_2O, 40 °C): δ [ppm] = 7.52-7.45 (m, 5H, Phenyl protons of gelatin); 6.07-5.99 (m, 1H, $-CH_2-C\mathit{H}=CH_2$); 5.29-5.20 (m, 2H, $-CH_2-CH=C\mathit{H}_2$); 4.59-1.11 (gelatin backbone and remaining protons from PA). Degree of substitution (DS) was determined as mmol of PA per gram of gelatin. Therefore, the proton integral of the double bond in PA was compared to the phenylalanine (Phe) signals in gelatin. The molecular weight (M) of Phe is the M of the amino acid minus M of H_2O, since Phe is bonded in gelatin:

$$M_{Phe\ in\ gelatin} = 165.19\frac{g}{mol} - 18.01\frac{g}{mol} = 147.18\frac{g}{mol} \quad \text{(equation 6).}$$

Due to Gelatin Handbook from Gelatin Manufacturers Institute of America [327], 1 g gelatin contains 21 mg (m) Phe. Thus, the amount of substance of Phe in 1 g gelatin is:

$$n_{Phe\ in\ gelatin} = \frac{m_{Phe\ in\ gelatin}}{M_{Phe\ in\ gelatin}} = \frac{0.021\frac{g}{mol}}{147.17\frac{g}{mol}} = 0.143\ mmol \quad \text{(equation 7).}$$

From ^{1}H-NMR, the integral of 1 Phe ring (5H) is compared to the integral of the single proton of the double bond (DB), which is representative for the number of PA substituted to gelatin compared to Phe. The DS's (mmol/g_{gelatin}) were calculated as follows:

$$n_{PA\ in\ gelatin} = n_{Phe\ in\ gelatin} \cdot \int Proton\ of\ DB$$

$$= 0.143\ mmol \cdot \int Proton\ of\ DB \quad \text{(equation 8)}$$

4.3.4 Kinetic studies

Kinetic studies were performed with the synthesis of GelPA described as above. After every 15 min 250 µL were withdrawn for dialysis at 40 °C. This procedure was repeated up to 4 h. The samples were freeze dried and characterized by ^{1}H-NMR and GPC.

4.3.5 Gel permeation chromatography (GPC)

Mass average molar mass M_w of gelatin and GelPA was determined by using a GPC system from Malvern (Herrenberg, Germany). The system consisted of a Viscotek GPCmax (in-line degasser, 2-piston-pump and autosampler), a column oven (35 °C), refractive index (RI) detector (Viscotek VE3580) and Viscotek A-columns (A2000/3000, length = 300 mm, width = 8 mm, porous poly(methyl methacrylate), particle size 13 µm). An aqueous solution of Millipore water with 8.5 g/L $NaNO_3$ and 0.2 g/L NaN_3 was used as eluent and solvent. The samples were dissolved with a concentration of 3.0 mg/mL overnight at RT and filtered with a 0.45 µm regenerated cellulose membrane. The measurements were performed with 100 µl of injected volume with an elution rate of 0.7 mL/min. The molecular weights of the gelatin and GelPA were calculated using conventional calibration with PEG standards.

4.3.6 2D gel electrophoresis

4.3.6.1 Isoelectric focusing dimension

Isoelectric focusing (IEF) was performed via nonequilibrium pH gel electrophoresis (NEPHGE) according to Gravel with modifications [328]. For NEPHGE, stock solutions were prepared as shown in **Table 6**.

Table 6: Contents for the stock solutions used for 2D gel electrophoresis.

Solution No.	Content
i	9.5 mol/L Urea 0.5 (*w*/*v*) SDS 5 % (*v*/*v*) β-mercaptoethanol 2 % (*w*/*v*) Ampholine pH 2-11
ii	9.5 mol/L Urea 5 wt% Nonidet® P40 5 % (*v*/*v*) β-mercaptoethanol 2 % (*w*/*v*) Ampholine pH 2-11
iii	6 mol/L Urea 2 % (*w*/*v*) Ampholine pH 2-11
iv	30 % acrylamide/bis solution
v	10 % (*v*/*v*) Nonidet P40
vi	anodic buffer with 10 mM H_3PO_4
vii	cathodic buffer with 20 mM NaOH

Glass capillary (length = 12 cm, Ø = 3 mm) tubes were silanized before use. For the gel precursor solution 5.5 g urea, 2 mL of **v**, 2 mL of ddH_2O and 1.33 mL of **iv** were mixed to a homogeneous solution under heating. Afterwards, 0.5 mL ampholine, 30 µL APS and 20 µL TEMED were added. The gel solution was filled into the silanized glass capillary tubes, which were capped with parafilm at one end, to a height of 11 cm and covered with ddH_2O until gelation. Gelatin, GelPA and cytochrom C were dissolved in 250 µL **i** at 37 °C and after dissolution 250 µL of **ii** was added to achieve a final concentration of 0.6 mg/µL for gelatin and GelPA and 1.2 mg/µL for cytochrome C as reference. After gelation of the precursor solutions in the tubes, parafilm was replaced by a thin mesh and the tubes were transferred into the tube holder of the tube cell model of the electrophoresis device. Empty slots of the holder were sealed with plugs. Every sample (20 µL) was pipetted into the remaining 1 cm of one tube each and covered thoroughly with **iii** (20 µL) and then H_3PO_4 solutions (**vi**) to the upper edge of the tube. The top chamber was completely filled with H_3PO_4 and the lower chamber was filled with NaOH solution (**vii**) until the tubes were soaked within the solution for around 2 cm. The top chamber was connected to the anode, whereas the lower chamber was connected to the cathode. Electrical conditions were 200 V for 15 min, 300 V for 30 min and 400 V afterwards until the cytochrome C reached the end of the tube. After IEF, the gels were forced out thoroughly from the glass tubes with a water filled syringe and stored at -20 °C until use for the SDS-PAGE. The reference gel with cytochrome C was cut into 0.5 mm pieces which were stored in ddH_2O at 4 °C over night for pH determination on the next day.

4.3.6.2 Second dimension electrophoresis using SDS-PAGE

A 12 % polyacrylamid gel using the standard protocol of Bio-Rad Laboratories was prepared for the second dimension electrophoresis. After transfer of the gel precursor solution into the chamber, the solution was covered with ddH_2O until gelation. The ddH_2O was removed and the collection gel was filled up to the frame of the chamber. Afterwards, the stored IEF gel was laid on top of the SDS-PAGE, sealed with 1 % agarose, whereas two tiny agarose gels loaded with Precisions Plus Protein^{TM} Western C^{TM} Blotting Standards were placed to the ends of the IEF gel. The SDS-PAGE was performed over night with 30 mA and stained with Coomassie® Brilliant Blue (SERVA and Electrophoresis GmbH).

4.3.7 Hydrogel formation

For hydrogel formation, GelPA and sPEG were dissolved in PBS at 37 °C for at least 2 h with final polymer concentrations of 3, 5 and 7 wt%. Molar ratios of 1:1, 2:1 and 3:1 were set as thiol:ene ratios. Stock solutions of Ru (10 mM) and SPS (100 mM) were used to achieve a final concentration of 0.1/1 mM of Ru/SPS in the hydrogel. The precursor solution was transferred into relevant transparent PDMS silicon molds and exposed to visible light (JOBMATE, 220-240 V, 50 Hz, 20 W LED, Steelfort, Palmerston North, New Zealand) for 30 and 60 s.

4.3.8 Mechanical testing

For mechanical testing, the hydrogel precursor solution was transferred into transparent PDMS molds with 4 mm height and diameter. All hydrogels were exposed to light for 30 s and 60 s. The linear compression testing was performed with a mechanical test instrument (ElectroForce 5500, TA Instruments, Eden Prairie, MN, USA) using a load cell of 250 g directly after preparation, 1 h, 24 h, 7 d, 14 d and 21 d. Before each measurement, height and diameter of each specimen were measured with a sliding calliper. The Young's modulus was calculated as described in chapter *3.3.9*. The strain γ was calculated by dividing displacement (disp) of the measurement by the height h_0 as shown equation 3. True stress was calculated as described in equation 4. The Young's modulus was received by plotting strain against true stress and applied by using linear fit to the strain-true stress curve. The slope was used for determination of the Young's modulus.

4.3.9 Wet weight change

For observation of the behaviour of the hydrogels after storage in 1 mL PBS, the hydrogels were taken out of the solution after 1 h, 24 h, 7 d, 14 d and 21 d, wiped dry, weighed, and compared to hydrogels after crosslinking. The hydrogels were covered with fresh PBS after each weighing. The ratio of the weight of stored hydrogels (w_s) and weight of non-stored hydrogels (w) were calculated with equation 5 as described in chapter *3.3.10*.

4.3.10 Rheological analysis

Rheological measurements were performed with a rheometer from Anton Paar (plate plate setting). The precursor solutions containing GelPA/sPEG (5 and 7 wt%, with all thiol:ene ratios) without initiator system were investigated on their thermo responsible properties. First, the samples were allowed to stabilize at 37 °C for 15 min. Then, amplitude sweep with strain from γ = 0.001 - 100 %, an angular frequency of ω = 10 rad/s run at 37 °C. Afterwards, the sample was allowed to stabilize again at 37 °C for 5 min, followed by a frequency sweep (γ = 0.1 %, ω = 100 bis 0.1 rad/s) at 37 °C. The temperature sweep was performed after the frequency sweep with γ = 0.1 %, ω = 10 rad/s and a cooling rate of 2 °C/min from 37 to 4 °C. The sample was allowed to stabilize at 4 °C for 5 min. Amplitude, stabilization and frequency sweep were repeated at 4 °C and temperature sweep was then performed with same adjustments as before from 4 to 37 °C.

4.3.11 3D (bio)printing

The 3D printed constructs were fabricated using a 3D Discovery robotic dispensing system (RegenHU, Villaz-St-Pierre, Switzerland). A PH2 print head (pneumatic driven print head, DD135N) was tempered to 21 °C or 12 °C to print the GelPA hydrogel precursor solution with a needle diameter of 0.33 µm (Nordson EFD, East Providence, Rhode Island, USA). The collector plate was cooled to 10 °C. The precursor solutions with thiol:ene ratio 1:1 were prepared as described above and transferred into 5 ml syringe barrel and cooled in the dark for 15 (3 %), 7 (5 %) and 5 min (7 %) at 4 °C. The constructs were printed in 4 layers and exposed to visible light (JOBMATE, 220-240 V, 50 Hz, 20 W LED, Steelfort, Palmerston North, New Zealand) for 60 s.

For 3D bioprinting, GelPA was weighed in a small glass vessel and sPEG in a 2 mL Eppendorf cup and the components were exposed to 254 nm UV light for at least 20 min for sterilization. Afterwards, GelPA was transferred into the 2 mL Eppendorf cup with sPEG and the polymers were dissolved in sterile PBS for at least 2 h and not longer than 4 h at 37 °C with 1000 rpm in the dark. The initiator solutions were filtered through a 0.2 µm membrane and kept at 4 °C in the dark until use. The MDA cells were suspended in the polymer solution with a concentration of 40k and 200k cells per mL by pipetting. Afterwards, the initiator solutions were added and the cell suspension thoroughly mixed. The printing was performed as describe above under sterile conditions. The printed constructs were cultivated in well plates with medium change on each second day.

4.3.12 Statistical Analysis

If not stated otherwise, mean and standard deviation and error of the mean (SEM) were calculated for Young's Modulus, migration speed and invasion distance using OriginPro 2018b. Statistical testing was done with Sigma Plot 12.5 by using two-way analysis of variance (ANOVA) followed by Tukey's post hoc test. Differences between mean values are considered statistically significant at $p \leq 0.05$ (*), $p \leq 0.01$ (**) and $p \leq 0.001$ (***).

4.4. Results

4.4.1 Synthesis of PA-NHS and GelPA

The successful synthesis of PA-NHS and GelPA was approved by NMR spectroscopy (**Figure 19A**) with the signals of the double bond from 6.084-5.206 ppm. For the kinetic study, control of the DS and the M_w after each 15 min for 4 h was performed in total. It could be shown that gelatin does not degrade massively at 40 °C for over 4 h (**Figure 19B**) and that the mild reaction conditions with 40 °C and pH between 8-9 prevent chain degradation of gelatin. The substitution is already finished after 15 min. The DS was about 0.36 mmol per gram gelatin and did not change much after 4 h (**Figure 19C**).

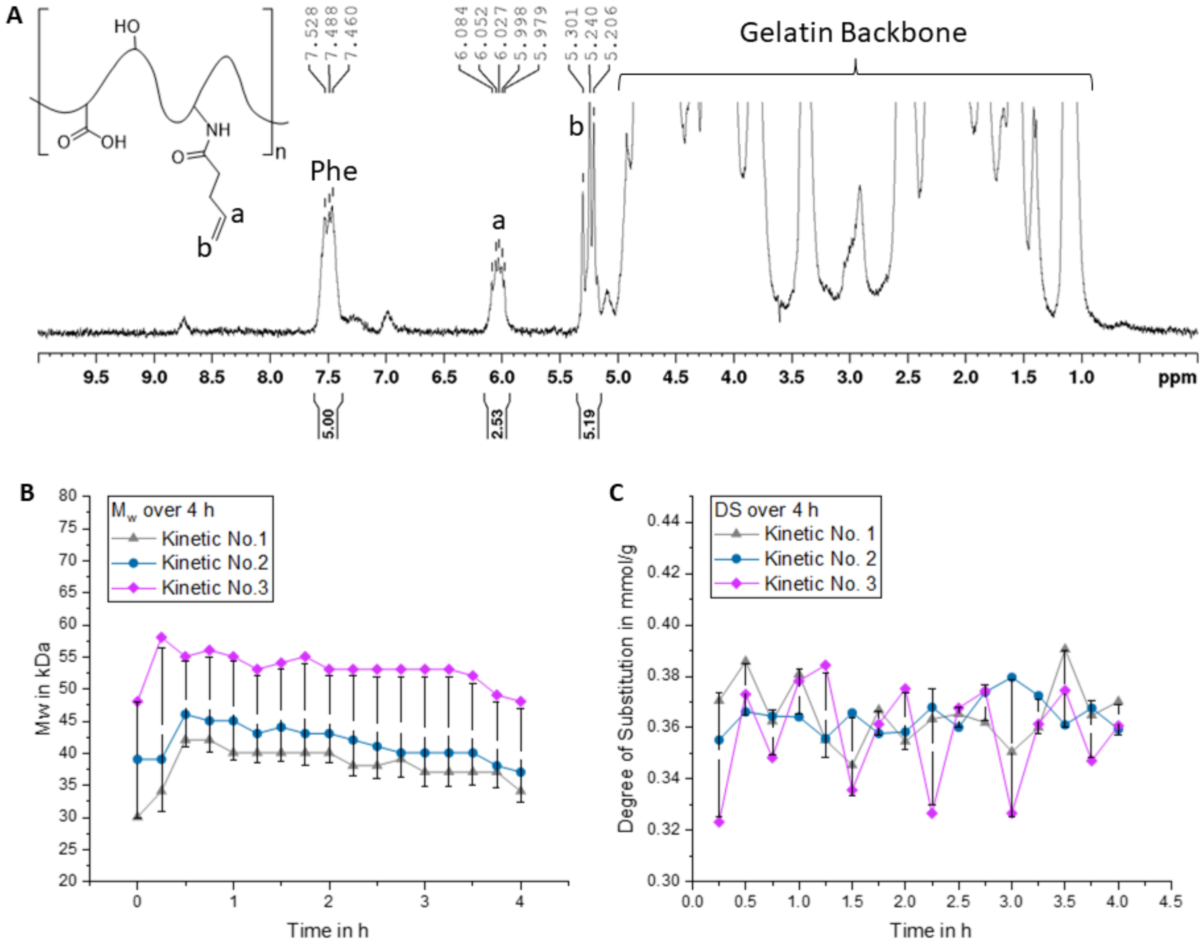

Figure 19: (**A**) NMR spectrum of GelPA with double bond signals between 6.084 and 5.206 ppm; (**B**) change of mass average molar mass Mw of GelPA over 4 h; (**C**) change of degree of substitution (DS) over 4 h.

The influence of different amounts of PA-NHS on the DS used for the reaction was also investigated. Therefore, different amounts of PA-NHS per gram gelatin (**Table 7**) were used.

A slight decrease of DS was observed with the lowest amount of PA-NHS (**Figure 20A**), whereas the DS did not increase with higher amount of substitution reagent.

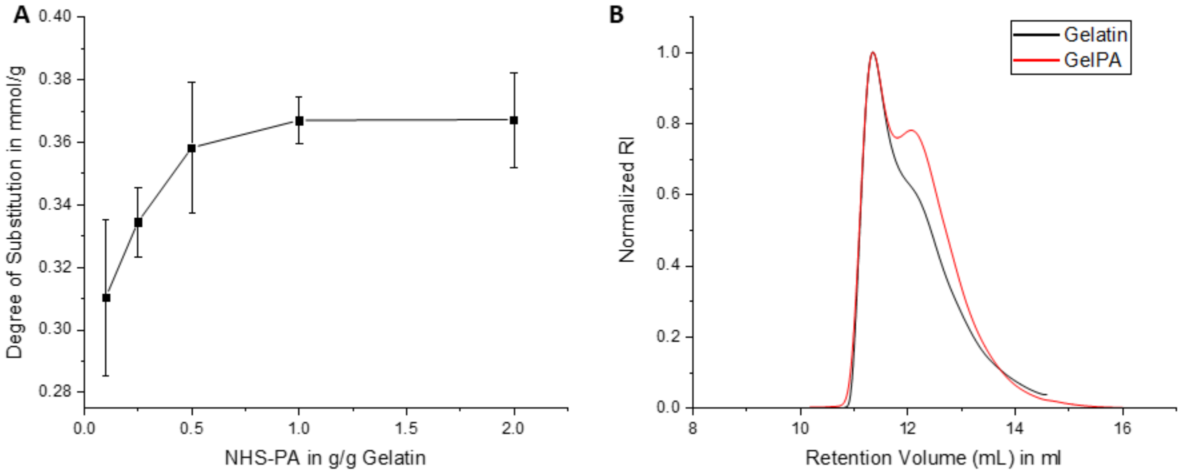

Figure 20: (**A**) Change of degree of substitution when using various amounts of substitution reagent PA-NHS, where lowest substitution degree was observed with 0.1 g PA-NHS per gram gelatin; (**B**) Gel permeation chromatography elugrams of GelPA compared to gelatin.

Table 7: Nomination of samples due to amounts of PA-NHS used for per gram gelatin.

Sample name	Amount of PA-NHS used for per gram gelatin [g]	Degree of Substitution (DO) [mmol/g]
GelPA$_{0.1}$	0.1	0.310±0.0251
GelPA$_{0.25}$	0.25	0.334±0.0110
GelPA$_{0.5}$	0.5	0.358±0.0210
GelPA$_{1}$	1	0.367±0.00753
GelPA$_{2}$	2	0.367±0.0153

4.4.2 Change of the isoelectric point of GelPA

Coincidentally, it was observed that GelPA is less soluble in water compared to gelatin, but completely solvable in PBS. It is suspected that the selective functionalization of lysine and hydroxylysine residues changes the isoelectric point, which results in less solubility of GelPA in water. After 2D electrophoresis with isoelectric focusing and SDS-PAGE, it was proven that the functionalization of amine containing residues changes the isoelectric point. Whereas gelatin (type A) has an IEP between 7-8, the IEP of GelPA shifts to an acidic pH range of around 4.8 (**Figure 21B**, unmodified and modified gelatin are highlighted with red boxes). The smears on both gels are caused by ampholine, since it has the properties of small proteins and occurs as intensely stained material at the dye front [329].

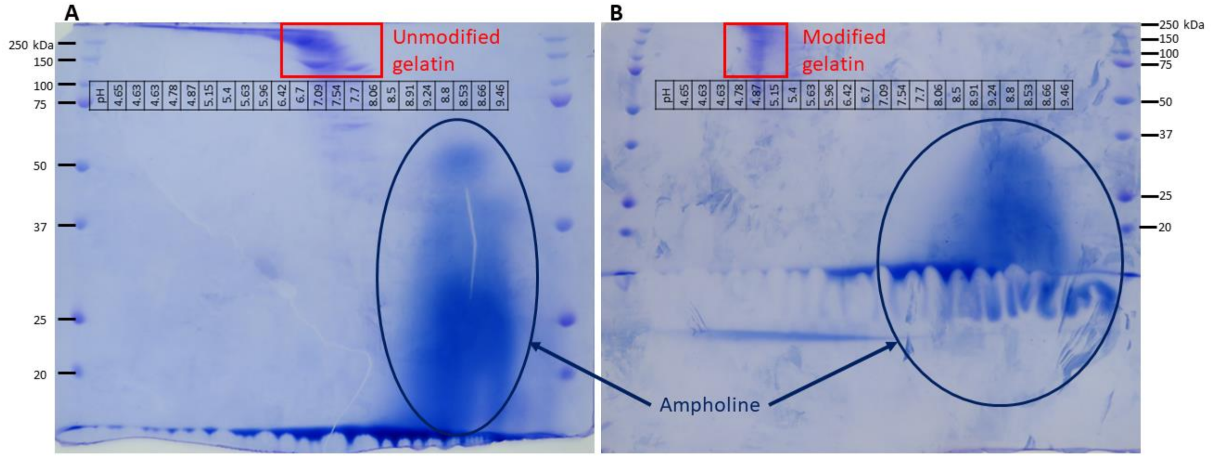

Figure 21: SDS-page of gelatin (**A**) and GelPA (**B**). Red boxes highlight the stained spots of gelatin and GelPA at the pH gradients, which are the values for the isoelectrical point (IEP). For gelatin, IEP is between 7-8, for GelPA around 4.8.

4.4.3 Hydrogel formation

The formation of the hydrogels with Ru/SPS (0.1/1 mM) and 30 s light exposure worked nicely. The precursor solution was mixed in the dark to avoid premature crosslinking by daylight. For hydrogels with 3 wt% and thiol:ene ratio of 1:1, a Young's modulus of 1.62±0.21 kPa was achieved directly after preparation (**Figure 22A**) and did not change significantly after 21 days (1.33±0.05 kPa). Due to the assumption that the crosslinking reaction was not completed with 30 s of light exposure and the mechanical properties can be increased by longer light exposure, the exposure time was extended to 60 s. The Young's modulus of same hydrogel compositions but longer exposure times is almost 1.1-2 times higher with 1.99±0.29 kPa for day 1 and 2.30±0.0.61 kPa for day 21. The effect of longer exposure time is more significant for hydrogels with higher polymer concentration. For 5 wt%, the Young's modulus increased around 1.3-1.6 times with 5.91±0.83 kPa for 30 s light exposure to 9.00±0.77 kPa for 60 s on day 21 (**Figure 22C**). For 7 wt%, up to 3.3 times higher Young's modulus (22.79±4.5 kPa) was achieved with 60 s light exposure on day 21 (**Figure 22E**). Consequently, increasing Young's modulus was observed with increasing polymer concentrations and there is no significant change after day 21. For all hydrogel concentration with 1:1 thiol:ene ratio, the Young's moduli did not change substantially over the 21 days.

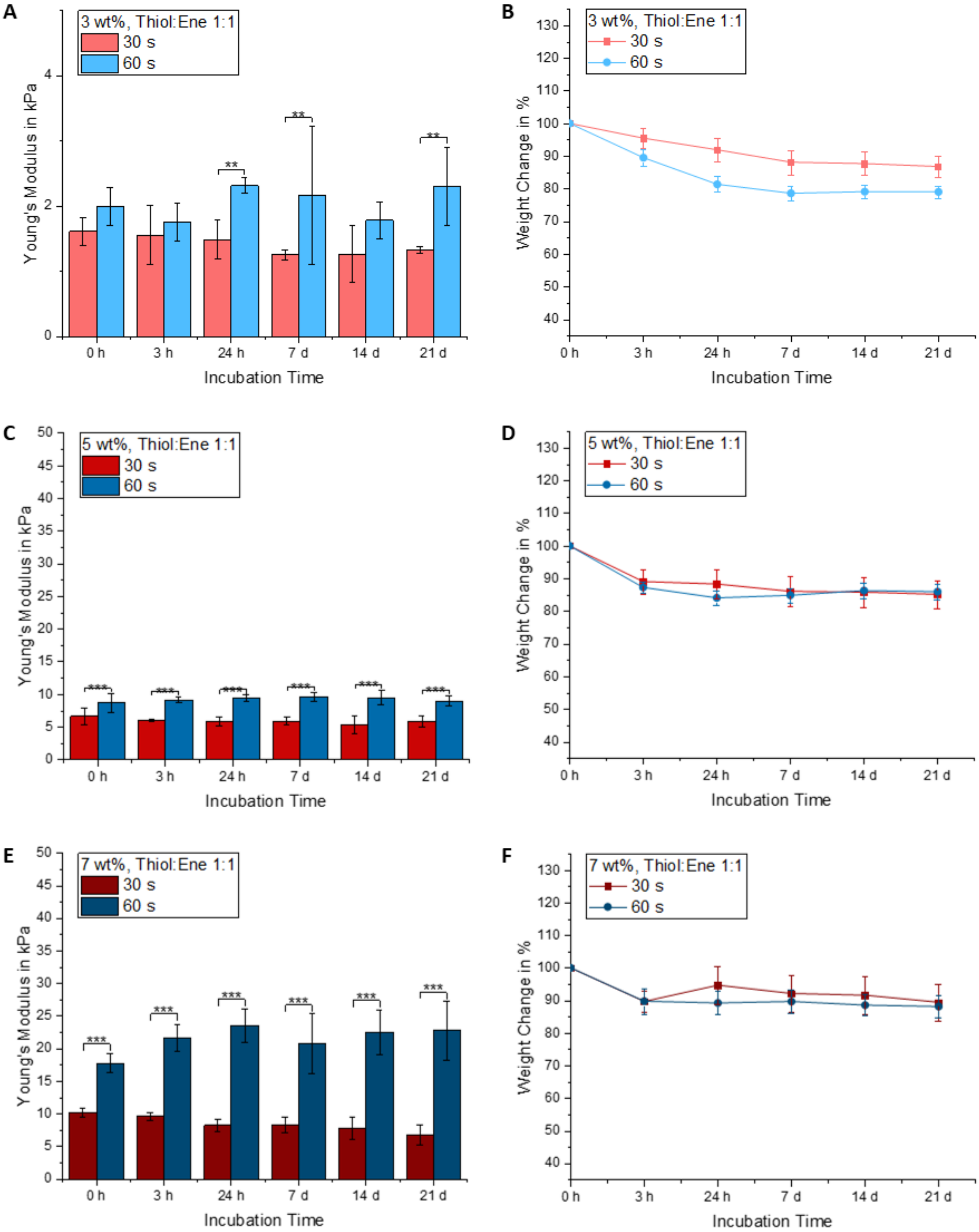

Figure 22: Young's Moduli (**A**, **C**, **E**) and weight change (**B**, **D**, **F**) of formed hydrogels with thiol:ene ratio of 1:1, directly after preparation and storage in 1 mL 1x PBS over 21 d. In general, longer exposure time to light led to higher Young's moduli. Young's modulus also increased with increasing polymer concentration of the hydrogels and did not change significantly over 21 d. Syneresis was observed for all hydrogels over 21 d.

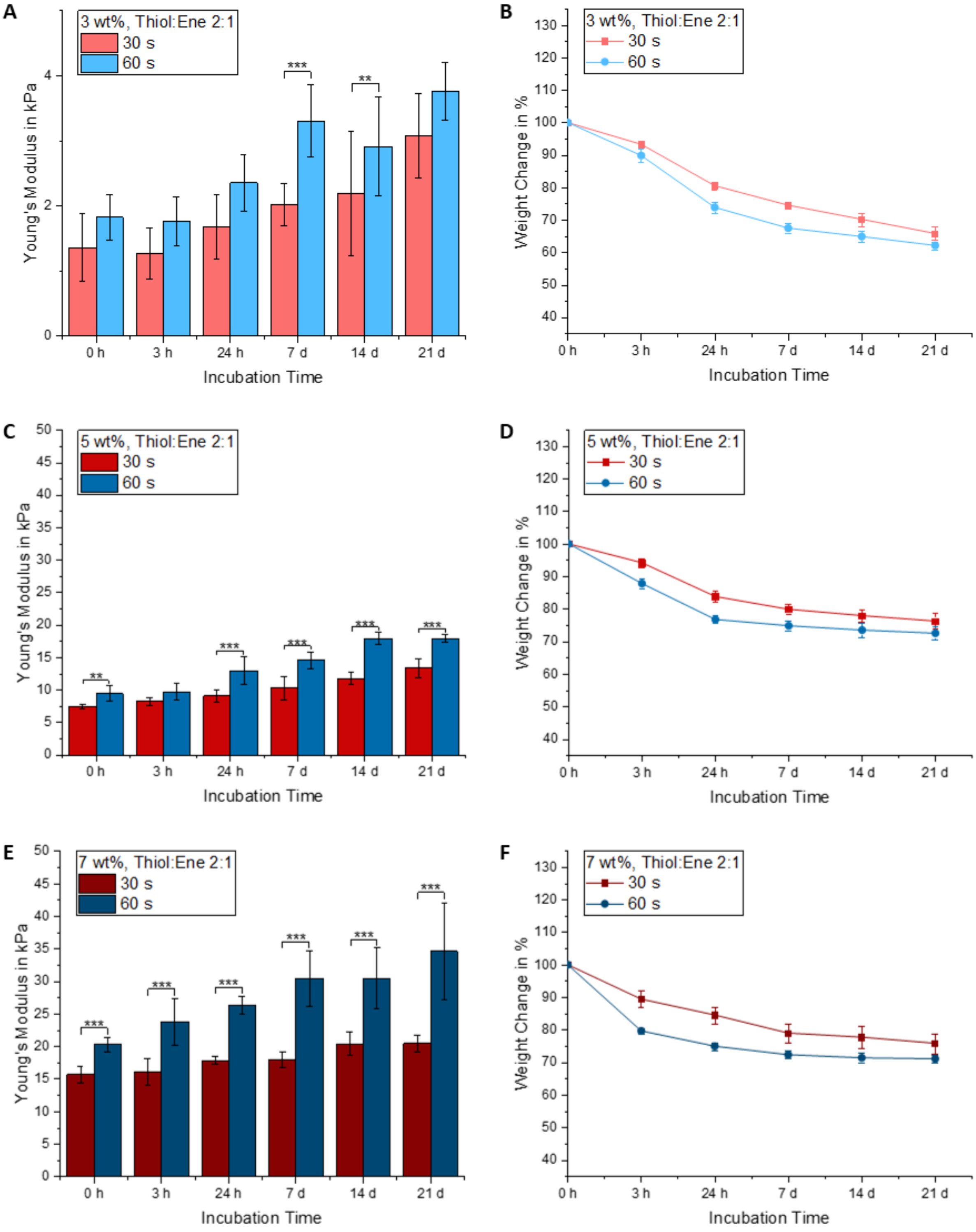

Figure 23: Young's Moduli (**A**, **C**, **E**) and weight change (**B**, **D**, **F**) of formed hydrogels with thiol:ene ratio of 2:1, directly after preparation and storage in 1 mL 1x PBS over 21 d. Highest Young's moduli were achieved with highest polymer concentration in the hydrogels. For all polymer concentrations, an increase over 21 d was observed. All hydrogels showed syneresis over 21 d.

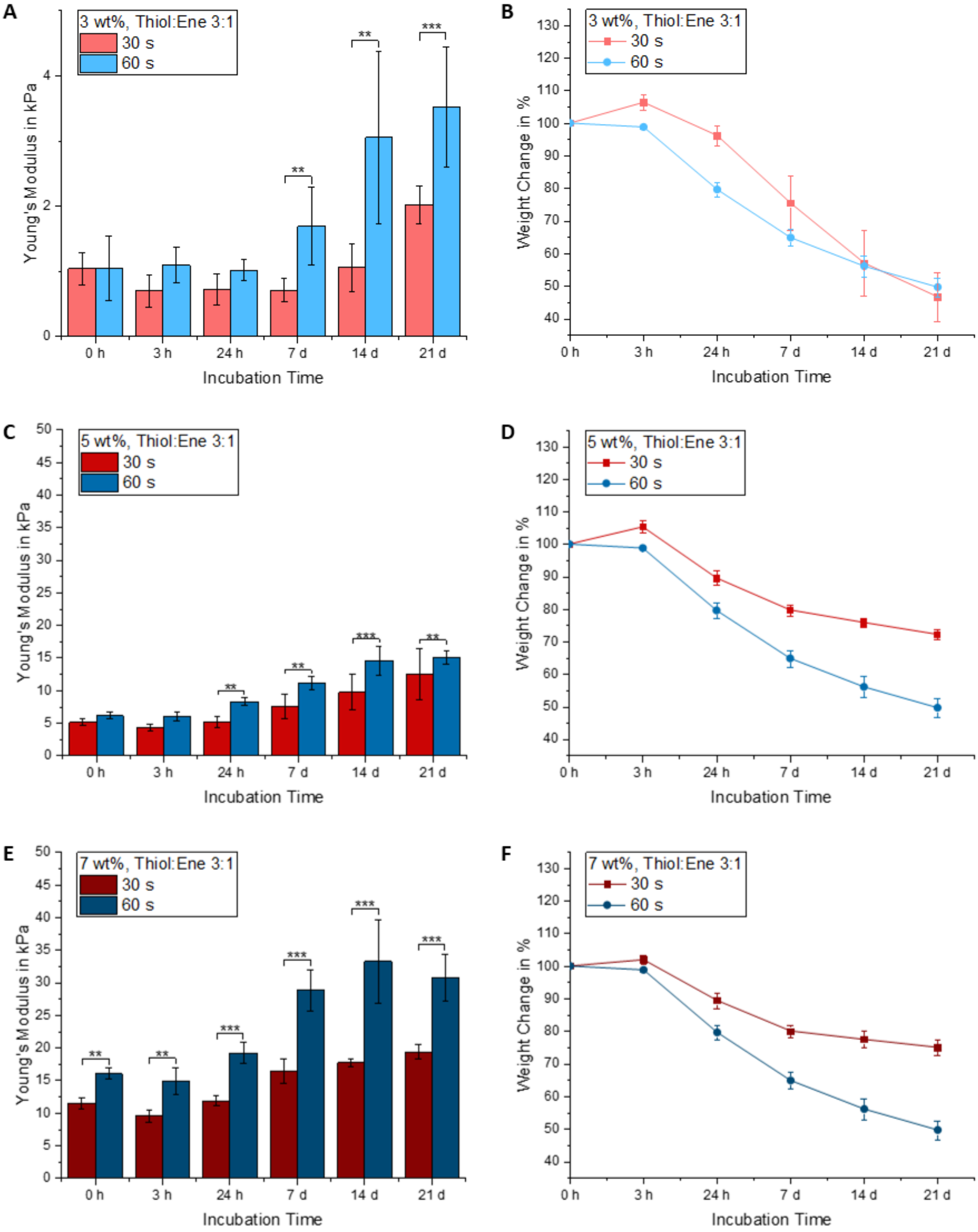

Figure 24: Young's Moduli (**A**, **C**, **E**) and weight change (**B**, **D**, **F**) of formed hydrogels with thiol:ene ratio of 3:1, directly after preparation and storage in 1 mL 1x PBS over 21 d. Highest polymer concentration of 7 wt% showed highest Young's modulus. An increase of Young's modulus over 21 d was observed for all three polymer concentrations which were used for hydrogel preparation. An initial swelling was also observed after 3 h, followed by syneresis of the hydrogels.

The influence of increasing thiol:ene ratio up to 3:1 (**Figure 23** and **Figure 24**) was also investigated. Here, it could be observed that the lowest polymer concentration of 3 wt% with lower amount of GelPA, the hydrogels showed less Young’s modulus compared to hydrogels with higher GelPA concentrations (**Figure 23** and **Figure 24**), especially at the beginning of the observed time period. For example, for 3 wt% and 60 s light exposure the values from day 1 with thiol:ene ratio of 1:1 (1.99±0.29 kPa) is 1.9-fold higher than a ratio of 3:1 (1.04±0.50 kPa) (**Figure 22A** and **Figure 24A**). Additionally, an increase of Young’s modulus was determined over the measured time for hydrogels with thiol excess. This effect is obvious for the highest thiol excess with a thiol:ene ratio of 3:1 (**Figure 24C and E**). For this ratio and 3 wt%, a more than three times higher modulus on day 21 was observed for 60 s light exposure (3.53±0.92 kPa) than on day 1 (1.04±0.50 kPa) (**Figure 24A**).

During storage of the hydrogels in PBS, no swelling was observed for hydrogels with thiol:ene ratio of 1:1 and 2:1 (**Figure 22**and **Figure 23B, D** and **F**). After 21 days, the weight of the hydrogels rather decreased to around 80 % of the initial mass directly after preparation for hydrogel with 3 wt% polymer content and 60 s light exposure. The weight loss for hydrogels crosslinked for 30 s was around 87 % (**Figure 22B**). Interestingly, the weight after storage in PBS also changed with higher amount of sPEG. Whereas lower sPEG concentration showed syneresis in most hydrogel compositions directly after 3 h in PBS, the gels with highest thiol excess (thiol:ene 3:1) and consequently highest sPEG amount kept or even gained their weights in the first 3 h and lost some mass after 24 h (**Figure 24B, D** and **F**). E.g., for 3 wt% hydrogels with thiol:ene ratio of 3:1 and 30 s crosslinking time, the weight increased to 106.40±2.32 % in the first 3 h, decreased after 24 h to 96.19±3.15 % to reach the minimum of weight on day 21 with less than 50 % of the initial weight.

4.4.4 Rheology of precursor solutions

The thermo responsive behavior of the GelPA/sPEG precursor solutions is important for 3D printing. Thus, precursor solutions with 5 and 7 wt% and all thiol:ene ratios were investigated by rheological measurements regards their temperature response. To avoid pre-crosslinking, the initiator system was left out and the measurements were performed in the dark. A temperature range from 4 to 37 °C was chosen for cooling down and heating up measurements to determine the melting and gel point of the precursor solutions.

When plotting the storage (G’) and loss (G’’) moduli of the single measurements, a shift of the gelation point (intersection of G’ and G’’) to lower temperature was observed (**Figure**

25A and **B**). The decrease is influenced by decreasing polymer content and the reduction of GelPA concentration, but independent whether cooling or heating was applied. The difference between cooling and heating is the temperature range of the gel point when cooling and melting point when heating. When the precursor solutions were cooled, the gel points were measured between 12.9 and 19.6 °C depending on composition of the solution, and the melting points were measured between 26.7 and 29.0 °C (**Figure 25C** and **Table 8**). In general, a decrease of melting and gelation temperature was observed when the thiol:ene ratio increased, which means a decrease of GelPA concentration. When comparing the GelPA/sPEG precursor solution with gelatin/sPEG solution with non-modified gelatin (**Figure 25D**), a shift of the gelation point was also observed. Interestingly, when cooling the solutions, a shift to higher temperature was observed to transfer GelPA/sPEG into gel state, whereas for heating, higher temperature was needed to liquify gelatin/sPEG mixture. Additionally, similar storage and loss modulus were observed during heating up process for both gelatin/sPEG and GelPA/sPEG, whereas during cool down, GelPA/sPEG mixture showed around 10 times higher storage and loss modulus.

Table 8: Melting and gelation temperature of precursor solutions with thiol:ene ratio 1:1, 2:1 and 3:1.

Thiol:Ene ratio / Polymer concentration	**7 wt%**		**5 wt%**	
	Melting T [°C]	Gelation T [°C]	Melting T [°C]	Gelation T [°C]
1:1	29.0 ± 0.4	19.6 ± 1.1	28.4 ± 0.0	15.5 ± 0.2
2:1	28.3 ± 0.1	16.8 ± 0.0	28.5 ± 0.6	16.0 ± 1.1
3:1	27.8 ± 0.1	16.1 ± 0.0	26.7 ± 0.9	12.9 ± 0.4

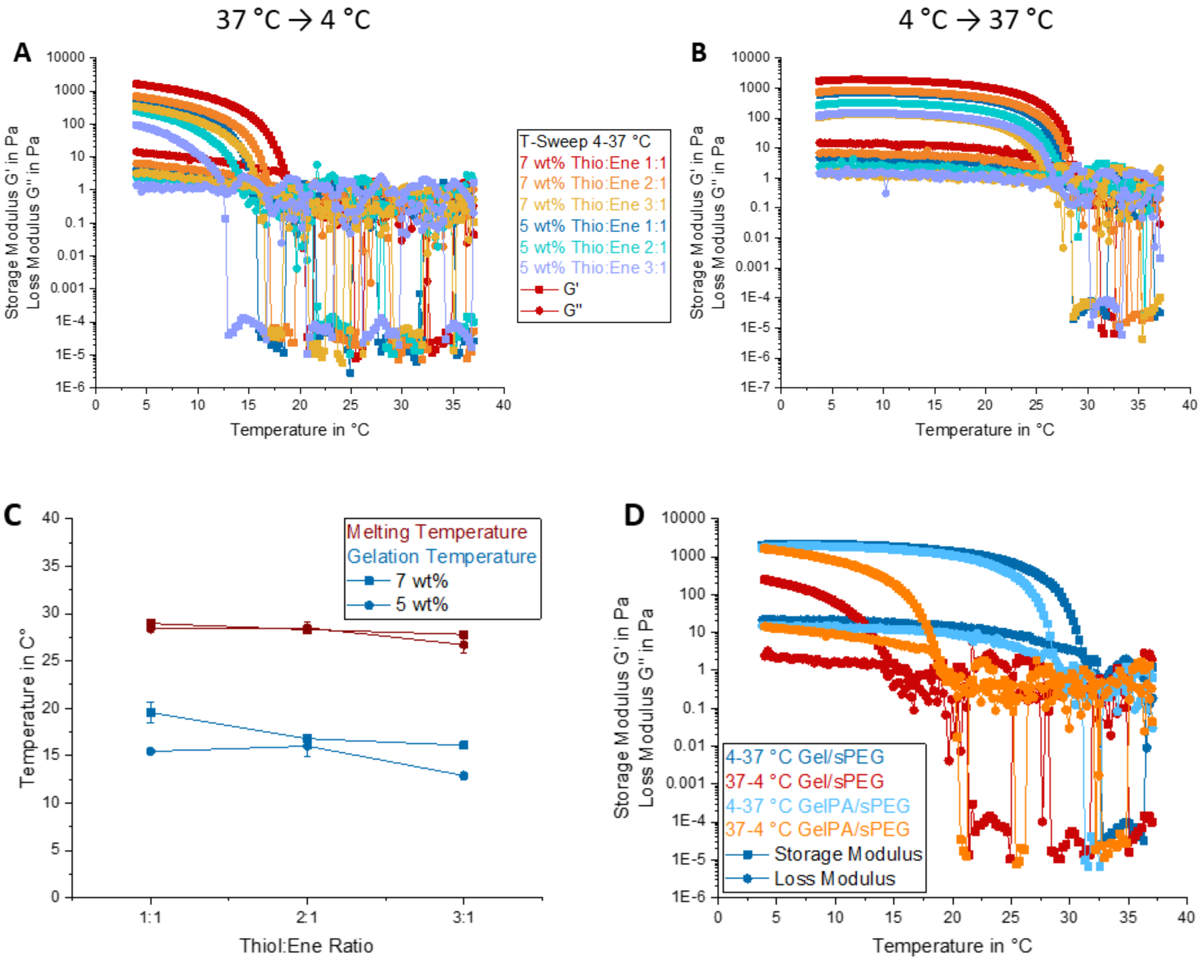

Figure 25: Rheological measurements of GelPA/sPEG precursor solutions without initiator system. Concentrations of 5 and 7 wt% with thiol:ene ratio of 1:1, 2:1 and 3:1 were investigated on their rheological behavior during cooling (**A**) and heating (**B**). The points of intersection were declared as gelation and melting point of the solutions and are summarized in (**C**). The comparison of unmodified gelatin and GelPA in precursor solutions of 7 wt% and 1:1 theoretical thiol:ene ratio is shown in (**D**).

4.4.5 3D printing and 3D bioprinting

All hydrogel concentrations could be printed (**Figure 26**). For 7 wt%, the hydrogel solution at around 37 °C needed to be cooled at 4 °C for 5 min to be printed afterwards at 21 °C with a pressure between 0.1 and 0.6 bar. The printing conditions for 5 wt% were similar to 7 wt%, except the cooling duration was increased slightly to 7 min. For 3 wt%, the cooling time needed to be extended to 15 min and the printing was processed at 12 °C. During printing, the collector plate was tempered at 10 °C to avoid diffluence of the printed constructs before crosslinking. The printed grids were crosslinked with visible light for 60 s. Bioprinted scaffolds containing human breast cancer cell line MDA-MB-231 are not shown in this work.

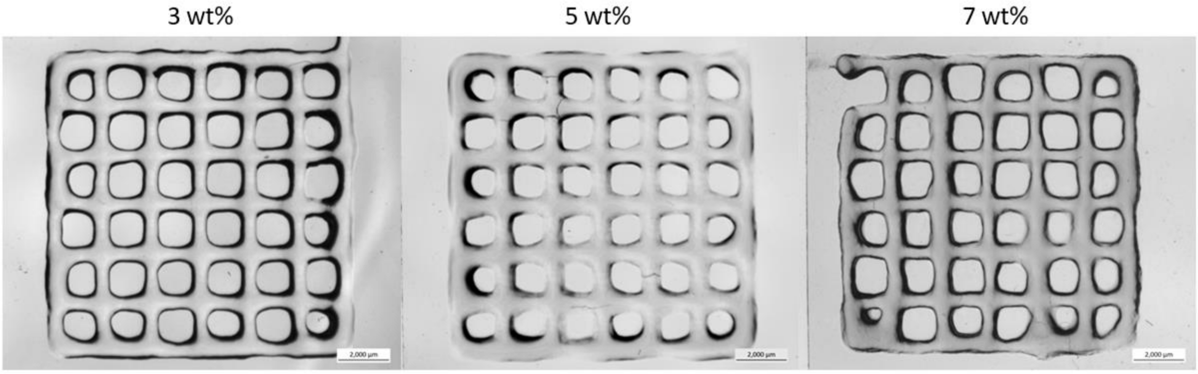
3 wt%
5 wt%
7 wt%
2,000 µm
2,000 µm
2,000 µm

Figure 26: Printed scaffolds using GelPA-sPEG bioink with 3, 5 and 7 wt%. Each scaffold contains 4 layers of material.

4.5 Discussion

4.5.1 Material properties

In this work, a new specific synthesis path for ene-functionalized gelatin has been developed. With this, lysins of gelatin were functionalized selectively via NHS activated ester of pentenoic acid [330]. Since the reaction was performed in an aqueous/DMSO mixture, NHS activated esters can undergo hydrolysis and lose the activity to react with amine functions [331]. Therefore, NHS-PA in different amounts was tested. The difference of DS is not immense, starting from using 0.5 g or more NHS-PA per gram gelatin. With less than 0.5 g of NHS-PA, the DS decreased slightly. Under the mild conditions with 40 °C and pH values between 8-9, chain degradation of gelatin was avoided successfully, and the thermo-responsive properties of gelatin were retained. Since longer reaction time has no effect on gelatin chain length and the lower amount of PA-NHS might decrease the DS, 2 h and 0.5 g NHS-PA per gram gelatin were chosen as reaction conditions to guarantee the complete reactions of amino groups in gelatin and the NHS-ester of PA. The shift of the IEP in GelPA is caused by substitution of amin containing amino acid residues via NHS-PA. The IEP of gelatin of Type A can vary between 7.5 and 9 [332]. With the 2D electrophoreses, an IEP between 7 and 8 was determined, which means that gelatin is uncharged in the statistical mean so the number of negatively and positively charged amino acid residues are the same. For GelPA, the IEP shifted to more acidic pH value of 4.8 and this implies that more acidic residues need to be protonated to achieve the uncharged state of the molecule. This state can only be obtained by decreasing the pH. For solubility, the usually positively charged lysine and hydroxylysine are substituted in GelPA, so the total number of charges is reduced. Additionally, pentenoate increases the hydrophobicity of GelPA. These facts probably cause the reduced solubility of GelPA in water.

It could be proven that GelPA hydrogels with Ru/SPS as initiator system can be controlled by light exposure time. By increasing the time from 30 s to 60 s, higher Young's moduli of the hydrogels were obtained. With the highest polymer concentration of 7 wt%, this effect was more apparent compared to the lower concentrated hydrogels with 3 wt% since the density of a network with higher polymer content can be more enhanced by longer crosslinking time. Compared to other thiol:ene systems with gelatin, such as GelAGE, the polymer concentration could be decreased down to 3 wt% without using a higher thiol:ene ratio [54].

An excess of thiol groups can be harmful for cells via autooxidation [333] and synthetic polymers, in our case 4-arm-SH-sPEG as crosslinker, do not provide inherent bioactive properties such as proteinic biopolymers, like gelatin [50]. Additionally, it was demonstrated that thiol excess leads to change of mechanical properties, probably by belated crosslinking via disulfide formation of the unreacted sPEG thiols [334]. Thiol excess also led to initial swelling of the hydrogels, which is not desirable if the material is intended for biomedical applications [335]. With a thiol:ene ratio of 1:1, these aspects could be avoided in our hydrogel system. The weight loss after storage in PBS is probably caused by diffusion of unbound crosslinker or GelPA chains. For 60 s crosslinked 3 wt% hydrogel, the network is denser and induces syneresis with water displacement as additionally appearing effect. Both effects together make the weight loss more apparent. For 5 and 7 wt%, the effect of syneresis probably dominates, since the polymer content is higher, and the crosslinking efficiency is increased due to spatial proximity and forms denser networks without remarkable polymer loss. Still, with highest sPEG content, an initial swelling of the hydrogels could be observed (**Figure 22**). This is probably caused by less crosslinking density due to reduced ene functions, so the hydrogel network can still absorb further PBS. Based on the hypothesis that thiol excess leads to belated crosslinking, the absorbed water can be displaced after longer time due to delayed crosslinking, resulting in increase of network density. Comparison of the three tested polymer concentrations show, that the highest concentration with 7 wt% resulted in highest Young’s moduli for all incubation times due to higher network density (**Figure 27A**). These hydrogels also show less weight loss during 21 d incubation time (**Figure 27B**), whereas hydrogels with lowest polymer concentration lost more than 20 % of their initial weight.

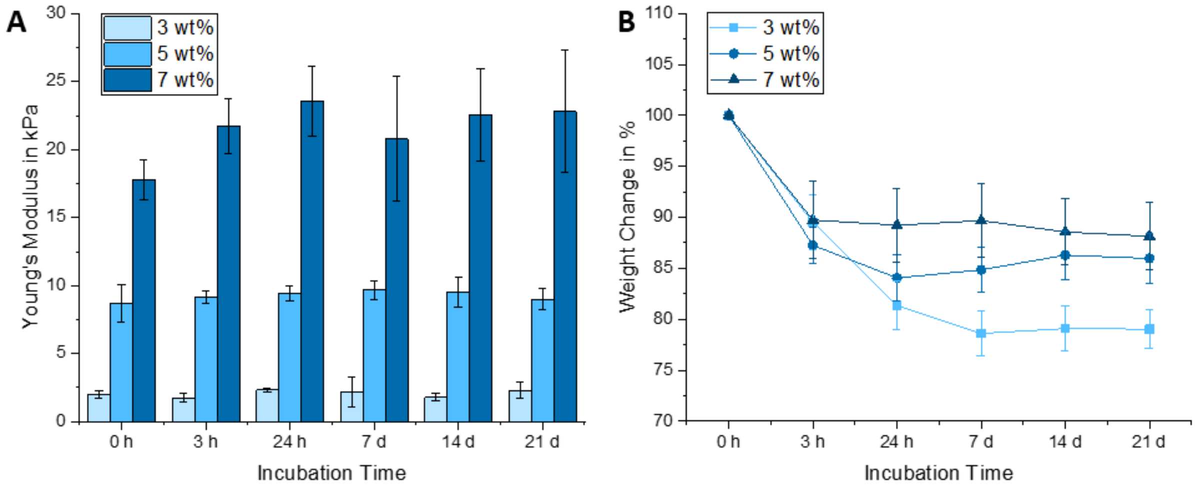

Figure 27: Young's moduli (**A**) and weight change (**B**) of 3, 5 and 7 wt% hydrogels with thiol:ene ratio of 1:1 and light exposure time of 60 s.

Rheology measurements proved the thermo responsive behavior of the precursor solutions. The gelation point during cooling, which has been proposed as the intersection of G' and G'' (G'=G'') with dependence on frequency [336,337], was determined. Cooling gelatin solutions to temperatures below the sol-gel transition temperature leads to a formation of triple helices by coiling of different gelatin chains [183]. The less a solution contains gelatin chains, the less helices are formed at same temperature or the solution needs longer time and lower temperature to achieve a similar helix concentration compared to more concentrated gelatin solutions [338]. With GelPA, when cooling the precursor solutions with same temperature rate and time but less GelPA concentration, the shift to lower temperatures to achieve the gel point was observed and can be explained with the lower concentration of formed helices. The increasing content of sPEG when higher thiol:ene ratio was investigated, might also hinder the helix formation of GelPA due to entanglement of the sPEG chains with GelPA chains. During heating of the solutions, energy in form of heat is needed to destroy the formed triple helices and transform the gel into a fluid state. The lower the present GelPA concentration the lower temperature is needed to liquify the gelled precursor solution. When comparing GelPA/spEG and gelatin/sPEG solutions, the influence of the lysin modifications were obvious. Higher temperature was needed to liquify the gelatin/sPEG solution, since unmodified lysin residues can still contribute, probably via hydrogen bonds, to the helix formation and more energy is needed to break these bonds during transition from gel to liquid state. These bonds cannot be formed when lysin is modified with pentenoate. When cooling, the formation of van-der-Waals interactions between the pentenoate residues probably also influences the gel formation by increasing the gelation temperature in comparison with unmodified gelatin. The difference of storage and loss modulus between gelatin/sPEG and GelPA/sPEG precursor solutions at 4 °C in the cool down phase is not obviously explainable. Since the temperature sweeps were always performed with the selfsame solution, similar values for both solutions were expected, such as during the heating up process. This observation could result from a measurement error and should be repeated in the future.

4.5.2 3D printing

For 3D printing, the handling and conditions before and during printing were adjusted for each concentration, since the polymer content strongly influences the thermal response of the precursor solution. Unmodified gelatin shows gelation behavior at critical concentrations of 0.4-1.0 % on cooling [339]. The GelPA concentration in each hydrogel used for printing is shown in **Table 9** and was always above the critical concentrations for gelation behavior of gelatin. Since liquid solutions or completely solid hydrogels are not suitable for 3D printing, the GelPA precursor solutions needed to be cooled to achieve a proper printing viscosity. To accelerate the cooling process for better cell viability, the precursor solutions were stored at 4 °C for several minutes, whereas the lowest concentration needed the longest time to accomplish the suitable printing texture. Additionally, the collector plate had to be cooled to preserve the printed constructs before crosslinking, since the lowest concentration liquifies at room temperature. During printing, the printing pressure needed to be adjusted to higher values constantly. This is caused by decomposition of persulfate to sulfate free radicals in aqueous solutions [340] and these free radicals can already initiate thiol-ene reactions without light sources. The effect of this primary crosslinking without light combined with increasing viscosity was also observed by Soliman *et al.* with GelAGE and thiolated crosslinkers [341]. Also, for every second layer, the printing speed needed to be decreased to avoid filament breakage due to higher cross section points.

Table 9: Printing conditions for the precursor solutions with 3, 5 and 7 wt% polymer content and information of the used GelPA amounts.

Polymer concentration [wt%]	GelPA content [wt%]	Cooling time at 4 °C [min]	Printing temperature [°C]
3	2.1	15	12
5	3.5	7	21
7	5	5	21

It is supposed that all the adjustments during printing process is due to the cooling of the bioink to achieve proper printing properties. This induced a definite rigidity of the hydrogel precursor solution. When pushing through the printing nozzle, the rigid hydrogel was destroyed by shear forces and the gel changed its nanostructure from homogeneous to an inhomogeneous hydrogel with nano fractures.

4.6 Conclusion

In this study, a new path for reproducible syntheses of an ene-containing gelatin derivative was established. For this, mild conditions were used to avoid chain degradation and to obtain stable substitution degrees. With Ru/SPS as the initiator system for thiol-ene reaction, it could be demonstrated that the hydrogel system with GelPA and 4-arm-SH-sPEG is light controllable in its mechanical strength with minor weight change under physiological conditions. Additionally, thermal controllable 3D printing is also performable due to thermo-responsive property of GelPA. Biocompatibility, cell morphology and cell migration were investigated with MDAs and the hydrogel system is proved to be cell friendly and suitable for biological or biomedical applications (data not shown in this thesis). To optimize the printing properties of GelPA, tuning the temperature or using other biopolymers as thickener during printing process might improve homogeneity after printing by avoiding over-gelation caused by cooling. In summary, it was able to introduce a new gelatin-based material for 3D bioprinting, which convinces with its reproducible synthesis, stable material properties and biocompatibility.

Chapter 5

3D PRINTING OF VARIOUS CELL CONCENTRATIONS FOR INVESTIGATION OF SCAFFOLD STABILITY USING PENTENOYL MODIFIED GELATIN AND MESENCHYMAL STEM CELLS

Parts of this chapter are intended to be published in the future (Junwen Shan, Julia Hauptstein, Theresa Zorn, Andrea Ewald, Ann-Christin Pöppler, Torsten Blunk, Jörg Teßmar, Jürgen Groll).

The content of this chapter is based on the work of the author of this thesis Junwen Shan, who performed all chemical, material scientifical and cell biological experiments, data evaluation and composition on the chemical, material scientifical and cell biological parts of the manuscript.

Chapter 5

The author contribution in the original research article was as followed:

Contributor	Contribution
Junwen Shan	Designed the research; performed the chemical, material scientific and cell biological part of the research; analyzed all chemical, material scientific data and cell biological results and all statistics; wrote the manuscript
Julia Hauptstein	Performed histological, immunohistochemical and biochemistry experiments; provided feedback on manuscript
Andrea Ewald	Supported 2D gel electrophoresis
Theresa Zorn	Performed NMR measurements; evaluated NMR spectra
Ann-Christin Pöppler	Provided feedback on manuscript
Torsten Blunk	Provided feedback on manuscript
Jörg Teßmar	Designed research; provided feedback on manuscript
Jürgen Groll	Designed research; provided feedback on manuscript

5.1 Abstract

The use of gelatin based hydrogels as bioinks is very popular in the field of biofabrication. Due to its thermo responsive property, the printing behavior can easily be tuned by temperature control. For the application as bioink, gelatin needs modifications beforehand for crosslinking reactions to achieve form stability under cell culture conditions. After crosslinking, the hydrogel network density is crucial for cell viability and can be regulated by polymer concentration, light exposure time and initiator concentration used for crosslinking. Still, the cell density used can also affect the cell behavior, especially when cells pass through the whole 3D printing process. This includes shear forces through needles with small diameters and printing conditions.

Since GelPA has recently been introduced as bioink for3D printing, it is desirable to investigate its printability with mesenchymal stem cells since they can differentiate into various cell types. For future use of GelPA as bioink for tissue engineering applications, it is also interesting to examine the suitable cell concentrations, which should be used for 3D printing to achieve high cell viability.

5.2 Introduction

The idea of 3D bioprinted organs pushes the research of biofabricated hydrogels forward for applications in tissue engineering and regenerative medicine. Therefore, polymers from natural origin are highly relevant since they already provide good biocompatibility, biodegradability and in most cases also bioactivity compared to most synthetic polymers [8,129,137]. Still, biopolymers without any chemical modifications or chemical crosslinking often do not contribute the right mechanical properties for form stability, which is crucial when they are used for hydrogel formation, e.g. hyaluronic acid or collagen [8,14]. A common biopolymer which shows good bioactivity but poor mechanical stability under cell culture conditions is gelatin due to its excellent solubility at 37 °C [342]. As a product of denatured collagen, gelatin shows non-immunogenic behavior in comparison to collagen [343]. For more mechanical stability, the conventional modification of gelatin is performed with methacrylate to obtain GelMA. GelMA is commercially available and usually photo-crosslinked with water soluble initiators via UV-light with Irgacure 2959 or visible light with LAP or Ru/SPS via radical chain polymerization with no necessary additional crosslinkers [251,344,345]. Another established gelatin based hydrogel system is GelAGE with thiol crosslinkers [54], which also needs UV or visible light crosslinking by using the thiol-ene reaction as chemical crosslinking step. Both systems have been 3D printed with extrusion-based techniques [54,111,346]. For GelAGE with thiolated 8-arm-starPEG, shape fidelity was achieved using excess of thiol crosslinker and 30 wt% GelAGE content whereas the total polymer concentration is higher [111]. With GelMA, 3 wt% hydrogels were printed with cooled collector plate since otherwise the printed hydrogel is not form stable [346]. In Chapter 4 , pentenoyl functionalized gelatin was successfully tested for 3D bioprinting with cancer cells using thiolated 4-arm-starPEG as crosslinker and Ru/SPS as initiator system. The concentration of the initiator system was kept low (01./1 mM Ru/SPS) since other ruthenium complexes are known to show anti-tumor activities without being toxic to normal cells [347]. However, this low initiator concentration effected the stability of printed constructs since the crosslinking efficiency is reduced.

For the printing process, hydrogels with application as bioinks are loaded with cells [15]. Ideally, the bioink fulfills following properties: mimicking of specific extracellular matrices (ECM) in their physical and chemical properties [348]; appropriate viscoelastic behavior for printability and shape fidelity after printing and simultaneously proper fluidity for cell protection during printing through a nozzle [349]; preservation of cell viability during and after printing, especially until regeneration and remodeling post-printing [350]. The cells undergo a shear stress depending on printing pressure, hydrogel viscosity and nozzle size and these factors also have influence on the long-term alteration and proliferation activity of the cells [73,351,352]. Still, shape fidelity, printability and printing resolution also relate to these factors [73]. One additional aspect with high influence on cell viability after 3D bioprinting is the cell concentration used in the bioink. Increasing cell concentrations induce higher cell-to-cell interaction and this limits proliferation and viability by physical stress enforced by neighboring cells [350]. Concurrently, cell density can also influence the stability of printed scaffolds [353].

From the biological and medical aspect, the migration of tumor cells in an extracellular matrix mimicking environment is highly interesting to understand the spreading and growth of carcinoma. For tissue engineering, the investigation of the behavior of mammalian cells in 3D printable hydrogels is also very attractive to promote the idea of 3D printed organs. Human mesenchymal stem cells can undergo myogenesis, adipogenesis, osteogenesis and chondrogenesis [354]. Since cell viability in GelPA was only investigated with tumor cells and until now, human bone marrow-derived stromal cells (hMSC), which can form various tissue types, are promising cells to look at if GelPA is intended to be used for tissue engineering.

This study aims to investigate the influence of initiator concentration on mechanical strength of GelPA hydrogels. Chondrogenesis with hMSCs is performed to determine cell viability with highest concentration of initiator. The impact of cell concentration on printability and cell survival after printing is examined by using high, medium and low cell density.

5.3 Materials and methods

As not stated otherwise, materials and methods for syntheses and characterization of GelPA and GelPA hydrogels are described in Chapter 4.3 or purchased from Sigma Aldrich.

5.3.1 Hydrogel formation with various initiator concentrations

The hydrogels were formed as described in chapter 4.3.7. Initiator concentrations of 0.3/3, 0.4/4 and 0.5/5 mM Ru/SPS were used additionally to investigate the influence of various initiator concentrations on hydrogel formation.

5.3.2 Determination of crosslinking degree with NMR

All NMR experiments with hydrogels were performed at a Bruker Avance III HD 600 spectrometer (Bruker, Karslruhe, Germany) operating at 600.4 MHz with a BBFO 5 mm probe head. The samples were prepared as described in 4.3.7 with 0.1/1, 0.2/2, 0.3/3, 0.4/4 and 0.5/5 mM Ru/SPS and the gelation was performed in NMR tubes. Afterwards, a coaxial insert with a TMS standard was imbedded into the hydrogel without air bubbles. ^{1}H-NMR experiments were then acquired at 37 °C with a 30° flip angle, 32 scans, recycle delay for 15.57 s and no sample spinning. All collected spectra were processed with the TopSpin 3.6.2 software, an exponential line broadening window function of 0.1 Hz, baseline correction confined to the regions of 10 to 5.5 ppm and 0.5 to -2.9 ppm and manual phasing.

5.3.3 Cell culture

Human mesenchymal stromal cells (hMSCs) were used for biological assessment of the GelPA hydrogels. The cell extraction was performed as described in 3.3.11. In short: hMSC were extracted from the cancellous bone of patients undergoing hip replacement (as approved by the Local Ethics Committee of the University of Wuerzburg (186/18) with the written informed consent of each donor patient). The hMSCs were isolated by extensively washing of the bone marrow and the bone fragments with PBS. Afterwards, the cell suspension was centrifuged and the received cell pellet was resuspended in proliferation medium

(DMEM/F12, complemented with 10 % FCS, 1 % PS, 50 µg/mL L-ascorbic acid, 2-phosphate sesquimagnesium salt hydrate and 5 ng/mL bFGF (BioLegend, London, UK)) and seeded into T175 cm^2 flasks (Greiner Bio-One, Frickenhausen, Germany). After several days, the non-attached cells were removed by washing thoroughly with PBS and adherent cells were cultured to a sub-confluent level at 37 °C and 5 % CO_2 in proliferation medium. Finally, the MSCs were detached with 0.25 % trypsin-EDTA and seeded at a density of 3-5x10^4 cells mL^{-1} in to T175 flasks.

5.3.4 hMSC encapsulation in GelPA hydrogels

hMSCs were encapsulated in 3, 5 and 7 wt% GelPA hydrogels. Therefore, GelPA and sPEG were sterilized separately using germicidal UV light at 254 nm (UVL hand lamp with filter, A. Hartenstein, Wuerzburg, Germany) for at least 20 min. GelPA is then combined with sPEG and dissolved in PBS at 37 °C under shaking in the dark. After 2 h, the solution was kept at 37 °C until use. Ru and SPS stock solutions were prepared fresh, filtered through a 0.2 µm syringe filter and kept at 4 °C until use. hMSCs at passage 4 were resuspended in the corresponding GelPA-sPEG solution. Afterwards, the initiator solutions were added with a concentration of 0.5/5 mM whereas Ru solution was added first, followed by SPS solution immediately. The cell containing precursor solution was pipetted into PDMS molds with 6 mm diameter and 2 mm height (60 µL). The hydrogels were crosslinked with visible light (JOBMATE, 220-240 V, 50 Hz, 20 W LED, Steelfort, Palmerston North, New Zealand) for 60 s. The cell-laden hydrogels were transferred into cell culture medium using a spatula and cultivated *in vitro* for 21 days either in proliferation medium or chondrogenic medium (Dulbecco's Modified Eagle's Medium high glucose 4.5 g/L, DMEM) supplemented with 1 % ITS+ Premix (Corning, NY, USA), 40 µg/mL L-proline, 50 µg/mL L-ascorbic acid 2-phosphate sesquimagnesium salt hydrate, 0.1 µM dexamethasone, 1 mM sodium pyruvate, 1% PS, and 10 ng/mL transforming growth factor-β1 (TGF-β1, BioLegend, London, UK)).

5.3.5 Cell viability assay

The cell viability of proliferated and differentiated MSCs was analyzed on day 1 and 21. Therefore, the cell-laden hydrogels were stained using calcein acetoxymethyl ester (Calcein-

AM) to detect viable cells and ethidium homodimer-I (EthD-I) for the detection of dead cells. The hydrogels were washed two times with PBS and subsequently incubated for 45 min at 37 °C in the staining solution containing 1 µM EthD-I (2 mM in DMSO) and 2 µM Calcein-AM (1 mg/mL in DMSO, Invitrogen, Carlsbad, CA, USA). Afterwards, the constructs were kept in PBS until top view imaging with a fluorescence microscope (Axio Observer.Z1, equipped with epifluorescence optics and a MRm camera, Carl Zeiss, Jena, Germany). The ratio of live and dead cells in hydrogels cultivated in proliferation medium was determined by using live/dead quantification via NIH ImageJ Fiji software (version 1.53c), counting at least at three different locations within each sample, whereas three samples per condition was used for counting. For live/dead quantification of chondrogenic differentiated cells, same software as for proliferation was used, except counting was performed at least at three different locations using two samples per condition.

5.3.6 Histology and immunohistochemistry

On day 1 and 21, MSC-laden hydrogels were harvested for histological, immunohistochemical and biochemical analyses, which are described in Hauptstein *et al.* [355]. Therefore, the hydrogels were fixed in 3.7 % PBS buffered formaldehyde at 4 °C over night. The constructs were then transferred to Tissue Tek O.C.T. (Sakura Finetek, Torrance, USA) and incubated at room temperature in a wet chamber over night. Afterwards, the samples were shock frozen in liquid nitrogen and stored at -20 °C. For histology and immunochemistry, the frozen hydrogels were sliced (8 µm per longitudinal section) using a cryostat (CM 3050S, Leica, Wetzlar, Germany) and fixed on SuperFrost plus glass slides (R. Langenbrick, Emmendingen, Germany). For staining of glycosaminoglycans (GAG) 0.1 % safranin O was utilized and cells were counterstained with 0.02 % fast green for histological analysis [293]. For immunohistochemical analysis, proteinase K was digested for 10 min at room temperature for antigen retrieval. The sections were washed in PBS and blocked with 1 % BSA in PBS for 1 h at room temperature. Afterwards, antibody staining (anti-aggrecan 969D4D11, 1:300; anti-collagen I ab34710, 1:500; anti-collagen II II-4C11, 1:500 in 1 % BSA in PBS) was performed at room temperature over night. After three times washing in PBS, the sections were incubated with secondary antibody (goat-anti-mouse Alexa488 115-545-146, 1:400; goat-anti-rabbit Alexa488 111-545-003, 1:400 in 1 % BSA in PBS) for 1 h at room temperature in the dark. Afterwards, the sections were washed with PBS and fixed with DAPI mounting medium ImmunoSelect. Fluorescence microscopy (Olympus BX51/DP71, Olympus, Hamburg, Germany) was used to visualize the stained ECM deposition.

5.3.7 Biochemical analysis

To quantify the DNA contents and GAG deposition, biochemical assays were performed with the hydrogels harvested on day 1 and 21. The constructs were washed with PBS and homogenized with a TissueLyser (Quiagen, Hilden, Germany) for 5 min at 25 Hz. The suspension was then digested with papain (3 U mL^{-1}) over night at 60 °C. A spectrofluorometer (Infinite M200 Pro, Tecan, Crailsheim, Germany) and salmon sperm DNA as defined DNA standard was used to quantify DNA with fluorescent DNA intercalating agent Hoechst 33258 at 340 nm and 465 nm [356]. Dimethylmethylene blue was used to bind to sulphated GAG to shift the absorption maximum. With this, GAG could be quantified at 525 nm using the spectrofluorometer and bovine chondroitin sulfate as standard.

5.3.8 3D bioprinting with different hMSC concentrations

3D bioprinting was performed as described in chapter 4.3.11 by using MSCs instead of MDAs. MSCs were printed with 0.2x10^6, 1x10^6 and 10x10^6 cells mL^{-1}. The printed constructs were cultured for 7 days. Cell viability was determined on day 1 and 7.

5.3.9 Statistical analysis

SigmaPlot 12.5 (Systat Software GmbH, Erkrath, Germany) was used for statistical analyses. Data are reported as the mean and standard deviation from at least three replicates if not stated otherwise. Two-way ANOVA with Tukey’s post hoc test was used as followed: for Young’s modulus with time (all measured time points) and initiator concentrations (0.1/1, 0.3/3, 0.4/4 and 0.5/5 mM); for cell viability with time (day 1, 7 and 21) with hydrogel contents (3, 5 and 7 wt%). Significant differences are marked as follows: *($p<0.05$), **($p<0.01$) and ***($p<0.001$).

5.4 Results

5.4.1 Influence of initiator concentration on hydrogel formation

5.4.1.1 Compression tests for Young's modulus and swelling behavior

Since printed scaffolds with 0.1/1 mM Ru/SPS concentration were not stable for longer than one day, it was suspected that the crosslinking density was too low to keep the scaffolds durable. Therefore, hydrogels with 7 wt%), thiol:ene ratio of 1:1 and higher concentrations of the initiator system were tested for their mechanical strength and wet behavior, using 0.3/3 mM, 0.4/4 mM and 0.5/5 mM Ru/SPS and compared with 0.1/1 mM (**Figure 28A**). Measurements of the Young's modulus showed increasing values with increasing initiator concentrations significantly, especially between 0.1/1 mM and all other concentrations ($p<0.001$). After 24 h, the hydrogels with 0.4/4 mM and 0.5/5 mM also showed differences ($p<0.05$) at each time point and on day 21, 0.3/3 mM and 0.4/4 mM showed significant differences ($p<0.001$) additionally. Highest Young's modulus was achieved with 0.4/4 mM Ru/SPS concentration with the highest value on day 7 (48.0 ± 5.5 kPa), which is 2.3-fold higher than with 0.1/1 mM, whereas lowest Young's modulus was reached with 0.5/5 mM with 35.3 ± 5.7 kPa on day 14, which is still 1.6 times higher than for the lowest initiator concentration. Since three different hydrogel concentrations were tested in former studies, these were also investigated here with 0.5/5 mM Ru/SPS. Compared to 4.4.3 the increase of Young's modulus with higher polymer concentration was observed within this study as well (**Figure 28C**). In general, there were no significant changes in Young's modulus for all hydrogel compositions. The weight changes during the 21 days were also moderate for all compositions (**Figure 28B** and **D**). Fewest changes were observed with 7 % polymer content and 0.5/5 mM Ru/SPS with around 90 % of the initial weight for almost all time points (**Figure 28D**).

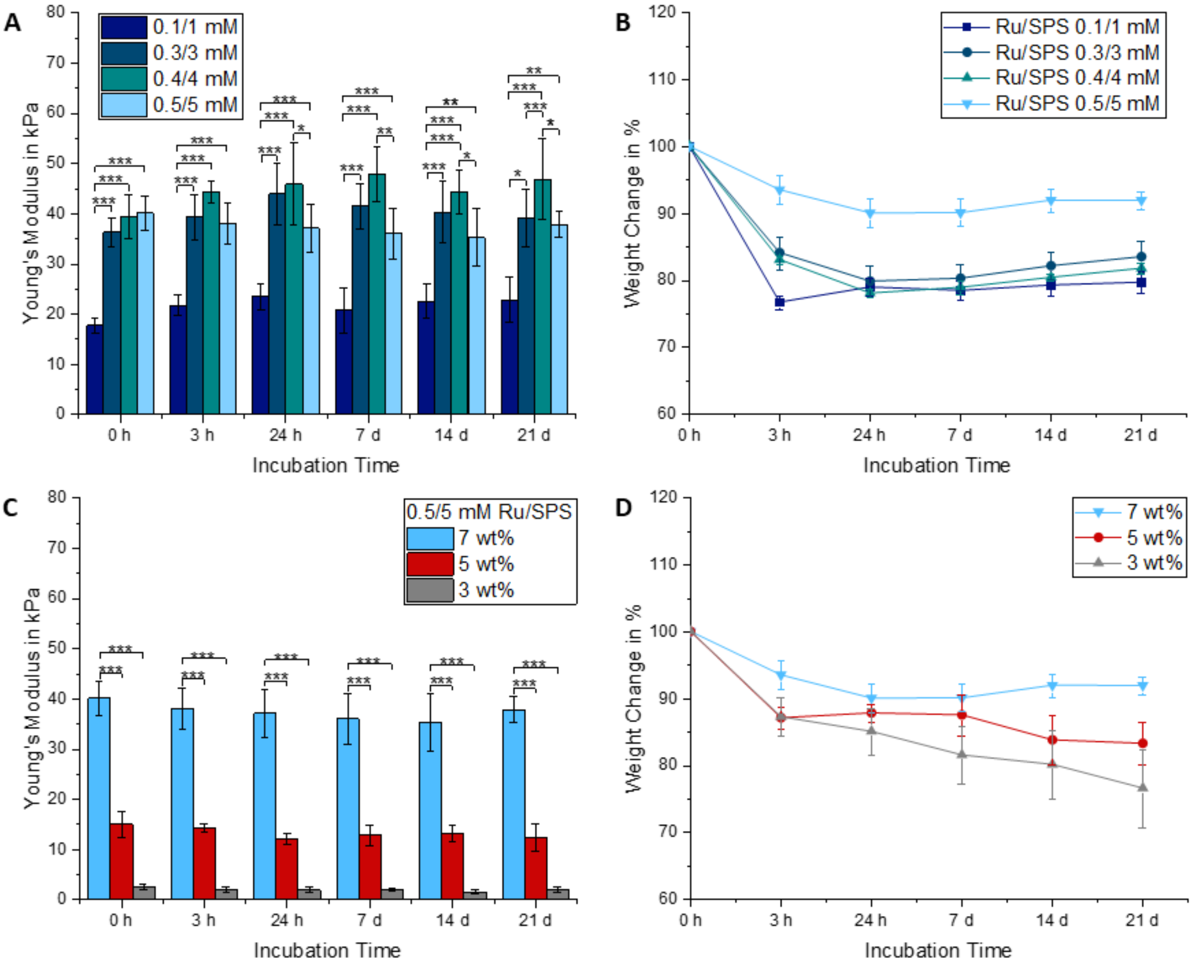

Figure 28: Young's moduli and swelling behavior of the hydrogels over 21 days with various concentration of the initiator system (**A-B**). Additionally, different hydrogel concentrations were investigated with an initiator concentration of 0.5/5 mM Ru/SPS on Young's modulus and swelling behavior over 21 days (**C-D**).

5.4.1.2 NMR measurements for determination of reacted ene-functions

To investigate how many ene-functions were consumed during crosslinking reaction, solid-state NMR measurements with the crosslinked hydrogels were performed and compared with a polymer sample without crosslinking. Surprisingly, none of the initiator concentrations led to a complete consumption of the ene-functions. The highest conversion of the ene-functions in thiol-ene reactions was achieved with 0.4/4 mM Ru/SPS concentration with 56.2 % of consumed ene-functions (**Figure 29**). This result fits within the values of the mechanical testing since the same composition has the highest Young's modulus.

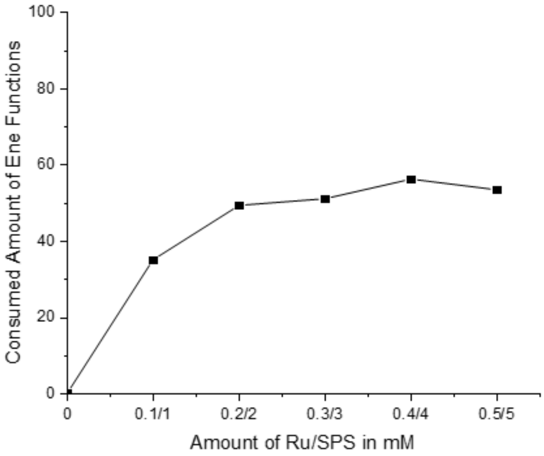

Figure 29: Consumed amount of ene-functions using various amounts of initiator system, measured with solid state NMR spectroscopy. An indicated plateau is observed beginning from 0.2/2 mM of Ru/SPS.

5.4.2 Cell viability of hMSCs

To investigate the biocompatibility, hydrogels with 3, 5 and 7 wt% polymer concentration and 1x10^7 hMSC mL^{-1} were cultivated for 21 days. Cell viability was determined on day 1, 7 and 21 by live dead staining (**Figure 30A** and **B**). At the same time, chondrogenically differentiated hMSCs were cultivated simultaneously, looking at the cell viability on day 1 and 21. The experiments showed very good cell viability both for proliferation and differentiation. For proliferation, significant differences were only determined for 3 wt% hydrogels compared to other concentrations on day 1 and 7. Over 21 days, 3 % hydrogels showed cell viabilities from 92.4±6.8 % to 98.3±1.0 %. Highest cell viability was achieved by hydrogels with 7 % with 98.9±0.4 % on day 21 **Figure 30C**). Still, live dead staining pictures also demonstrated cell spreading for 3 % hydrogels, starting already on day 7. On day 21, almost all live detected cells were spread, which indicates cell attachment to the hydrogel matrix [357]. For chondrogenic differentiated cells, 82.1±16.5 % for day 1 and 87.4±13.7 % viable cells were determined for 3 % hydrogels (**Figure 30D**). Highest viability of 99.1±0.3 % was reached on day 21 with 5 % hydrogels. Here, cell spreading was observed on day 21 for 3 %, whereas single cells are spread in 5 % or remained roundish in 7 %.

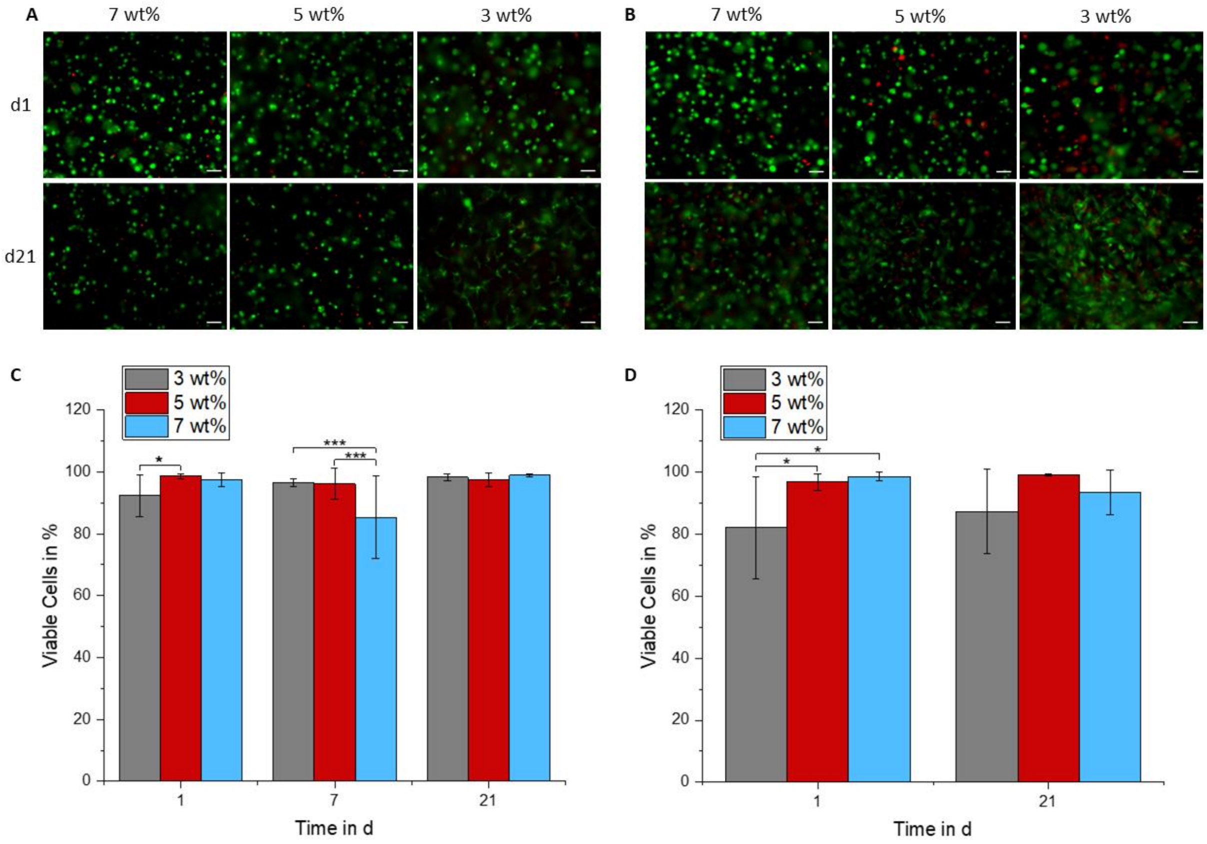

Figure 30: Live-dead staining of MSC's cultivated in cast hydrogels with various concentrations of polymers and an initiator concentration of 0.5/5 mM Ru/SPS. Viable cells were labeled with calcein-AM and dead cells with EthD-I (**A-B**). Scale bars are 100 µm. Quantification of live-dead staining for proliferated cells was performed with n = 3 per condition and time point, counting at least 9 locations each hydrogel (**C**). For differentiated hydrogels (**D**), quantification of live-dead staining was performed with n = 3 per condition and time point, counting at least 6 locations each hydrogel.

5.4.3 Chondrogenic differentiation of hMSCs in GelPA

Evaluation of deposition of extra cellular matrix (ECM) during chondrogenic differentiation of hMSCs in GelPA was performed with histological, immunohistochemical and biochemical analyses. Therefore, the hydrogels were harvested on day 1 and 21. Quantification of glycosaminoglycan with biochemical analysis showed almost no GAG/DNA production on day 1 (**Figure 31A**) but increased on day 21 to 32.32±4.16 µg/µg for 3 %, 43.4±3.0 µg/µg for 5 % and 33.5±2.6 µg/µg for 7 % (**Figure 31B and C**). However, the safranin O, aggrecan and collagen II staining of the hydrogels with different concentrations showed on day 21, that ECM production increased with decreasing polymer concentration in hydrogels (**Figure 31B**). The results of the staining confirmed the comparison of day 1 and 21 and approved the deposition of ECM during chondrogenic differentiation. However, collagen/DNA ratio could not be performed since GelPA is synthesized from gelatin, which is denatured collagen and consequently interferes with determination of collagen/DNA ratio.

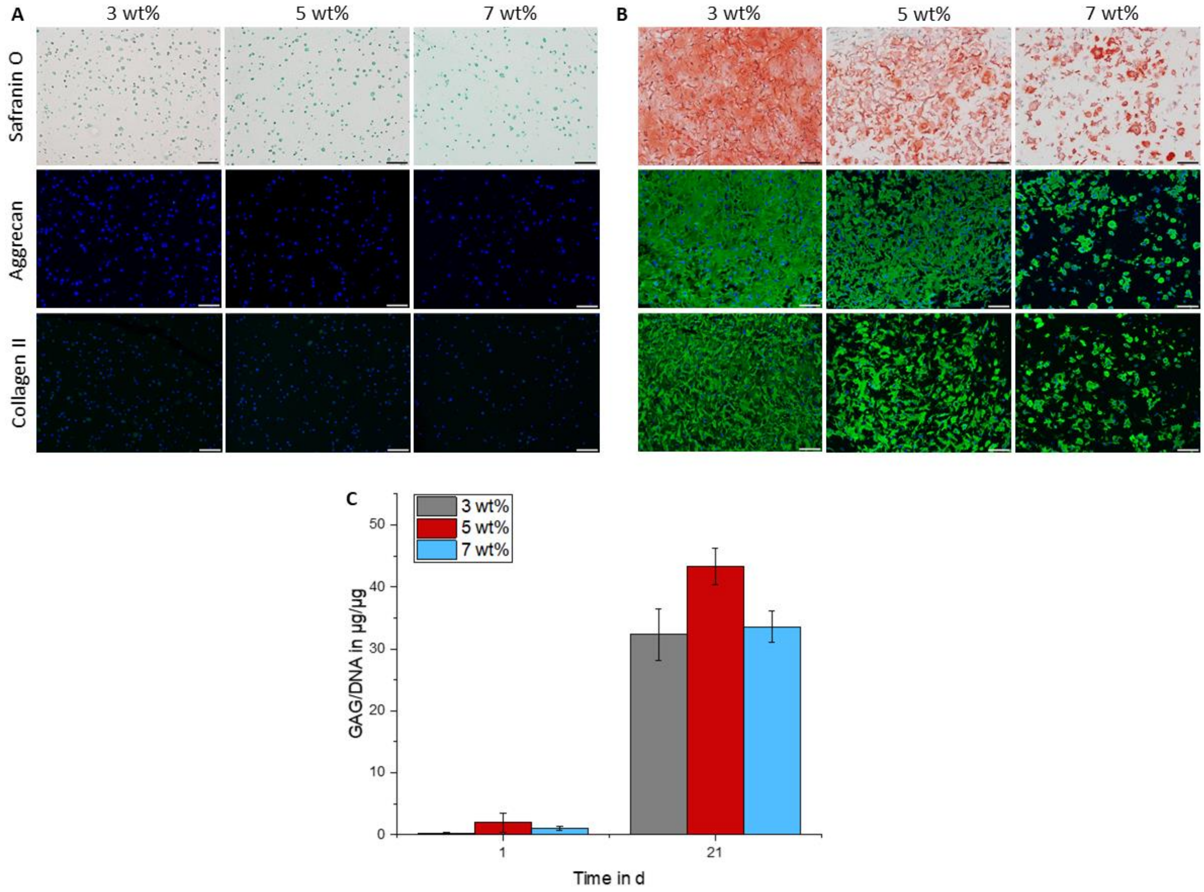

Figure 31: Safranin O, aggrecan and collagen II staining of differentiated hydrogels after 1 day (**A**) and 21 days (**B**). Immunohistochemical staining for aggrecan (green) and collagen type II (green), with nuclei stained with DAPI (blue). Scale bars are 100 µm. Quantification of the GAG production shows very high values after 21 days compared to 1 day. Data are presented as means ± standard deviation (n = 3).

5.4.4 Scaffold stability with various cell numbers

Printing with various different cell concentration was performed to analyze the scaffold stability depending on cell density. Therefore, cell concentrations of 10×10^6, 1×10^6 and 0.2×10^6 were printed with hydrogels with 5 % polymer content. It could be observed that with highest cell concentration of 10×10^6, some areas of the construct already started to breakdown on day 1, especially the strands in between the points of intersection (**Figure**

32A). After day 7, this effect was still existing, and cells were released out of the scaffold and spread on the coverslips which were used for 3D printing. Additionally, the high density of cells led to very intensive and overlapping fluorescence signal of the printed constructs. With lower cell concentrations, the breakdown of the construct was not observed even after day 7 under culture conditions. This could be found already with 10 times less cell concentration of 1×10^6 cells mL^{-1}. The quantification of live/dead staining showed that high cell density causes less viable cells (45.78±1.51 % for 10×10^6 cells mL^{-1} on day 7, **Figure 32B**). Best cell viability was achieved by printing 0.2×10^6 cells mL^{-1} with 85.00±0.78 % after day 1, which dropped significantly to 77.74±1.62 % after day 7. Altogether, a significant decrease of cell viability was observed for all cell concentrations from day 1 to day 7.

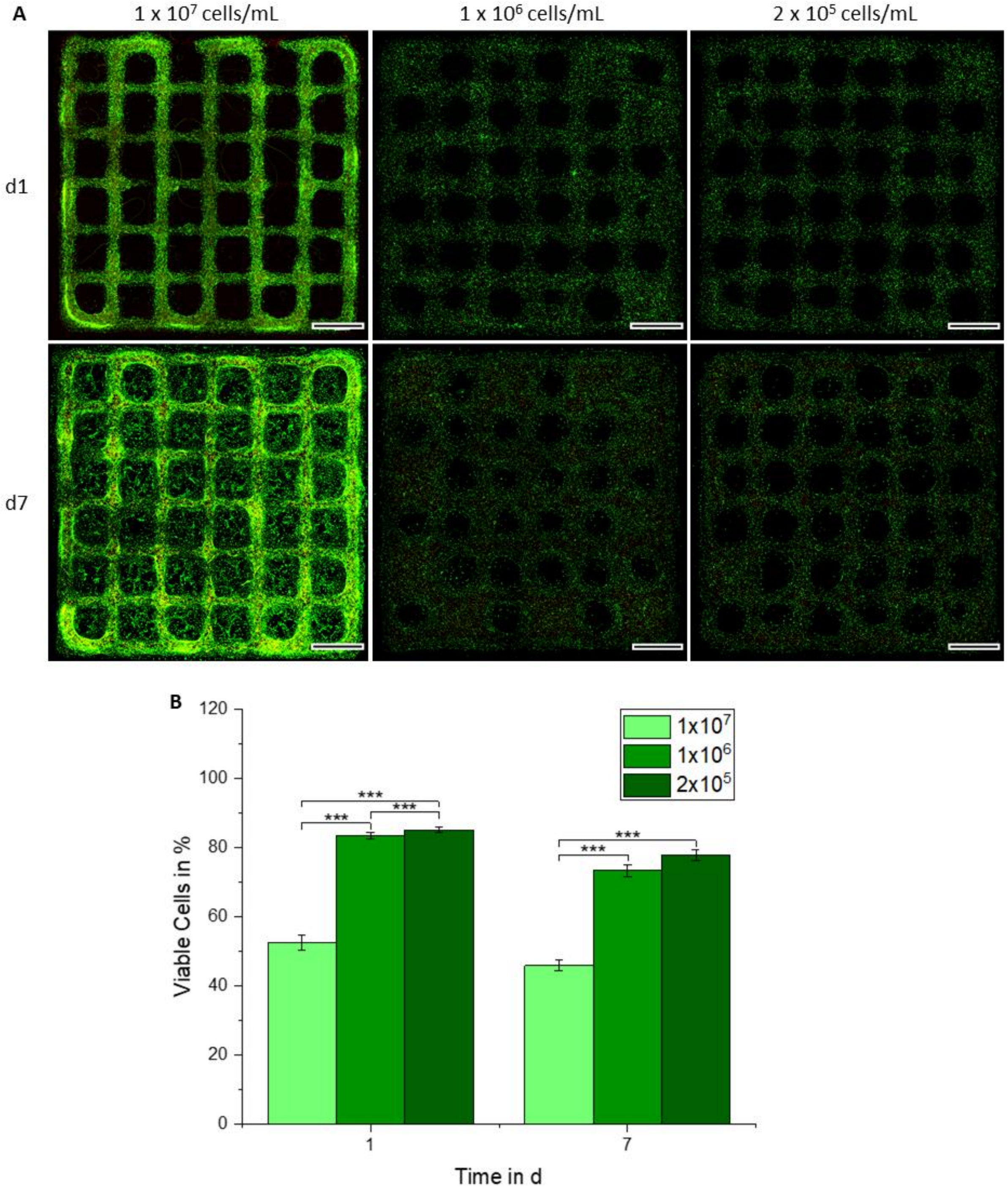

Figure 32: Live-dead staining of MSC's after printing and day 1 and 7 (**A**). Living cells were labeled with calcein-AM and dead cells with EthD-I. Quantification of live-dead staining for printed cells was performed with n = 3 per condition and time point, counting at least 9 locations each hydrogel (**B**).

5.5 Discussion

The determination of Young's modulus showed that the mechanical strength of the hydrogels can be tuned by using higher concentrations of initiators. The used Ru complex is known to absorb visible light in aqueous solutions [358]. With increasing concentration of Ru, more visible light can be absorbed and this can improve the radical formation of Ru^{2+} to the excited state which induces decomposition of persulfate to sulfate radicals [359], resulting in better crosslinking efficiency of the thiol-ene reaction. For other materials, e.g. GelMA, the concentration of Ru/SPS with 0.2/2 mM was already sufficient to complete the crosslinking of the GelMA macromers, whereas for GelAGE, highest Young's modulus was achieved by using 1/10 mM Ru/SPS [54,359]. In the study with GelPA, the highest Young's modulus was not achieved by highest concentration of 0.5/5 mM, but with 0.4/4 mM of Ru/SPS. The NMR measurements also indicate the consumed amount of ene-functions increased with ascending Ru/SPS concentration with maximum at 0.4/4 mM. The differences of the concentrations of Ru/SPS used to achieve highest Young's modulus is probably caused by the usage of different light sources. Since the properties of the materials and the crosslinking mechanism are also diverse, the most efficient concentration of Ru/SPS need probably to be detected for each system. Still, with 0.5/5 mM the swelling behavior was most moderate compared to other initiator concentrations. For this reason, this concentration was used for all follow-up cell experiments since a change of the dimension of the hydrogels by swelling is not desirable for tissue engineering applications due to loss of mechanical performance and deformation [360].

In the experiments with hMSCs, GelPA showed excellent biocompatibility due to high cell viability with all polymer concentrations. Even cell spreading was affected by decrease of the polymer content. Compared to other hydrogels systems, only a cell viability of over 80 % was observed with GelMA [136], whereas in most cases with GelPA, cell viability of over 90 % was obtained. With GelAGE, cell viability around 90 % could also be achieved with 20 % hydrogels, but a spreading of cells was not observed [54]. During chondrogenic differentiation, the production of ECM was also influenced by the concentration of the hydrogels and increased with decreasing polymer content. Still, the GAG production is lower compared to hyaluronic acid hydrogels or GelMA hydrogels, which were enhanced with inner meniscus or outer meniscus ECM [355,361]. Nevertheless, the staining pictures show an equal distribution of the newly formed ECM by the differentiated MSCs, especially for the lowest hydrogel concentration of 3 % although the lowest GAG production was detected for these hydrogels. This is probably caused by the low polymer concentration, so the disposed ECM can diffuse more easily through looser network density into the cell medium [355].

For bioprinting, three different cell concentrations were used to investigate the cell density on printability, stability of printed constructs and cell viability after printing. Therefore, $10x10^6$, $1x10^6$ and $0.2x10^{6*}$ cells mL^{-1} suspended in precursor solution were used. All three cell-polymer solutions could be printed with low pressure (< 0.5 bar). The constructs with highest cell concentration lost the stability and the printed strands dissolved partially. Since these strands are filled with cells, polymer relaxation occurs [350] and consequently results in spatial separation of the reactive groups for the thiol-ene crosslinking reaction. The constructs with both lower concentrations remained stable even after day 7 and the phenomenon of dissolving strands could not be observed. Cell viability after printing was also investigated after day 1 and 7. Highest cell density also led to immense cell death of over 50 % dead cells after day 7 and already over 40 % for day 1. High cell density can cause cell damage by hypoxia, saturation and disruptive cell-cell interaction and due to polymer relaxation, the cells in higher concentration loose their protection by encapsulation in the material. With this, it is necessary to select proper cell concentration for bioprinting, since a too low cell density can also cause reduced cell growth [350]. However, better cell viability with lower cell density during printing could be demonstrated with cell concentrations of $1x10^6$ and $0.2x10^6$ cells mL^{-1}.

5.6 Conclusion

The experiments of Chapter 5 engrossed the investigation of GelPA properties as material itself and for the use as bioink with hMSCs. The mechanical characteristics cannot only be tuned by exposure time of the precursor solutions to light or polymer concentration, but also with the initiator concentration. The use of GelPA as a material for chondrogenic differentiation is highly promising with nice cell viability and ECM production. It was demonstrated that cell printing is decidedly dependent on cell density of the used bioink for cell viability since the ink material plays a protective role during the whole printing process. Additionally, the stability of printed constructs is also dependent on the cell concentration. The chondrogenic differentiation with printed cells should be performed in the future to investigate whether the cells behave differently compared to casted hydrogels.

Chapter 6

CONCLUDING DISCUSSION AND OUTLOOK

In this doctoral thesis, the performed chemical investigations were focused on the synthesis of two different biopolymer derivatives, a) based on oxidation of hyaluronic acid and b) a specific functionalization of the lysin residues of gelatin.

For the modification of hyaluronic acid, the oxidation of the primary alcohol enabled a minimal alteration of the polymer chains by only converting the primary alcohol into an aldehyde function. With this modification no additional ring-opening occurs and a major intervention into the chain structure is avoided. Additionally, the carboxylic acid function of the group of the glucuronic acid is retained, which is known to interact with CD44 receptors due to its negative charge in neutral pH [290]. The oxidation with TEMPO/TCC however caused a massive degradation of the hyaluronic acid chain, which was not surprising since degradation of hyaluronic acid also occurs under oxidative conditions [156,301,302]. The additional alkaline ion exchange procedure with *tert*-butylammonium hydroxide might also be additionally responsible for this observation, since strong pH values also degrade hyaluronic acid chains. Still, very high degrees of oxidation could be achieved, and this strongly influenced the mechanical and long-term stability of the resulting hydrogels, despite the reversible nature of the crosslinking via Schiff Base chemistry. The batch-to-batch variation between identical modification reactions was still an observed problem, therefore blending of multiple products was performed to yield a more uniform product from the various syntheses. So far the modification of hyaluronic acid was only possible in small batch size due to the huge effort of working under inert gas and the need for water free solvents. An up-scaling of the reaction would be desirable in the future, especially if demands for larger batches are coming up.

For the additional functionalization of gelatin with pentenoate, the synthesis was much less complex compared to the TEMPO/TCC oxidation of hyaluronic acid. The only additionally established step is the synthesis of the educt, the NHS-ester of pentenoic acid using EDC chemistry, which was a quite simple procedure without laborious purification of the product. Due to the mild reaction conditions applied during the GelPA synthesis, no degradation of gelatin chain occurred and its thermo-responsive behavior was retained and only slightly changed due to the modification. Additionally, the achieved reproducibility of the products was very acceptable, as far as the consistency of the used biological starting material was given. The syntheses were already performed with batches of 10 g gelatin, so a subsequent up-scaling of the reaction is much easier to implement and thereby favorable for the development of a bioink.

Both modified biopolymers could be easily transformed in consistent and stable hydrogels, which additionally offered to control mechanical strength and degradability. The obvious differences of both hydrogel formulations are the used type of crosslinker and the type of crosslinking reaction. Whereas a low molecular weight crosslinker (adipic acid dihydrazide) was used for the Schiff Base formation with aldehyde containing hyaluronic acid, a polymeric crosslinker with 5 kDa molecular weight (thiolated 4-arm-star-PEG) was used for thiol-ene reaction with the ene containing gelatin. Schiff Base formation occurred very fast within seconds without the addition of any initiators or reaction triggers. Accordingly, the reaction was not temporally controllable after adding the crosslinker to the HA solution. The resulting hydrogels were mechanically strong, but stiff and brittle, which impeded an application as bioink since the gels could only be extruded with destruction of the gel structure and this additionally led to a necessary adjustment of the penetration depth for mechanical testing as the gels still increased in strength. For the GelPA-sPEG hydrogels, the penetration depth could be kept constant for all time points which indicates no further solidification due to the formation of new crosslinks. The Young's moduli for the gelatin-based hydrogels were in general lesser than HA hydrogels (except 2 wt%), even with the highest polymer concentration of 7 wt% and longest irradiation time of 60 s. During the storage in PBS GelPA hydrogels also did not shrink compared to the reversibly crosslinked hyaluronic acid hydrogels. This leads to the conclusion that the highest network density was achieved after re-arrangement of the Schiff Base bonds, whereas the network structure in GelPA hydrogels did not change massively after storage in PBS. The gelatin hydrogels accordingly showed a better elastic behavior than the hyaluronic acid hydrogels and were less brittle. Still, the irreversible bond formed by the thiol-ene reaction resulted in stable hydrogels over three weeks also in cell culture media, whereas hydrogels based on Schiff Base chemistry dissolved completely under the cell culture conditions. A possible other application of the HA based hydrogels is based on their time dependent dissolution in cell culture media founded in the reversible binding of the network. This property was already used in an article published by Blum *et al.*, where the HA hydrogels were used as sacrificial coating material to protect modified PCL scaffolds from an enzymatic attack by neutrophiles [362]. One additional aspect for the developed GelPA hydrogels is the choice of the initiator system for light induced crosslinking. In this thesis, the investigation was focused on the Ru/SPS system. Yet, the initiator system containing ruthenium complexes might not fit to all cell types, since ruthenium containing agents have shown a specific potential antitumor activity [347,363]. Other initiators using visible light, such as LAP or riboflavin [249,250], could be investigated in the future to broaden the applicability of GelPA as bioink.

The differences of the two hydrogels are most likely caused by various factors:
1.) size of the crosslinker (small bifunctional molecule versus polymeric 4 arm crosslinker);
2.) crosslinking mechanism (reversible versus irreversible bond formation);
3.) type of biopolymer (polysaccharide vs. polypeptide).

Therefore, hydrogel systems containing both types of biopolymers could be interesting for future investigations. Additionally, a systematic variation of the crosslinker size or the combination of both crosslinking mechanisms might be appealing for further research.

Due to the fast gelation and the stiffness of HA based hydrogels, it was not able to use the system as a bioink. However, these hydrogels can be eventually printed by using extrusion fragmentation, where the bulk hydrogel is fragmented into microgels using mechanic force [115]. The subsequent addition of multifunctional crosslinkers then might stabilies the strand of fractured microgels. To use the HA hydrogel system as bioink, future experiments should focus on a controlled process of microgel fabrication and subsequent fixation of the particles. For GelPA, a printability is already given by the retention of the thermo responsive properties of the native gelatin. However, further improvements are also needed for this bioink, since printing of the lower hydrogel concentrations led to significantly different optical properties than for the casted bulk hydrogels due to occurring micro fissures and fractures, which were caused by the printing of the cooled and partially already gelated precursor solution. In general, the influence of the printing process on hydrogel property should be investigated in more detail to efficiently develop bioinks suitable also for imaging applications.

From the biological point of view, both hydrogel systems were investigated on their impact on chondrogenic differentiation using hMSCs. First, cell viability was investigated and both hydrogels were proven to be cell friendly and biocompatible. For chondrogenesis, both systems were suitable and best results for GAG and collagen production were generally achieved for lower polymer concentrations in the hydrogels. For GelPA, cells however also produced lower amounts of ECM in the 3 wt% compared to the 5 wt% hydrogels, which can be explained by a significant lower network density und resulting loss of produced GAG and collagen out of the much wider hydrogel network. This should be examined in future by also quantifying the released GAG and collagen in the used cell media [355]. During handling, an increase of rigidity was observed for both chondrogenically differentiated hydrogels, which indicates a successful deposition of cartilage ECM. Thus, both systems can be used for further *in vitro* investigations and should be considered as potential new ECM mimetic hydrogels.

For the GelPA system, cell viability was also investigated after printing for different applied cell concentrations. Here, it was further proven that printing at high cell density harms the cells and that the cell concentration of a bioink should be chosen carefully to accomplish the tasks of the ink with the appropriate amount of cells.

Chapter 7

SUMMARY / ZUSAMMENFASSUNG

7.1 Summary

The **focus of this thesis** was to investigate novel synthesis paths for hyaluronic acid (HA) and gelatin derivatives, and study their reproducibility and consistency for the application as biomaterial. The resulting materials were examined regarding their material properties, chemically and physically, pure and as hydrogels in combination with suitable crosslinkers. Biocompatibility and the supportive role of the hydrogels in chondrogenic differentiation were investigated using human mesenchymal stromal cells. Also, gelatin hydrogels were used to observe migration behavior of malignant tumor cells in bulk and printed hydrogels in a side project performed by collaboration partners within the TRR225.

The investigation of the selective oxidation of the primary alcohol group in HA with TEMPO/TCC was described in **chapter 3**. Here, the aim was to establish a reaction to functionalize HA with aldehyde groups without massive alterations for the backbone structure. Even though massive chain degradation occurred during the oxidation reaction, it was possible to increase the degree of oxidation to generate more aldehyde functions for Schiff base crosslinking. The intended higher degree of oxidation resulted in hydrogels which were longer stable in cell culture medium than hydrogels containing the $NaIO_4$ oxidized HA with dialdehyde functionalization, generated together with a ring-opening of the respective saccharide. Thus, the reproducibility of the oxidation was still problematic and needed further improvements in the reaction steps. The influence of the batch-to-batch variation on hydrogel property was investigated using three batches and one blend batch of all three. In cell culture, the hydrogels with TEMPO/TCC oxidized HA showed good cell compatibility and were supportive for hMSCs during chondrogenesis. Due to the possibility of a time dependent dissolution by cause of the reversible Schiff base chemistry, this hydrogel system can be further used as sacrificial material for temporary coatings. Here, the influencing factors on dissolution, e.g. the pH variation or use of hypotonic aqueous solutions should be focus of further investigations. The last possibility of using the hydrogel as sacrificial material by storage in hypotonic buffers has already been investigated in some initial experiments by Carina Blum and the results were published in a research article [362].

After using a polysaccharide as starting biomaterial, gelatin was chosen as an alternative proteinogenic biopolymer. The results of functionalization of gelatin with pentenoate specifically to lysin residues were presented in **chapter 4**. Here, the successful two steps

synthesis of pentenoate modified gelatin (GelPA) was shown with very good reproducibility and in a large scale. The kinetic of the reaction of gelatin with the NHS-ester of pentenoic acid was investigated with regard to the influence of reaction time and amount of modification reagents. Additionally, since mainly the lysin residues of the protein were functionalized, the isoelectrical point of the modified gelatin (GelPA) was determined and compared to the native gelatin. The resulting polymers could be crosslinked with thiol functionalized 4-arm-star-PEG (sPEG) via thiol-ene reaction using a visible light initiator system and the resulting hydrogels were tested on their mechanical properties depending on polymer amounts and irradiation times. Due to the thermo responsive nature of GelPA, the hydrogel precursor solutions with various polymer concentrations were well suited for the application as bioink. For this, the thermal response was investigated with temperature sweeps using rheological measurements. All three concentrations of the precursor solution containing GelPA and sPEG were printed using an extrusion based bioprinter. With the initial printing experiments, the printability of the GelPA/sPEG system was proven, but there is still some room for improvement. Cell viability and migration behavior before and after printing were investigated using human breast cancer cells and the results are not presented in this work.

In order to compare the support of the chondrogenic differentiation of hMSCs between polysaccharide based and proteinogenic biopolymers, GelPA hydrogels were also cultivated with hMSCs and differentiated chondrogenically. Both HA and gelatin-based hydrogels showed excellent support of chondrogenesis, especially when the polymer concentration in the hydrogels was kept quite low. In the future, the hydrogels should be compared directly with each other in cell culture experiments. Additionally, cell viability of hMSCs after printing with 3 different cell concentrations in the GelPA/sPEG bioink was investigated and the results are presented in **chapter 5**. The successful 3D bioprinting with hMSCs and the influence of cell density on cell viability was demonstrated.

7.2 Zusammenfassung

Der **Fokus dieser Doktorarbeit** lag auf der Untersuchung neuer Synthesewege für Hyaluronsäure- und Gelatinederivate sowie die Untersuchung derer Reproduzierbarkeit und Beständigkeit für die Anwendung als Biomaterial. Die daraus resultierten Materialien wurden auf ihre Materialeigenschaften, sowohl chemisch als auch physikalisch, als Rohmaterial und als Hydrogele in Kombination mit Vernetzern untersucht. Die Biokompatibilität und unterstützende Rolle der Hydrogele während der chondrogenen Differenzierung wurde mit menschlichen mesenchymale Stromazellen (hMSCs) untersucht. Gelatine basierte Hydrogele wurden in einem Nebenprojekt in Zusammenarbeit mit Kooperationspartnern von TRR225 auch zur Beobachtung von Migrationsverhalten von bösartigen Tumorzellen in Bulkhydrogele und als gedruckte Hydrogele eingesetzt.

Die Untersuchung der selektiven Oxidation der primären Alkoholgruppe in Hyaluronsäure mit TEMPO/TCC wurde in **Kapitel 3** beschrieben. Das Ziel dabei war eine Reaktion einzuführen, die die Hyaluronsäure mit Aldehydgruppen funktionalisiert, ohne massive Änderung der Hauptstrangstruktur. Auch wenn starken Kettenabbau während der Oxidationsreaktion stattfand, war es möglich den Oxidationsgrad zu erhöhen, sodass mehr Aldehydfunktionen für die Vernetzung über Schiffsche Base generiert wurde. Die Erhöhung des Oxidationsgrades resultierte in Hydrogele, die länger in Zellkulturmedium stabil waren als Hydrogele, die $NaIO_4$-oxidierte Hyaluronsäure mit einer Dialdehydfunktionalisierung enthielten, die über eine Ringöffnung der betroffenen Saccharideinheit entstanden sind. Dennoch war die Reproduzierbarkeit der Oxidation immer noch problematisch und hier bedarf es in Zukunft noch Verbesserung der Reaktionsschritte. Der Einfluss dieser Änderung zwischen den einzelnen Chargen auf die Hydrogeleigenschaften wurde untersucht, indem drei verschiedenen Chargen einzeln und vermengt untersucht wurden. In der Zellkultur zeigten die TEMPO/TCC oxidierten Hyaluronsäure gute Zellkompatibilität und unterstützten die hMSCs während der Chondrogenese. Aufgrund der Möglichkeit, dass die Hydrogele sich in Abhängigkeit von der Zeit auflösen können wegen der Reversibilität der Schiffschen Base, könnte dieses Hydrogelsystem als Opfermaterial für temporäre Beschichtung genutzt werden. Hier sollten in weiterführenden Untersuchungen die Faktoren, die die Auflösung beeinflussen können, untersucht werden, wie zum Beispiel die pH-Wertänderung oder der Einsatz von hypotonen wässrigen Lösungen. Die zuletzt genannte Möglichkeit, das Hydrogel als Opfermaterial zu nutzen, indem es in hypotonen Pufferlösungen gelagert wird, wurde bereits in einigen anfänglichen Experimenten von Carina Blum untersucht und die Ergebnisse in einem wissenschaftlichen Artikel veröffentlicht.

Nachdem ein Polysaccharid als Ausgangmaterial genutzt wurde, wurde Gelatine als alternatives proteinogenes Biopolymere ausgewählt. Die Ergebnisse der spezifischen Funktionalisierung von Gelatine mit Pentenoat an Lysinreste sind in **Kapitel 4** dargestellt. Darin wurde die erfolgreiche Synthese von Pentenoat-modifizierte Gelatine (GelPA) in zwei Schritten mit sehr guter Reproduzierbarkeit und in großem Maßstab gezeigt. Die Kinetik der Reaktion von Gelatine mit NHS-Ester der Pentensäure wurde auf den Einfluss durch die Reaktionszeit und der Menge des eingesetzten Modifikationsreagenzes untersucht. Da hauptsächlich die Lysinreste der Gelatine funktionalisiert wurden, wurde zusätzlich der isoelektrische Punkt der modifizierten Gelatine (GelPA) bestimmt und mit dem der nativen Gelatine verglichen. Für Hydrogele wurde GelPA mit Thiol-funktionalisiertem 4-Arm-Stern-PEG (sPEG) über Thiol-En-Reaktion mit Hilfe eines Initiatorsystems, das über sichtbares Licht aktiviert wird, vernetzt. Die Hydrogele wurden auf ihre mechanischen Eigenschaften in Abhängigkeit vom Polymergehalt und von der Belichtungszeit untersucht. Aufgrund der thermoresponsiven Eigenschaft von GelPA waren die Präkursorlösungen mit unterschiedlichen Polymerkonzentrationen für die Anwendung als Biotinte gut geeignet. Dafür wurde die Thermoresponsibilität durch Temperatur-Sweeps mit Hilfe von rheologischen Messungen untersucht. Alle drei getesteten Konzentrationen der Präkursorlösung mit GelPA und sPEG wurden mit einem Extrusionsbiodrucker gedruckt. Mit den ersten Druckexperimenten konnte die Druckbarkeit von GelPA /sPEG-System gezeigt werden, jedoch ist diese noch verbesserungsfähig. Die Viabilität und das Migrationsverhalten von Zellen vor und nach dem Druck wurden mit Hilfe von menschlichen Brustkrebszellen untersucht.

Um einen Vergleich zwischen Polysaccharid- und proteinogen basierte Polymere in deren unterstützenden Funktion während der chondrogenen Differenzierung zu bekommen, wurden GelPA-Hydrogele auch mit hMSCs kultiviert und zusätzlich chondrogen differenziert. Sowohl Hyaluronsäure- also auch Gelatine-basierte Hydrogele zeigten hervorragende unterstützende Eigenschaften für die Chondrogenese, insbesondere wenn die Polymerkonzentration in den Hydrogelen niedrig gehalten wurde. In Zukunft sollten beide Hydrogel in Zellversuche direkt miteinander verglichen werden. Zusätzlich wurde auch die

Zellviabilität mit drei unterschiedlichen Zellkonzentrationen in der GelPA/sPEG Biotinte nachdem Drucken untersucht und die Ergebnisse wurden in **Kapitel 5** vorgestellt. Der erfolgreiche 3D-Biodruck mit hMSCs und der Einfluss der Zelldichte auf die Zellviabilität konnten gezeigt werden.

Chapter 8

REFERENCES

[1] L.G. Griffith, G. Naughton, *Science* **2002**, *295*(5557) 1009-1014.

[2] C.A. Vacanti, *J. Cell Mol. Med.* **2006**, *10*(3) 569-576.

[3] S. Parveen, K. Krishnakumar, S. Sahoo, *J. Stem Cells Regen. Med.* **2006**, *1*(1) 8-24.

[4] A. Persidis, *Nat. Biotechnol.* **1999**, *17*(5) 508-510.

[5] A. Shafiee, A. Atala, *Annu. Rev. Med.* **2017**, *68*(1) 29-40.

[6] K.Y. Lee, D.J. Mooney, *Chem. Rev.* **2001**, *101*(7) 1869-1880.

[7] M.W. Tibbitt, K.S. Anseth, *Biotechnol. Bioeng.* **2009**, *103*(4) 655-663.

[8] M. Gelinsky, in *3D Bioprinting for Reconstructive Surgery*, (Eds: D.J. Thomas, Z.M. Jessop, I.S. Whitaker), Woodhead Publishing **2018**, 125-136.

[9] B.-S. Kim, D.J. Mooney, *Trends Biotechnol.* **1998**, *16*(5) 224-230.

[10] J. Groll, T. Boland, T. Blunk, J.A. Burdick, D.-W. Cho, P.D. Dalton, B. Derby, G. Forgacs, Q. Li, V. Mironov, A., L. Moroni, M. Nakamura, W. Shu, S. Takeuchi, G. Vozzi, T.B.F. Woodfield, T. Xu, J.J. Yoo, J. Malda, *Biofabrication* **2016**, *8*(1) 013001.

[11] M. Fritz, A.M. Belcher, M. Radmacher, D.A. Walters, P.K. Hansma, G.D. Stucky, D.E. Morse, S. Mann, *Nature* **1994**, *371*(6492) 49-51.

[12] H. Fong, S.N. White, M.L. Paine, W. Luo, M.L. Snead, M. Sarikaya, *J. Bone Miner. Res.* **2003**, *18*(11) 2052-2059.

[13] P.S. Gungor-Ozkerim, I. Inci, Y.S. Zhang, A. Khademhosseini, M.R. Dokmeci, *Biomater. Sci.* **2018**, *6*(5) 915-946.

[14] T. Jungst, W. Smolan, K. Schacht, T. Scheibel, J. Groll, *Chem. Rev.* **2016**, *116*(3) 1496-1539.

[15] J. Groll, J.A. Burdick, D.-W. Cho, B. Derby, M. Gelinsky, S.C. Heilshorn, T. Juengst, J. Malda, V.A. Mironov, K. Nakayama, A. Ovsianikov, W. Sun, S. Takeuchi, J.J. Yoo, T.B.F. Woodfield, *Biofabrication* **2019**, *11* 013001.

[16] S.V. Murphy, A. Atala, *Nat. Biotechnol.* **2014**, *32*(8) 773-785.

[17] A.M. Vladimir, N. Reis, D. Brian, *Tissue Eng.* **2006**, *12*(4) 631-634.

[18] I.T. Ozbolat, W. Peng, V. Ozbolat, *Drug Discovery Today* **2016**, *21*(8) 1257-1271.

[19] G. Gao, A.F. Schilling, T. Yonezawa, J. Wang, G. Dai, X. Cui, *Biotechnol. J.* **2014**, *9*(10) 1304-1311.

[20] T. Xu, C. Baicu, M. Aho, M. Zile, T. Boland, *Biofabrication* **2009**, *1*(3) 035001.

[21] X. Cui, K. Breitenkamp, M.G. Finn, M. Lotz, D.D. D'Lima, *Tissue Eng Part A* **2012**, *18*(11-12) 1304-1312.

[22] A. Faulkner-Jones, C. Fyfe, D.-J. Cornelissen, J. Gardner, J. King, A. Courtney, W. Shu, *Biofabrication* **2015**, *7*(4) 044102.

[23] L. Horváth, Y. Umehara, C. Jud, F. Blank, A. Petri-Fink, B. Rothen-Rutishauser, *Sci. Rep.* **2015**, *5*(1) 7974.

[24] Y.-B. Lee, S. Polio, W. Lee, G. Dai, L. Menon, R.S. Carroll, S.-S. Yoo, *Exp. Neurol.* **2010**, *223*(2) 645-652.

[25] V. Lee, G. Singh, J.P. Trasatti, C. Bjornsson, X. Xu, T.N. Tran, S.S. Yoo, G. Dai, P. Karande, *Tissue Eng. Part C Methods* **2014**, *20*(6) 473-484.

[26] S. Vijayavenkataraman, J.Y.H. Fuh, W.F. Lu, *Bioeng.* **2017**, *4*(3) 63.

[27] M. Jafarkhani, Z. Salehi, A. Aidun, M.A. Shokrgozar, *Iran Biomed. J.* **2019**, *23*(1) 9-20.

[28] Y. Zhang, Y. Yu, I.T. Ozbolat, *J. Nanotechnol. Eng. Med.* **2013**, *4*(2) 0210011-0210017.

[29] Y. Yu, Y. Zhang, J.A. Martin, I.T. Ozbolat, *J. Biomech. Eng.* **2013**, *135*(9) 91011.

[30] K. Christensen, C. Xu, W. Chai, Z. Zhang, J. Fu, Y. Huang, *Biotechnol. Bioeng.* **2015**, *112*(5) 1047-1055.

[31] A. Blaeser, D.F. Duarte Campos, M. Weber, S. Neuss, B. Theek, H. Fischer, W. Jahnen-Dechent, *BioRes. Open Access* **2013**, *2*(5) 374-384.

[32] R. Xiong, Z. Zhang, W. Chai, Y. Huang, D.B. Chrisey, *Biofabrication* **2015**, *7* 045011.

[33] N. Noor, A. Shapira, R. Edri, I. Gal, L. Wertheim, T. Dvir, *Adv. Sci.* **2019**, *6*(11) 1900344.

[34] H. Geckil, F. Xu, X. Zhang, S. Moon, U. Demirci, *Nanomedicine* **2010**, *5*(3) 469-484.

[35] M.E. Cooke, S.W. Jones, B. ter Horst, N. Moiemen, M. Snow, G. Chouhan, L.J. Hill, M. Esmaeli, R.J.A. Moakes, J. Holton, R. Nandra, R.L. Williams, A.M. Smith, L.M. Grover, *Adv. Mater.* **2018**, *30*(14) 1705013.

[36] M.S. Jhon, J.D. Andrade, *J. Biomed. Mater. Res.* **1973**, *7*(6) 509-522.

[37] R.O. Hynes, *Science* **2009**, *326*(5957) 1216-1219.

[38] C. Frantz, K.M. Stewart, V.M. Weaver, *J. Cell. Sci.* **2010**, *123*(24) 4195-4200.

[39] A.D. Theocharis, S.S. Skandalis, C. Gialeli, N.K. Karamanos, *Adv. Drug Delivery Rev.* **2016**, *97* 4-27.

[40] K.C. Clause, T.H. Barker, *Current Opinion in Biotechnology* **2013**, *24*(5) 830-833.

[41] T.J. McKee, G. Perlman, M. Morris, S.V. Komarova, *Sci. Rep.* **2019**, *9*(1) 10542.

[42] R.V. Iozzo, L. Schaefer, *Matrix Biol.* **2015**, *42* 11-55.

[43] D. Vigetti, E. Karousou, M. Viola, S. Deleonibus, G. De Luca, A. Passi, *Biochim. Biophys. Acta* **2014**, *1840*(8) 2452-2459.

[44] G. Karsenty, R.W. Park, *Int. Rev. Immunol.* **1995**, *12*(2-4) 177-185.

[45] S.M. Mithieux, A.S. Weiss, in *Advances in Protein Chemistry*, (Eds: D. Parry, J. Squire), Academic Press **2005**, 437-461.

[46] Y. Mao, J.E. Schwarzbauer, *Matrix Biol.* **2005**, *24*(6) 389-399.

[47] R. Timpl, H. Rohde, P.G. Robey, S.I. Rennard, J.M. Foidart, G.R. Martin, *J. Biol. Chem.* **1979**, *254*(19) 9933-9937.

[48] T. Rozario, D.W. DeSimone, *Dev. Biol.* **2010**, *341*(1) 126-140.

[49] J.L. Drury, D.J. Mooney, *Biomaterials* **2003**, *24*(24) 4337-4351.

[50] S. Bhatia, *Natural Polymers vs Synthetic Polymer*, Springer, Cham (Switzerland), **2016**, 95-118.

[51] C.A. DeForest, K.S. Anseth, *Annu. Rev. Chem. Biomol. Eng.* **2012**, *3*(1) 421-444.

[52] J. Malda, J. Visser, F.P. Melchels, T. Jüngst, W.E. Hennink, W.J.A. Dhert, J. Groll, D.W. Hutmacher, *Adv. Mater.* **2013**, *25*(36) 5011-5028.

[53] A.S. Asghari Adib, A.; Shahhosseini, M.; Simeunovic A.; Wu, S.; Castro, C. E.; Zhao, R.; Khademhosseini, A.; Hoelzle, D.J. , *Biofabrication* **2020**, *12*(4) 045006.

[54] S. Bertlein, G. Brown, K. Lim, T. Jungst, T. Böck, T. Blunk, J. Tessmar, G. J. Hooper, T. Woodfield, J. Groll, *Adv. Mater.* **2017**, *29*(44) 1703404.

[55] I. Rault, V. Frei, D. Herbage, N. Abdul-Malak, A. Huc, *J. Mater. Sci. Mater. Med.* **1996**, *7*(4) 215-221.

[56] M.D. Brigham, A. Bick, E. Lo, A. Bendali, A.B. Jason, A. Khademhosseini, *Tissue Eng. Part A* **2009**, *15*(7) 1645-1653.

[57] W. Ding, J. Zhou, Y. Zeng, Y.-n. Wang, B. Shi, *Carbohydr. Polym.* **2017**, *157* 1650-1656.

[58] F. Croisier, C. Jérôme, *Eur. Polym. J.* **2013**, *49*(4) 780-792.

[59] B. Yue, *J. Glaucoma* **2014**, *23*(8) 20-23.

[60] A. Padhi, A.S. Nain, *Ann. Biomed. Eng.* **2020**, *48*(3) 1071-1089.

[61] A. Peloso, L. Urbani, P. Cravedi, R. Katari, P. Maghsoudlou, M.E. Fallas, V. Sordi, A. Citro, C. Purroy, G. Niu, J.P. McQuilling, S. Sittadjody, A.C. Farney, S.S. Iskandar, J.P. Zambon, J. Rogers, R.J. Stratta, E.C. Opara, L. Piemonti, C.M. Furdui, S. Soker, P. De Coppi, G. Orlando, *Ann. Surg.* **2016**, *264*(1) 169-179.

[62] A.J. Engler, S. Sen, H.L. Sweeney, D.E. Discher, *Cell* **2006**, *126*(4) 677-689.

[63] C.J. Little, N.K. Bawolin, X. Chen, *Tissue Eng. Part B Rev.* **2011**, *17*(4) 213-227.

[64] R.S. Tuan, A.F. Chen, B.A. Klatt, *J. Am. Acad. Orthop. Surg.* **2013**, *21*(5) 303-311.

[65] J. Hazur, R. Detsch, E. Karakaya, J. Kaschta, J. Teßmar, D. Schneidereit, O. Friedrich, D.W. Schubert, A.R. Boccaccini, *Biofabrication* **2020**, *12*(4) 045004.

[66] S. Shen, J. Shen, H. Shen, C. Wu, P. Chen, Q. Wang, *Front. Chem.* **2020**, *8*(36) 1-10.

[67] L.L. Wang, C.B. Highley, Y.C. Yeh, J.H. Galarraga, S. Uman, J.A. Burdick, *J. Biomed. Mater. Res. A* **2018**, *106*(4) 865-875.

[68] M.E. Cooke, D.H. Rosenzweig, *APL Bioeng.* **2021**, *5*(1) 011502.

[69] B.A. Aguado, W. Mulyasasmita, J. Su, K.J. Lampe, S.C. Heilshorn, *Tissue Eng. Part A* **2012**, *18*(7-8) 806-815.

[70] R. Chang, J. Nam, W. Sun, *Tissue Eng. Part A* **2008**, *14*(1) 41-48.

[71] N.C. Crawford, L.B. Popp, K.E. Johns, L.M. Caire, B.N. Peterson, M.W. Liberatore, *J. Colloid Interface Sci.* **2013**, *396* 83-89.

[72] J. Kim, J.-Y. Chang, Y.-Y. Kim, M.-J. Kim, H.-S. Kho, *Arch. Oral Biol.* **2018**, *89* 55-64.

[73] A. Blaeser, D.F. Duarte Campos, U. Puster, W. Richtering, M.M. Stevens, H. Fischer, *Adv. Healthcare Mater.* **2016**, *5*(3) 326-333.

[74] S.J. Müller, E. Mirzahossein, E.N. Iftekhar, C. Bächer, S. Schrüfer, D.W. Schubert, B. Fabry, S. Gekle, *PLoS One* **2020**, *15*(7) e0236371.

[75] J. Mewis, N.J. Wagner, *Adv. Colloid Interface Sci.* **2009**, *147-148* 214-227.

[76] M.M. Cross, *J. Colloid Sci.* **1965**, *20*(5) 417-437.

[77] G. Yang, Z. Xiao, X. Ren, H. Long, H. Qian, K. Ma, Y. Guo, *PeerJ* **2016**, *4* e2497.

[78] M. Norouzi, B. Nazari, D.W. Miller, *Drug Discovery Today* **2016**, *21*(11) 1835-1849.

[79] L. García-Fernández, M. Olmeda-Lozano, L. Benito-Garzón, A. Pérez-Caballer, J. San Román, B. Vázquez-Lasa, *Mater. Sci. Eng. C* **2020**, *110* 110702.

[80] Y.-J. Seol, H.-W. Kang, S.J. Lee, A. Atala, J.J. Yoo, *Eur. J. Cardio-Thorac. Surg.* **2014**, *46*(3) 342-348.

[81] D. Ji, S. Choi, J. Kim, *Small* **2018**, *14*(26) 1801042.

[82] L. Zhou, H. Ramezani, M. Sun, M. Xie, J. Nie, S. Lv, J. Cai, J. Fu, Y. He, *Biomater. Sci.* **2020**, *8*(18) 5020-5028.

[83] S. Liu, A.K. Bastola, L. Li, *ACS Appl. Mater. Interfaces* **2017**, *9*(47) 41473-41481.

[84] M. Weis, J. Shan, M. Kuhlmann, T. Jungst, J. Tessmar, J. Groll, *Gels (Basel, Switzerland)* **2018**, *4*(4) 82.

[85] C. Xu, G. Dai, Y. Hong, *Acta Biomater.* **2019**, *95* 50-59.

[86] V. Guryča, R. Hobzová, M. Přádný, J. Širc, J. Michálek, *Cont. Lens Anterior Eye* **2007**, *30*(4) 215-222.

[87] S. Shahzad, M. Yar, S.A. Siddiqi, N. Mahmood, A. Rauf, Z.-u.-A. Qureshi, M.S. Anwar, S. Afzaal, *J. Mater. Sci. Mater. Med.* **2015**, *26*(3) 136.

[88] A. Motta, C. Migliaresi, F. Faccioni, P. Torricelli, M. Fini, R. Giardino, *J. Biomater. Sci. Polym. Ed.* **2004**, *15*(7) 851-864.

[89] L. Huang, C. Li, W. Yuan, G. Shi, *Nanoscale* **2013**, *5*(9) 3780-3786.

[90] Y. Luo, K.R. Kirker, G.D. Prestwich, *J. Control. Release* **2000**, *69*(1) 169-184.

[91] H. Najaf Zadeh, T. Huber, V. Nock, C. Fee, D. Clucas, *Bioeng.* **2020**, *7*(2) 58.

[92] A.W. Justin, R.A. Brooks, A.E. Markaki, *J. R. Soc. Interface* **2016**, *13*(125) 20160768.

[93] S. Das, B. Basu, *Indian Inst. Sci* **2019**, *99* 405-428.

[94] L. Ning, X. Chen, *Biotechnol. J.* **2017**, *12*(8) 1600671.

[95] S. Kyle, Z.M. Jessop, A. Al-Sabah, I.S. Whitaker, *Adv. Healthcare Mater.* **2017**, *6*(16) 1700264.

[96] J.K. Placone, A.J. Engler, *Adv. Healthcare Mater.* **2018**, *7*(8) 1701161.

[97] R. Suntornnond, E.Y.S. Tan, J. An, C.K. Chua, *Mater.* **2016**, *9*(9) 756.

[98] W. Liu, Y.S. Zhang, M.A. Heinrich, F. De Ferrari, H.L. Jang, S.M. Bakht, M.M. Alvarez, J. Yang, Y.-C. Li, G. Trujillo-de Santiago, A.K. Miri, K. Zhu, P. Khoshakhlagh, G. Prakash, H. Cheng, X. Guan, Z. Zhong, J. Ju, G.H. Zhu, X. Jin, S.R. Shin, M.R. Dokmeci, A. Khademhosseini, *Adv. Mater.* **2017**, *29*(3) 1604630.

[99] D. Chimene, K.K. Lennox, R.R. Kaunas, A.K. Gaharwar, *Ann. Biomed. Eng.* **2016**, *44*(6) 2090-2102.

[100] M. Müller, J. Becher, M. Schnabelrauch, M. Zenobi-Wong, *Biofabrication* **2015**, *7*(3) 035006.

[101] S. Stichler, T. Jungst, M. Schamel, I. Zilkowski, M. Kuhlmann, T. Böck, T. Blunk, J. Tessmar, J. Groll, *Ann. Biomed. Eng.* **2016**, *45*(1) 273-285.

[102] D. Petta, U. D’Amora, L. Ambrosio, D.W. Grijpma, D. Eglin, M. D’Este, *Biofabrication* **2020**, *12*(3) 032001.

[103] J. Ku, H. Seonwoo, S. Park, K.-J. Jang, J. Lee, M. Lee, J.W. Lim, J. Kim, J.H. Chung, *Appl. Sci.* **2020**, *10*(7) 2455.

[104] W. Kim, C.H. Jang, G.H. Kim, *Nano Lett.* **2019**, *19*(12) 8612-8620.

[105] W. Liu, M.A. Heinrich, Y. Zhou, A. Akpek, N. Hu, X. Liu, X. Guan, Z. Zhong, X. Jin, A. Khademhosseini, Y.S. Zhang, *Adv. Healthcare Mater.* **2017**, *6*(12) 1601451.

[106] S.H. Kim, Y.K. Yeon, J.M. Lee, J.R. Chao, Y.J. Lee, Y.B. Seo, M.T. Sultan, O.J. Lee, J.S. Lee, S.-i. Yoon, I.-S. Hong, G. Khang, S.J. Lee, J.J. Yoo, C.H. Park, *Nat. Commun.* **2018**, *9*(1) 1620.

[107] A. Abbadessa, V.H.M. Mouser, M.M. Blokzijl, D. Gawlitta, W.J.A. Dhert, W.E. Hennink, J. Malda, T. Vermonden, *Biomacromolecules* **2016**, *17*(6) 2137-2147.

[108] S.A. Othman, C.F. Soon, N.L. Ma, K.S. Tee, G.P. Lim, M. Morsin, M.K. Ahmad, A.I. Abdulmaged, S.C. Cheong, *Polym. Bull.* **2020**, *78* 6115-6135.

[109] Y.P. Singh, A. Bandyopadhyay, B.B. Mandal, *ACS Appl. Mater. Interfaces* **2019**, *11*(37) 33684-33696.

[110] P. Thayer, H. Martinez, E. Gatenholm, in *3D Printing. Methods in Molecular Biology*, (Eds: J. Crook), Humana, New York, NY, **2020**, 3-18.

[111] B.G. Soliman, G.C.J. Lindberg, T. Jungst, G.J. Hooper, J. Groll, T.B.F. Woodfield, K.S. Lim, *Adv Healthc Mater* **2020**, *9*(15) e1901544.

[112] A.C. Daly, L. Riley, T. Segura, J.A. Burdick, *Nat. Rev. Mater.* **2020**, *5*(1) 20-43.

[113] D. Dendukuri, K. Tsoi, T.A. Hatton, P.S. Doyle, *Langmuir* **2005**, *21*(6) 2113-2116.

[114] S. Sohrabi, N. kassir, M. Keshavarz Moraveji, *RSC Adv.* **2020**, *10*(46) 27560-27574.

[115] V.G. Muir, T.H. Qazi, J. Shan, J. Groll, J.A. Burdick, *ACS Biomater Sci Eng* **2021**, *7*(9) 4269-4281.

[116] C.B. Highley, K.H. Song, A.C. Daly, J.A. Burdick, *Adv. Sci.* **2019**, *6*(1) 1801076.

[117] E. Sideris, D.R. Griffin, Y. Ding, S. Li, W.M. Weaver, D. Di Carlo, T. Hsiai, T. Segura, *ACS Biomater. Sci. Eng.* **2016**, *2*(11) 2034-2041.

[118] D.L. Kaplan, in *Macromolecular Systems - Materials Approach*, (Eds: D.L. Kaplan), Springer, Berlin, Heidelberg, **1998**, 1-29.

[119] R. Rebelo, M. Fernandes, R. Fangueiro, *Procedia Eng.* **2017**, *200* 236-243.

[120] M.G. Rao, P. Bharathi, R. Akila, *Sci. Revs. Chem. Commun* **2014**, *4*(2) 61-68.

[121] S.O. Andersen, T. Weis-Fogh, in *Advances in Insect Physiology*, (Eds: J.W.L. Beament, J.E. Treherne, V.B. Wigglesworth), Academic Press **1964**, 1-65.

[122] L. Day, M.A. Augustin, I.L. Batey, C.W. Wrigley, *Trends Food Sci. Technol.* **2006**, *17*(2) 82-90.

[123] H.E. Swaisgood, *Int. J. Dairy Sci.* **1993**, *76*(10) 3054-3061.

[124] T. Peters, in *Advances in Protein Chemistry*, (Eds: C.B. Anfinsen, J.T. Edsall, F.M. Richards), Academic Press **1985**, 161-245.

[125] C.S.K. Reddy, R. Ghai, Rashmi, V.C. Kalia, *Bioresour. Technol.* **2003**, *87*(2) 137-146.

[126] R.E. Drumright, P.R. Gruber, D.E. Henton, *Adv. Mater.* **2000**, *12*(23) 1841-1846.

[127] Y. Farag, C. Leopold, *Dissolut. Technol.* **2009**, *16* 33-39.

[128] H. Mooibroek, K. Cornish, *Appl. Microbiol. Biotechnol.* **2000**, *53*(4) 355-365.

[129] B. Balakrishnan, R. Banerjee, *Chem. Rev.* **2011**, *111*(8) 4453-4474.

[130] L. Meng, F. Xie, B. Zhang, D.K. Wang, L. Yu, *ACS Sustainable Chem. Eng.* **2019**, *7*(2) 2792-2802.

[131] S. Bencherif, O. Gsib, C. Egles, *J. Mol. Biol. Biotech* **2017**, *2*(1) 3.

[132] T. Andersen, P. Auk-Emblem, M. Dornish, *Microarrays* **2015**, *4*(2) 133-161.

[133] B.H. Lee, H. Shirahama, N.-J. Cho, L.P. Tan, *RSC Adv.* **2015**, *5*(128) 106094-106097.

[134] X. Zhang, Y. Yang, J. Yao, Z. Shao, X. Chen, *ACS Sustainable Chem. Eng.* **2014**, *2*(5) 1318-1324.

[135] N. Reddy, R. Reddy, Q. Jiang, *Trends Biotechnol* **2015**, *33*(6) 362-369.

[136] K. Yue, G. Trujillo-de Santiago, M.M. Alvarez, A. Tamayol, N. Annabi, A. Khademhosseini, *Biomaterials* **2015**, *73* 254-271.

[137] B. ter Horst, N.S. Moiemen, L.M. Grover, in *Biomaterials for Skin Repair and Regeneration*, (Eds: E. García-Gareta), Woodhead Publishing **2019**, 151-192.

[138] K. Meyer, J.W. Palmer, *J. Biol. Chem.* **1934**, *107*(3) 629-634.

[139] R.D. Price, M.G. Berry, H.A. Navsaria, *J. Plast. Reconstr. Aesthet. Surg.* **2007**, *60*(10) 1110-1119.

[140] J. Necas, L. Bartosikova, P. Brauner, J. Kolar, *Vet. Med.* **2008**, *53*(8) 397-411.

[141] J.A. Burdick, G.D. Prestwich, *Adv. Mater.* **2011**, *23*(12) H41-H56.

[142] E.D.T. Atkins, J.K. Sheehan, *Nat. New Biol.* **1972**, *235*(60) 253-254.

[143] P.D. Ward, S.L. Thibeault, S.D. Gray, *J. Voice* **2002**, *16*(3) 303-309.

[144] M.K. Cowman, S. Matsuoka, *Carbohydr. Res.* **2005**, *340*(5) 791-809.

[145] L. Ambrosio, A. Borzacchiello, P.A. Netti, L. Nicolais, *J. Macromol. Sci. A* **1999**, *36*(7-8) 991-1000.

[146] M.N. Collins, C. Birkinshaw, *J. Mater. Sci. Mater. Med.* **2008**, *19*(11) 3335-3343.

[147] J.W. Kuo, D.A. Swann, G.D. Prestwich, *Bioconjugate Chem.* **1991**, *2*(4) 232-241.

[148] L.B. Dahl, T.C. Laurent, B. Smedsrød, *Anal. Biochem.* **1988**, *175*(2) 397-407.

[149] A. Bignami, M. Hosley, D. Dahl, *Anat. Embryol.* **1993**, *188*(5) 419-433.

[150] R.J. Peach, D. Hollenbaugh, I. Stamenkovic, A. Aruffo, *J. Cell Biol.* **1993**, *122*(1) 257-264.

[151] D. Bhattacharya, D. Svechkarev, J.J. Souchek, T.K. Hill, M.A. Taylor, A. Natarajan, A.M. Mohs, *J. Mater. Chem. B* **2017**, *5*(41) 8183-8192.

[152] A. Lee, S.E. Grummer, D. Kriegel, E. Marmur, *Dermatol. Surg.* **2010**, *36*(7) 1071-1077.

[153] E. Payan, J.Y. Jouzeau, F. Lapicque, N. Muller, P. Netter, *Int. Rev. Immunol.* **1993**, *25*(3) 325-329.

[154] Y. Tokita, A. Okamoto, *Polym. Degrad. Stab.* **1995**, *48*(2) 269-273.

[155] Y. Tokita, K. Ohshima, A. Okamoto, *Polym. Degrad. Stab.* **1997**, *55*(2) 159-164.

[156] A.e.-r. Tamer, in *Engineering of Polymers and Chemical Complexity*, (Eds: W.F. Walter, H.-J. Radusch), Apple Academic **2014**, 107-144.

[157] P. Andre, *Semin. Cutan. Med. Surg.* **2004**, *23*(4) 218-222.

[158] K.L. Goa, P. Benfield, *Drugs* **1994**, *47*(3) 536-566.

[159] C. Longinotti, *Burn. Trauma* **2014**, *2*(4) 162-168.

[160] V. Nobile, D. Buonocore, A. Michelotti, F. Marzatico, *J. Cosmet. Dermatol.* **2014**, *13*(4) 277-287.

[161] T. Pavicic, G.G. Gauglitz, P. Lersch, K. Schwach-Abdellaoui, B. Malle, H.C. Korting, M. Farwick, *J Drugs Dermatol* **2011**, *10*(9) 990-1000.

[162] S.N.A. Bukhari, N.L. Roswandi, M. Waqas, H. Habib, F. Hussain, S. Khan, M. Sohail, N.A. Ramli, H.E. Thu, Z. Hussain, *Int. J. Biol. Macromol.* **2018**, *120* 1682-1695.

[163] C.N. Soparkar, J.R. Patrinely, J. Tschen, *Ophthalmic Plast Reconstr Surg* **2004**, *20*(4) 317-336.

[164] E.A. Balazs, J.L. Denlinger, *J Rheumatol Suppl* **1993**, *39* 3-9.

[165] E.A. Balazs, D. Watson, I.F. Duff, S. Roseman, *Arthritis & Rheumatism* **1967**, *10*(4) 357-376.

[166] M. Litwiniuk, A. Krejner, M.S. Speyrer, A.R. Gauto, T. Grzela, *Wounds* **2016**, *28*(3) 78-88.

[167] E.A. Turley, P.W. Noble, L.Y. Bourguignon, *J. Biol. Chem.* **2002**, *277*(7) 4589-4592.

[168] M.W. Holmes, M.T. Bayliss, H. Muir, *Biochem. J.* **1988**, *250*(2) 435-441.

[169] N. Gerwin, C. Hops, A. Lucke, *Adv. Drug Delivery Rev.* **2006**, *58*(2) 226-242.

[170] M. Akmal, A. Singh, A. Anand, A. Kesani, N. Aslam, A. Goodship, G. Bentley, *J Bone Joint Surg B* **2005**, *87*(8) 1143-1149.

[171] W.S. Toh, T.C. Lim, M. Kurisawa, M. Spector, *Biomaterials* **2012**, *33*(15) 3835-3845.

[172] Y. Liu, X.Z. Shu, G.D. Prestwich, *Tissue Eng.* **2006**, *12*(12) 3405-3416.

[173] M.N. Collins, C. Birkinshaw, *Carbohydr. Polym.* **2013**, *92*(2) 1262-1279.

[174] I.L. Kim, R.L. Mauck, J.A. Burdick, *Biomaterials* **2011**, *32*(34) 8771-8782.

[175] I.J. Haug, K.I. Draget, in *Handbook of Food Proteins*, (Eds: G.O. Phillips, P.A. Williams), Woodhead Publishing **2011**, 92-115.

[176] K.B. Djagny, Z. Wang, S. Xu, *Crit. Rev. Food* **2001**, *41*(6) 481-492.

[177] A.A. Mariod, H. Fadul, *Acta Sci Pol Technol Aliment.* **2013**, *12*(2) 135-147.

[178] J. Poppe, in *Thickening and gelling agents for food*, 1 (Eds: A. Imeson), Springer **1992**, 98-123.

[179] W. Babel, *Chem. Unserer Zeit* **1996**, *30*(2) 86-95.

[180] H. Wang, O.C. Boerman, K. Sariibrahimoglu, Y. Li, J.A. Jansen, S.C.G. Leeuwenburgh, *Biomaterials* **2012**, *33*(33) 8695-8703.

[181] K. Su, C. Wang, *Biotechnol. Lett.* **2015**, *37*(11) 2139-2145.

[182] L. Guo, R.H. Colby, C.P. Lusignan, T.H. Whitesides, *Macromolecules* **2003**, *36*(26) 9999-10008.

[183] J. Ahmed, in *Advances in Food Rheology and Its Applications*, (Eds: J. Ahmed, P. Ptaszek, S. Basu), Woodhead Publishing **2017**, 377-404.

[184] S.M. Tosh, A.G. Marangoni, *Appl. Phys. Lett.* **2004**, *84*(21) 4242-4244.

[185] M. Djabourov, J. Leblond, P. Papon, *J. phys.* **1988**, *49*(2) 333-343.

[186] V. Normand, S. Muller, J.-C. Ravey, A. Parker, *Macromolecules* **2000**, *33*(3) 1063-1071.

[187] A.O. Elzoghby, W.M. Samy, N.A. Elgindy, *J. Control. Release* **2012**, *161*(1) 38-49.

[188] G.V. Rathna, *J Mater Sci Mater Med* **2008**, *19*(6) 2351-2358.

[189] F. Zhang, C. He, L. Cao, W. Feng, H. Wang, X. Mo, J. Wang, *Int. J. Biol. Macromol.* **2011**, *48*(3) 474-481.

[190] S. Dawlee, A. Sugandhi, B. Balakrishnan, D. Labarre, A. Jayakrishnan, *Biomacromolecules* **2005**, *6*(4) 2040-2048.

[191] Y. Fang, R. Takahashi, K. Nishinari, *Biomacromolecules* **2005**, *6*(6) 3202-3208.

[192] Á.J. Leite, B. Sarker, T. Zehnder, R. Silva, J.F. Mano, A.R. Boccaccini, *Biofabrication* **2016**, *8*(3) 035005.

[193] M. Neufurth, X. Wang, H.C. Schröder, Q. Feng, B. Diehl-Seifert, T. Ziebart, R. Steffen, S. Wang, W.E.G. Müller, *Biomaterials* **2014**, *35*(31) 8810-8819.

[194] D. Loessner, C. Meinert, E. Kaemmerer, L.C. Martine, K. Yue, P.A. Levett, T.J. Klein, F.P. Melchels, A. Khademhosseini, D.W. Hutmacher, *Nat. Protoc.* **2016**, *11*(4) 727-746.

[195] T.U.S. Rashid, Sadia; Biswas, Shanta; Ahmed, Tanvir; Mallik, Abul K.; Shahruzzaman, Md.; Sakib, Md. Nurus; Haque, Papia; Rahman, Mohammed Mizanur, in *Polymers and Polymeric Composites: A Reference Series*, (Eds: M. Mondal), Springer, Cham, **2019**, 1601-1641.

[196] W. Schuurman, P.A. Levett, M.W. Pot, P.R. van Weeren, W.J.A. Dhert, D.W. Hutmacher, F.P.W. Melchels, T.J. Klein, J. Malda, *Macromol. Biosci.* **2013**, *13*(5) 551-561.

[197] P.A. Levett, F.P.W. Melchels, K. Schrobback, D.W. Hutmacher, J. Malda, T.J. Klein, *Acta Biomater.* **2014**, *10*(1) 214-223.

[198] P.A. Levett, F.P.W. Melchels, K. Schrobback, D.W. Hutmacher, J. Malda, T.J. Klein, *J. Biomed. Mater. Res. A* **2014**, *102*(8) 2544-2553.

[199] S.R. Shin, B. Aghaei-Ghareh-Bolagh, T.T. Dang, S.N. Topkaya, X. Gao, S.Y. Yang, S.M. Jung, J.H. Oh, M.R. Dokmeci, X. Tang, A. Khademhosseini, *Adv. Mater.* **2013**, *25*(44) 6385-6391.

[200] M.B. Chen, S. Srigunapalan, A.R. Wheeler, C.A. Simmons, *Lab Chip* **2013**, *13*(13) 2591-2598.

[201] N. Annabi, Š. Selimović, J.P. Acevedo Cox, J. Ribas, M. Afshar Bakooshli, D. Heintze, A.S. Weiss, D. Cropek, A. Khademhosseini, *Lab Chip* **2013**, *13*(18) 3569-3577.

[202] W. Hu, Z. Wang, Y. Xiao, S. Zhang, J. Wang, *Biomater. Sci.* **2019**, *7*(3) 843-855.

[203] J. Berger, M. Reist, J.M. Mayer, O. Felt, R. Gurny, *Eur. J. Pharm. Biopharm.* **2004**, *57*(1) 35-52.

[204] C.B. Highley, C.B. Rodell, J.A. Burdick, *Adv. Mater.* **2015**, *27*(34) 5075-5079.

[205] L. Ouyang, C.B. Highley, C.B. Rodell, W. Sun, J.A. Burdick, *ACS Biomater. Sci. Eng.* **2016**, *2*(10) 1743-1751.

[206] C. Hiemstra, L.J. van der Aa, Z. Zhong, P.J. Dijkstra, J. Feijen, *Macromolecules* **2007**, *40*(4) 1165-1173.

[207] A.D. Augst, H.J. Kong, D.J. Mooney, *Macromol. Biosci.* **2006**, *6*(8) 623-633.

[208] P. Sautrot-Ba, N. Razza, L. Breloy, S.A. Andaloussi, A. Chiappone, M. Sangermano, C. Hélary, S. Belbekhouche, T. Coradin, D.L. Versace, *J. Mater. Chem. B* **2019**, *7*(42) 6526-6538.

[209] L.S. Teixeira, J. Feijen, C.A. van Blitterswijk, P.J. Dijkstra, M. Karperien, *Biomaterials* **2012**, *33*(5) 1281-1290.

[210] J. Gopinathan, I. Noh, *J. Tissue Eng. Regen. Med.* **2018**, *15*(5) 531-546.

[211] J. Xu, Y. Liu, S.-h. Hsu, *Molecules* **2019**, *24*(16) 3005.

[212] O. Guaresti, S. Basasoro, K. González, A. Eceiza, N. Gabilondo, *Eur. Polym. J.* **2019**, *119* 376-384.

[213] A.H. Khan, J.K. Cook, W.J. Wortmann III, N.D. Kersker, A. Rao, J.A. Pojman, A.T. Melvin, *J. Biomed. Mater. Res. Part B Appl. Biomater.* **2020**, *108*(5) 2294-2307.

[214] J. Xu, X. Liu, X. Ren, G. Gao, *Eur. Polym. J.* **2018**, *100* 86-95.

[215] J.-Y. Sun, X. Zhao, W.R.K. Illeperuma, O. Chaudhuri, K.H. Oh, D.J. Mooney, J.J. Vlassak, Z. Suo, *Nature* **2012**, *489*(7414) 133-136.

[216] H. Schiff, *Justus Liebigs Ann. Chem.* **1866**, *140*(1) 92-137.

[217] N.E. Hall, B.J. Smith, *J. Phys. Chem A* **1998**, *102*(25) 4930-4938.

[218] E. Erdtman, E.A.C. Bushnell, J.W. Gauld, L.A. Eriksson, *Comput. Theor. Chem.* **2011**, *963*(2) 479-489.

[219] Y. Liu, S.-h. Hsu, *Front. Chem.* **2018**, *6*(449) 1-10.

[220] J. Kalia, R.T. Raines, *Angew. Chem. Int. Ed.* **2008**, *47*(39) 7523-7526.

[221] K.A. Kristiansen, A. Potthast, B.E. Christensen, *Carbohydr. Res.* **2010**, *345*(10) 1264-1271.

[222] J.M. Bobbitt, in *Advances in Carbohydrate Chemistry*, (Eds: M.L. Wolfrom, R.S. Tipson), Academic Press **1956**, 1-41.

[223] C.G. Gomez, M. Rinaudo, M.A. Villar, *Carbohydr. Polym.* **2007**, *67*(3) 296-304.

[224] I.M.N. Vold, B.E. Christensen, *Carbohydr. Res.* **2005**, *340*(4) 679-684.

[225] R. Montgomery, S. Nag, *Biochim. Biophys. Acta* **1963**, *74* 300-302.

[226] E. Maekawa, T. Koshijima, *J. Appl. Polym. Sci.* **1991**, *42*(1) 169-178.

[227] B. Sarker, D.G. Papageorgiou, R. Silva, T. Zehnder, F. Gul-E-Noor, M. Bertmer, J. Kaschta, K. Chrissafis, R. Detsch, A.R. Boccaccini, *J. Mater. Chem. B* **2014**, *2*(11) 1470-1482.

[228] K.H. Bouhadir, D.S. Hausman, D.J. Mooney, *Polymer* **1999**, *40*(12) 3575-3584.

[229] S. Hafeez, H.W. Ooi, F.L.C. Morgan, C. Mota, M. Dettin, C. Van Blitterswijk, L. Moroni, M.B. Baker, *Gels (Basel, Switzerland)* **2018**, *4*(4) 85.

[230] Y.-C. Chen, W.-Y. Su, S.-H. Yang, A. Gefen, F.-H. Lin, *Acta Biomater.* **2013**, *9*(2) 5181-5193.

[231] K.P. Vercruysse, D.M. Marecak, J.F. Marecek, G.D. Prestwich, *Bioconjugate Chem.* **1997**, *8*(5) 686-694.

[232] T. Posner, *Ber. Dtsch. Chem. Ges.* **1905**, *38*(1) 646-657.

[233] A.K. Sinha, D. Equbal, *Asian J. Org. Chem.* **2019**, *8*(1) 32-47.

[234] C.E. Hoyle, T.Y. Lee, T. Roper, *J. Polym. Sci. A Polym. Chem.* **2004**, *42*(21) 5301-5338.

[235] S.K. Reddy, N.B. Cramer, C.N. Bowman, *Macromolecules* **2006**, *39*(10) 3681-3687.

[236] C.R. Morgan, F. Magnotta, A.D. Ketley, *J. Polym. Sci. A Polym. Chem.* **1977**, *15*(3) 627-645.

[237] B.H. Northrop, R.N. Coffey, *J. Am. Chem. Soc.* **2012**, *134*(33) 13804-13817.

[238] C.E. Hoyle, C.N. Bowman, *Angew. Chem. Int. Ed.* **2010**, *49*(9) 1540-1573.

[239] B.D. Mather, K. Viswanathan, K.M. Miller, T.E. Long, *Prog. Polym. Sci.* **2006**, *31*(5) 487-531.

[240] D.P. Nair, M. Podgorski, S. Chatani, T. Gong, W. Xi, C.R. Fenoli, C.N. Bowman, *Chem. Mater.* **2014**, *26*(1) 724-744.

[241] H.C. Kolb, M.G. Finn, K.B. Sharpless, *Angew. Chem. Int. Ed.* **2001**, *40*(11) 2004-2021.

[242] M. Uygun, M.A. Tasdelen, Y. Yagci, *Macromol. Chem. Phys.* **2010**, *211*(1) 103-110.

[243] T.J. McKenzie, P.S. Heaton, K. Rishi, R. Kumar, T. Brunet, G. Beaucage, O. Mondain-Monval, N. Ayres, *Macromolecules* **2020**, *53*(10) 3719-3727.

[244] A. Dondoni, *Angew. Chem. Int. Ed.* **2008**, *47*(47) 8995-8997.

[245] L.A. Sawicki, A.M. Kloxin, *Biomater. Sci.* **2014**, *2*(11) 1612-1626.

[246] M. Bartnikowski, N.J. Bartnikowski, M.A. Woodruff, K. Schrobback, T.J. Klein, *Acta Biomater.* **2015**, *27* 66-76.

[247] B.J. Klotz, D. Gawlitta, A. Rosenberg, J. Malda, F.P.W. Melchels, *Trends Biotechnol* **2016**, *34*(5) 394-407.

[248] J. Dahle, E. Kvam, T. Stokke, *J Carcinog* **2005**, *4* 11.

[249] B.D. Fairbanks, M.P. Schwartz, C.N. Bowman, K.S. Anseth, *Biomaterials* **2009**, *30*(35) 6702-6707.

[250] J. Hu, Y. Hou, H. Park, B. Choi, S. Hou, A. Chung, M. Lee, *Acta Biomater.* **2012**, *8*(5) 1730-1738.

[251] K.S. Lim, B.S. Schon, N.V. Mekhileri, G.C.J. Brown, C.M. Chia, S. Prabakar, G.J. Hooper, T.B.F. Woodfield, *ACS Biomater. Sci. Eng.* **2016**, *2*(10) 1752-1762.

[252] J. Liang, X. Zhang, Z. Chen, S. Li, C. Yan, *Polymers* **2019**, *11*(12) 2102.

[253] S. Stichler, T. Böck, N. Paxton, S. Bertlein, R. Levato, V. Schill, W. Smolan, J. Malda, J. Teßmar, T. Blunk, J. Groll, *Biofabrication* **2017**, *9*(4) 044108.

[254] R. Holmes, X.-B. Yang, A. Dunne, L. Florea, D. Wood, G. Tronci, *Polymers* **2017**, *9*(6) 226.

[255] N. Rajabi, M. Kharaziha, R. Emadi, A. Zarrabi, H. Mokhtari, S. Salehi, *J. Colloid Interface Sci.* **2020**, *564* 155-169.

[256] T.V.C. McOscar, W.M. Gramlich, *Cellulose* **2018**, *25*(11) 6531-6545.

[257] H.W. Ooi, C. Mota, A.T. ten Cate, A. Calore, L. Moroni, M.B. Baker, *Biomacromolecules* **2018**, *19*(8) 3390-3400.

[258] Y. Li, Y. Tan, K. Xu, C. Lu, P. Wang, *Polym. Degrad. Stab.* **2017**, *137* 75-82.

[259] L. Russo, A. Sgambato, R. Visone, P. Occhetta, M. Moretti, M. Rasponi, F. Nicotra, L. Cipolla, *Monatsh. Chem.* **2016**, *147*(3) 587-592.

[260] C.E. Schanté, G. Zuber, C. Herlin, T.F. Vandamme, *Carbohydr. Polym.* **2011**, *85*(3) 469-489.

[261] K. Bergman, C. Elvingson, J. Hilborn, G. Svensk, T. Bowden, *Biomacromolecules* **2007**, *8*(7) 2190-2195.

[262] J.-Y. Lai, *J. Mater. Sci. Mater. Med.* **2013**, *24*(9) 2201-2210.

[263] J. Mergy, A. Fournier, E. Hachet, R. Auzély-Velty, *J. Polym. Sci. A Polym. Chem.* **2012**, *50*(19) 4019-4028.

[264] Z. Mũnoz, H. Shih, C.-C. Lin, *Biomater. Sci.* **2014**, *2*(8) 1063-1072.

[265] N.O. Sonntag, *Chem. Rev.* **1953**, *52*(2) 237-416.

[266] E. van den Bosch, C. Gielens, *Int. J. Biol. Macromol.* **2003**, *32*(3) 129-138.

[267] W.M. Ames, *Chem. Ind.* **1947**, *66*(8) 279-284.

[268] M. Zhu, Y. Wang, G. Ferracci, J. Zheng, N.-J. Cho, B.H. Lee, *Sci. Rep.* **2019**, *9*(1) 6863.

[269] B.F. Lee, M.J. Kade, J.A. Chute, N. Gupta, L.M. Campos, G.H. Fredrickson, E.J. Kramer, N.A. Lynd, C.J. Hawker, *J. Polym. Sci. A Polym. Chem.* **2011**, *49*(20) 4498-4504.

[270] X. Jia, J.A. Burdick, J. Kobler, R.J. Clifton, J.J. Rosowski, S.M. Zeitels, R. Langer, *Macromolecules* **2004**, *37*(9) 3239-3248.

[271] W.-Y. Su, Y.-C. Chen, F.-H. Lin, *Acta Biomater.* **2010**, *6*(8) 3044-3055.

[272] S. Hofmann, C.T. Foo, F. Rossetti, M. Textor, G. Vunjak-Novakovic, D.L. Kaplan, H.P. Merkle, L. Meinel, *J Control Release* **2006**, *111*(1-2) 219-227.

[273] S.A. Sell, M.J. McClure, K. Garg, P.S. Wolfe, G.L. Bowlin, *Advanced Drug Delivery Reviews* **2009**, *61*(12) 1007-1019.

[274] G. Kogan, L. Šoltés, R. Stern, P.J.B.L. Gemeiner, **2007**, *29*(1) 17-25.

[275] S. Gorgieva, V. Kokol, in *Biomaterials applications for nanomedicine*, (Eds: R. Pignatello), InTech **2011**, 17-52.

[276] E.A. Balazs, in *Chemistry and Biology of Hyaluronan*, (Eds: H.G. Garg, C.A. Hales), **2004**, 415-455.

[277] A. Aruffo, I. Stamenkovic, M. Melnick, C.B. Underhill, B. Seed, *Cell* **1990**, *61*(7) 1303-1313.

[278] P. Teriete, S. Banerji, M. Noble, C.D. Blundell, A.J. Wright, A.R. Pickford, E. Lowe, D.J. Mahoney, M.I. Tammi, J.D. Kahmann, I.D. Campbell, A.J. Day, D.G. Jackson, *Mol. Cell* **2004**, *13*(4) 483-496.

[279] M.J. Kujawa, A.I. Caplan, *Dev. Biol.* **1986**, *114*(2) 504-518.

[280] C.G. Pfeifer, A. Berner, M. Koch, W. Krutsch, R. Kujat, P. Angele, M. Nerlich, J. Zellner, *Materials (Basel)* **2016**, *9*(5) 381.

[281] T. Coviello, P. Matricardi, C. Marianecci, F. Alhaique, *J. Control. Release* **2007**, *119*(1) 5-24.

[282] H.J. Lee, G.M. Fernandes-Cunha, D. Myung, *React. Funct. Polym.* **2018**, *131* 29-35.

[283] K.A. Smeds, M.W. Grinstaff, *J. Biomed. Mater. Res.* **2001**, *54*(1) 115-121.

[284] S.-L. Yu, S.-K. Lee, *Mol. Cell. Toxicol.* **2017**, *13*(1) 21-28.

[285] J. Moan, M.J. Peak, *J. Photochem. Photobiol. B: Biol.* **1989**, *4*(1) 21-34.

[286] G.N. Grover, R.L. Braden, K.L. Christman, *Advanced materials (Deerfield Beach, Fla.)* **2013**, *25*(21) 2937-2942.

[287] L. Weng, H. Pan, W. Chen, *J. Biomed. Mater. Res. A* **2008**, *85A*(2) 352-365.

[288] M. Angelin, M. Hermansson, H. Dong, O. Ramström, *Eur. J. Org. Chem.* **2006**, *2006*(19) 4323-4326.

[289] R. Buffa, S. Kettou, L. Pospisilova, G. Huerta-Angeles, D. Chladkova, V. Velebný, Method of Preparation of an Oxidized Derivative of Hyaluronic Acid and a Method of Modification thereof, United States Patent, Contipro Pharma a.s., Dolni Dobrouc, **2016**.

[290] M.Y. Kwon, C. Wang, J.H. Galarraga, E. Puré, L. Han, J.A. Burdick, *Biomaterials* **2019**, *222* 119451.

[291] M.H.M. Oudshoorn, R. Rissmann, J.A. Bouwstra, W.E. Hennink, *Polymer* **2007**, *48*(7) 1915-1920.

[292] J. Schindelin, I. Arganda-Carreras, E. Frise, V. Kaynig, M. Longair, T. Pietzsch, S. Preibisch, C. Rueden, S. Saalfeld, B. Schmid, J.-Y. Tinevez, D.J. White, V. Hartenstein, K. Eliceiri, P. Tomancak, A. Cardona, *Nat. Methods* **2012**, *9*(7) 676-682.

[293] I. Martin, B. Obradovic, L.E. Freed, G. Vunjak-Novakovic, *Ann. Biomed. Eng.* **1999**, *27*(5) 656-62.

[294] N. Schmitz, S. Laverty, V.B. Kraus, T. Aigner, *Osteoarthr. Cartil.* **2010**, *18 Suppl 3* S113-S116.

[295] R.W. Farndale, D.J. Buttle, A.J. Barrett, *Biochim. Biophys. Acta* **1986**, *883*(2) 173-177.

[296] J.F. Woessner, *Arch. Biochem. Biophys.* **1961**, *93*(2) 440-447.

[297] A.P. Hollander, T.F. Heathfield, C. Webber, Y. Iwata, R. Bourne, C. Rorabeck, A.R. Poole, *J. Clin. Investig.* **1994**, *93*(4) 1722-1732.

[298] L.A. Carpino, *Acc. Chem. Res.* **1973**, *6*(6) 191-198.

[299] R.P. van Summeren, A. Romaniuk, E.G. Ijpeij, P.L. Alsters, *Catal. Sci. Technol.* **2012**, *2*(10) 2052-2056.

[300] B. Jiang, E. Drouet, M. Milas, M. Rinaudo, *Carbohydr. Res.* **2000**, *327*(4) 455-461.

[301] H. Sies, *Angewandte Chemie International Edition in English* **1986**, *25*(12) 1058-1071.

[302] G. Kogan, L. Šoltés, R. Stern, J. Schiller, R. Mendichi, in *Studies in Natural Products Chemistry*, (Eds: R. Atta ur), Elsevier **2008**, 789-882.

[303] Y. Lei, S. Gojgini, J. Lam, T. Segura, *Biomaterials* **2011**, *32*(1) 39-47.

[304] S. Ouasti, R. Donno, F. Cellesi, M.J. Sherratt, G. Terenghi, N. Tirelli, *Biomaterials* **2011**, *32*(27) 6456-6470.

[305] C. Chung, M. Beecham, R.L. Mauck, J.A. Burdick, *Biomaterials* **2009**, *30*(26) 4287-4296.

[306] A.J. Sutherland, G.L. Converse, R.A. Hopkins, M.S. Detamore, *Adv. Healthcare Mater.* **2015**, *4*(1) 29-39.

[307] I.E. Erickson, A.H. Huang, S. Sengupta, S. Kestle, J.A. Burdick, R.L. Mauck, *Osteoarthr. Cartil.* **2009**, *17*(12) 1639-1648.

[308] L. Bian, C. Hou, E. Tous, R. Rai, R.L. Mauck, J.A. Burdick, *Biomaterials* **2013**, *34*(2) 413-421.

[309] J. Hauptstein, T. Bock, M. Bartolf-Kopp, L. Forster, P. Stahlhut, A. Nadernezhad, G. Blahetek, A. Zernecke-Madsen, R. Detsch, T. Jungst, J. Groll, J. Tessmar, T. Blunk, *Adv Healthc Mater* **2020**, *9*(15) e2000737.

[310] S. Sultan, A.P. Mathew, *Nanoscale* **2018**, *10*(9) 4421-4431.

[311] W.L. Ng, M.H. Goh, W.Y. Yeong, M.W. Naing, *Biomater Sci* **2018**, *6*(3) 562-574.

[312] R. Levato, W.R. Webb, I.A. Otto, A. Mensinga, Y. Zhang, M. van Rijen, R. van Weeren, I.M. Khan, J. Malda, *Acta Biomater.* **2017**, *61* 41-53.

[313] P. Snetkov, K. Zakharova, S. Morozkina, R. Olekhnovich, M. Uspenskaya, *Polymers* **2020**, *12*(8) 1800.

[314] K.I. Draget, G. Skjåk Bræk, O. Smidsrød, *Carbohydr. Polym.* **1994**, *25*(1) 31-38.

[315] J. Kim, Y. Park, G. Tae, K.B. Lee, C.M. Hwang, S.J. Hwang, I.S. Kim, I. Noh, K. Sun, *J. Biomed. Mater. Res. A* **2009**, *88A*(4) 967-975.

[316] J. Yin, M. Yan, Y. Wang, J. Fu, H. Suo, *ACS Appl. Mater. Interfaces* **2018**, *10*(8) 6849-6857.

[317] J.W. Nichol, S.T. Koshy, H. Bae, C.M. Hwang, S. Yamanlar, A. Khademhosseini, *Biomaterials* **2010**, *31*(21) 5536-5544.

[318] S.S. Gandhi, H. Yan, C. Kim, *ACS Macro Lett.* **2014**, *3*(11) 1210-1214.

[319] C.Y. Kuo, T. Guo, J. Cabrera‐Luque, N. Arumugasaamy, L. Bracaglia, A. Garcia‐Vivas, M. Santoro, H. Baker, J. Fisher, P. Kim, *J. Biomed. Mater. Res. A 106*(6) 1476-1487.

[320] L.E. Bertassoni, J.C. Cardoso, V. Manoharan, A.L. Cristino, N.S. Bhise, W.A. Araujo, P. Zorlutuna, N.E. Vrana, A.M. Ghaemmaghami, M.R. Dokmeci, A. Khademhosseini, *Biofabrication* **2014**, *6*(2) 024105.

[321] D.B. Denney, M.A. Greenbaum, *J. Am. Chem. Soc.* **1957**, *79*(14) 3701-3705.

[322] H. Tsumoto, K. Takahashi, T. Suzuki, H. Nakagawa, K. Kohda, N. Miyata, *Bioorganic Med. Chem. Lett.* **2008**, *18*(2) 657-660.

[323] O. Koniev, A. Wagner, *Chem. Soc. Rev.* **2015**, *44* 5495-5551.

[324] W.H. Binder, H. Gruber, *Macromol. Chem. Phys.* **2000**, *201*(9) 949-957.

[325] G.W. Cline, S.B. Hanna, *J. Org. Chem.* **1988**, *53*(15) 3583-3586.

[326] G.W. Anderson, J.E. Zimmerman, F.M. Callahan, *J. Am. Chem. Soc.* **1964**, *86*(9) 1839-1842.

[327] G. HANDBOOK, Gelatin Manufacturers Institute of America Members as of January 2012, **2012**, 7.

[328] P. Gravel, *The Protein Protocols Handbook*, 2nd ed., Springer, Totowa (NJ, USA), **2002**, 163-168.

[329] P.H. O'Farrell, *J Biol Chem* **1975**, *250*(10) 4007-21.
[330] Z. Grabarek, J. Gergely, *Anal. Biochem.* **1990**, *185*(1) 131-135.
[331] O. Klykov, M.G. Weller, *Anal. Methods* **2015**, *7*(15) 6443-6448.
[332] F.A. Johnston-Banks, *Food Gels*, Springer, Dordrecht, **1990**, 233-289.
[333] R. Munday, *Free Radic. Biol. Med.* **1989**, *7*(6) 659-673.
[334] M. Perera, N. Ayres, *Polym. Chem.* **2017**, *8* 6741-6749.
[335] H. Kamata, X. Li, U.-i. Chung, T. Sakai, *Adv. Healthcare Mater.* **2015**, *4*(16) 2360-2374.
[336] C.-Y.M. Tung, P.J. Dynes, *J. Appl. Polym. Sci.* **1982**, *27*(2) 569-574.
[337] H.H. Winter, M. Mours, *Neutron spin echo spectroscopy viscoelasticity rheology* **1997**, 165-234.
[338] M. Djabourov, J. Leblond, P. Papon, *J. phys.* **1988**, *49*(2) 319-332.
[339] S.B. Ross-Murphy, *Polymer* **1992**, *33*(12) 2622-2627.
[340] I.M. Kolthoff, I.K. Miller, *J. Am. Chem. Soc.* **1951**, *73*(7) 3055-3059.
[341] B.G. Soliman, G.C.J. Lindberg, T. Jungst, G.J. Hooper, J. Groll, T.B.F. Woodfield, K.S. Lim, *Advanced Healthcare Materials* **2020**, *9*(15) 1901544.
[342] P.N. Jaipan, Alexander; Narayan, Roger J., *MRS Communications* **2017**, *7* 416-426.
[343] B.F. Pierce, E. Pittermann, N. Ma, T. Gebauer, A.T. Neffe, M. Hölscher, F. Jung, A. Lendlein, *Macromol Biosci* **2012**, *12*(3) 312-321.
[344] I. Pepelanova, K. Kruppa, T. Scheper, A. Lavrentieva, *Bioengineering (Basel, Switzerland)* **2018**, *5*(3) 55.
[345] A.K. Nguyen, P.L. Goering, V. Reipa, R.J. Narayan, *Biointerphases* **2019**, *14*(2) 021007.
[346] H. Ding, N.P. Illsley, R.C. Chang, *Sci. Rep.* **2019**, *9*(1) 18854.
[347] E.S. Antonarakis, A. Emadi, *Cancer Chemother Pharmacol* **2010**, *66*(1) 1-9.
[348] Z. Wu, X. Su, Y. Xu, B. Kong, W. Sun, S. Mi, *Sci. Rep.* **2016**, *6*(1) 24474.
[349] S. Hong, D. Sycks, H.F. Chan, S. Lin, G.P. Lopez, F. Guilak, K.W. Leong, X. Zhao, *Adv. Mater.* **2015**, *27*(27) 4035-4040.
[350] G. Cidonio, M. Glinka, J.I. Dawson, R.O.C. Oreffo, *Biomaterials* **2019**, *209* 10-24.
[351] J.E. Trachtenberg, M. Santoro, C. Williams, C.M. Piard, B.T. Smith, J.K. Placone, B.A. Menegaz, E.R. Molina, S.-E. Lamhamedi-Cherradi, J.A. Ludwig, V.I. Sikavitsas, J.P. Fisher, A.G. Mikos, *ACS Biomater. Sci. Eng.* **2018**, *4*(2) 347-356.
[352] K. Nair, M. Gandhi, S. Khalil, K.C. Yan, M. Marcolongo, K. Barbee, W. Sun, *Biotechnol. J.* **2009**, *4*(8) 1168-1177.
[353] K. Holzl, S. Lin, L. Tytgat, S. Van Vlierberghe, L. Gu, A. Ovsianikov, *Biofabrication* **2016**, *8*(3) 032002.
[354] M. Crisan, S. Yap, L. Casteilla, C.W. Chen, M. Corselli, T.S. Park, G. Andriolo, B. Sun, B. Zheng, L. Zhang, C. Norotte, P.N. Teng, J. Traas, R. Schugar, B.M. Deasy, S. Badylak, H.J. Buhring, J.P. Giacobino, L. Lazzari, J. Huard, B. Péault, *Cell Stem Cell* **2008**, *3*(3) 301-313.
[355] J. Hauptstein, T. Böck, M. Bartolf-Kopp, L. Forster, P. Stahlhut, A. Nadernezhad, G. Blahetek, A. Zernecke-Madsen, R. Detsch, T. Jüngst, J. Groll, J. Teßmar, T. Blunk, *Adv. Healthcare Mater.* **2020**, *9*(15) 2000737.
[356] Y.-J. Kim, R.L.Y. Sah, J.-Y.H. Doong, A.J. Grodzinsky, *Anal. Biochem.* **1988**, *174*(1) 168-176.
[357] I.C. Ng, P. Pawijit, J. Tan, H. Yu, in *Encyclopedia of Biomedical Engineering*, (Eds: R. Narayan), Elsevier, Oxford, **2019**, 225-236.
[358] K. Kalyanasundaram, *Coord. Chem. Rev.* **1982**, *46* 159-244.
[359] K.S. Lim, B.J. Klotz, G.C.J. Lindberg, F.P.W. Melchels, G.J. Hooper, J. Malda, D. Gawlitta, T.B.F. Woodfield, *Macromol. Biosci.* **2019**, *19*(6) 1900098.
[360] H. Kamata, Y. Akagi, Y. Kayasuga-Kariya, U.-i. Chung, T. Sakai, *Science* **2014**, *343*(6173) 873-875.
[361] B.B. Rothrauff, K. Shimomura, R. Gottardi, P.G. Alexander, R.S. Tuan, *Acta Biomater.* **2017**, *49* 140-151.
[362] C. Blum, M.B. Taskin, J. Shan, T. Schilling, K. Schlegelmilch, J. Teßmar, J. Groll, *Small* **2021**, *17*(13) 2007551.
[363] I. Kostova, *Curr Med Chem* **2006**, *13*(9) 1085-107.

Acknowledgements / Danksagung

Als Erstes möchte ich mich bei Prof. Dr. Jürgen Groll bedanken, der es mir ermöglicht hat dieses besonders interessante Thema an seinem Lehrstuhl unter seiner Betreuung zu bearbeiten. Danke für die von Ihnen mitgegebene Erfahrung, selbstständig und systematisch zu arbeiten, an meine eigenen Grenzen zu gehen und über mich selbst hinauszuwachsen. Außerdem vielen Dank für die Möglichkeit, dass ich an zahlreichen Konferenzen und Seminaren teilnehmen durfte. Besonders durch die Teilnahme am PONTEA-Seminar habe ich nicht nur für die Doktorarbeit, sondern auch für die Zeit nach der Doktorarbeit viel gelernt, wofür ich mich besonders bedanken möchte.

Dem Prof. Dr. Torsten Blunk danke ich für anregende Diskussionen in vielen Besprechungen, für die sehr angenehme Kooperation und die Zeit, die er in meine Arbeit investiert hat. Außerdem herzlichen Dank dafür, dass er die Rolle des 2. Gutachters meiner Doktorprüfung übernimmt.

Bei Prof. Dr. Ann-Christin Pöppler möchte ich mich für die NMR-Messzeiten, die sehr gute Zusammenarbeit und ihre Funktion als 3. Gutachterin für meine Arbeit bedanken.

Ganz besonders möchte ich mich bei Dr. Jörg Teßmar bedanken, da ohne ihn diese Arbeit nicht möglich gewesen wäre. Vielen Dank für die immer offene Tür trotz deines vollen Terminkalenders, für die zahlreichen Diskussionen über Wissenschaft oder Gott und die Welt. Vielen Dank dafür, dass du mir mit Rat und aufbauenden Worten zur Seite standst, als ich selbst nicht mehr an mich geglaubt hatte. Ich konnte mich stets darauf verlassen, dass du dein Wissen mit mir teilst und mich unterstützt, meine Ideen umzusetzen und weiterzuverfolgen. Danke auch, dass du meine Dissertation Korrektur gelesen hast.

Bei Dr. Thomas Böck möchte ich mich für die vielen Stunden, die wir zusammen im Zelllabor verbracht haben und auch erfolgreichen waren, bedanken. Danke, dass ich als Biolaie immer zu dir kommen konnte und „dumme“ Fragen stellen durfte. Ein Dank gilt auch Dr. Julia Hauptstein, die nach Thomas die Analyse meiner Hydrogele bzgl. Chondrogenese übernommen hatte. Zusätzlich möchte ich an dieser Stelle auch Hannes Horder, der MBA-Zellversuche mit GelPA durchgeführt hat, für die angenehme Zusammenarbeit danken.

Ein herzliches Dankeschön geht an Dr. Carina Blum, Dr. Tina Tylek und Dr. Matthias Ryma. Danke euch, dass ich wegen den MSCs, Mikroskopie- und Zellversuchen jederzeit zu euch kommen konnte, wenn ich Hilfe und Rat brauchte.

Acknowledgements / Danksagung

Danke an Michael Bartolf-Kopp und Ruben Scheuring, die mir den 3D-Drucker und die Kunst des G-Code-Schreibens nähergebracht haben, für eure Geduld und Hilfsbereitschaft.

Additionally, I want to thank Ali Nadernezhad for his help with rheology and interesting conversations and discussions.

Weiterhin möchte ich mich bei Dr. Andrea Ewald und Prof. Dr. Uwe Gburek bedanken. Danke Andrea, dass du mir bei biologischen Fragen immer mit Rat und Tat weitergeholfen hast. Danke Uwe, dass du mit deinen Kochkünsten diverse FMZ-Parties und Grillabende unvergesslich gemacht hast.

An Dr. Tatjana Schilling, Alice Schaaf und Alevtina Rosenthal ein herzliches Dankeschön, dass ihr mich in der Zellkultur und bei biologischen Fragestellungen immer unterstützt habt.

Danke an die guten Seelen vom FMZ, Tanja Dambach, Birgit Langner-Bischof, Harald Hümpfer und Anton Hofmann, für die Hilfe und Unterstützung in allen möglichen Situationen!

Ich danke Philipp Stahlhut, der wunderbare Aufnahmen am REM gemacht hat (auch wenn sie’s nicht in die Arbeit geschafft haben) und mir einen näheren Einblick in meine Hydrogelstruktur gegeben hat.

Für die schönen Mittagsstunden, angenehme, witzige und spannende Konversationen in der Küche oder auch auf der Dachterrasse möchte ich den Mädels aus der alten Chemie und der Biofab-Gruppe danken. Ein Dankeschön außerdem an die FMZ-Oldies, vorallem an Willi Smolan, die mir zu Anfang meiner Doktorarbeit immer mit Rat und Tat zur Seite standen. Ein Dank geht auch an alle nicht namentlich erwähnten FMZ-Mitarbeitern für die angenehme Arbeitsatmosphäre und die ständige Hilfsbereitschaft.

An die besten Bürokollegen der Welt Ilona Paulus, Viktoria Niklaus, Leonard Forster und Berat Taskin: auch wenn wir nicht durchgehend Bürokollegen waren, vielen Dank, dass ihr immer ein offenes Ohr für mich hattet, egal um was es ging! Die regelmäßigen Plaudereien haben mir immer sehr gutgetan und auch die freizeitlichen Aktivitäten waren immer ein Highlight für mich.

Zuletzt möchte ich meiner Familie danken. Ein besonderes Dankeschön geht an meine Eltern Changyu Wang und Jianfeng Shan, die mir in jeder Lebenssituation zur Seite standen, mir den Rücken gestärkt haben und immer stolz auf mich waren. Christoph, Danke, dass du in jeglicher Lage immer für mich da warst und mir immer so viel Geduld entgegenbringst, dass du immer an mich geglaubt hast und mich so akzeptierst, wie ich bin.